



THE UNIVERSITY *of* EDINBURGH
School of GeoSciences



Confirmation Report

Investigating geothermal heat resources of legacy mine workings, why
are some mine waters hotter than others?

Mylene Receveur

Christopher McDermott, Stuart Gilfillan, Andrew Fraser-Harris, Ian Watson



PhD in Geology

School of Geosciences
University of Edinburgh, Scotland
May 12, 2020

Abstract

This confirmation report has been realized as part of the confirmation process for the PhD in Geology at the university of Edinburgh, taking place with the 6-9th month from the start of the PhD. This PhD consists in investigating the geothermal heat resources of legacy mine workings in the UK and understand why waters from different mines have different temperatures.

Abandoned flooded coal mines in the UK represent low-temperature geothermal reservoirs that can potentially be used for heat storage or production (Adams and Younger, 2001). The presence of mining voids inherited from the extraction of coal seams in e.g. the Carboniferous layers of the Midland Valley of Scotland, has led to the formation of high-permeability reservoirs in which large volume of water are stored. Hot mine water therefore constitutes a low carbon heat source from which heat can be extracted using open-loop ground source heat pump systems.

However, a little is known about the heat potential, the heat sources and the recharge mechanisms in mine systems (Coal Authority, Pers. Com., 2019). Temperature measurements in several shafts in the UK have shown the lack of correlation between the depth of the measurement and the temperature of the mine water (Gillespie et al., 2013). In addition to the regional geothermal gradient, it is suggested that other factors might contribute to defining the mine water temperature. The complexity of the interconnections between mine workings represents one of the most challenging barriers in understanding mines hydro-geology.

The conducted PhD research will therefore aim to understand the temperature distribution in the mines by identifying the main factors controlling heat recharge. A key outcome of this work will be the development of a predictive tool, model or conceptual approach that enables the scientific estimation of the extent and nature of the heat available over the long term in abandoned flooded coal mines.

Contents

	Page
1 Context	4
1.1 Background	4
1.2 Abandonned mines geothermal resources	4
1.3 Knowledge gap and research area	5
2 Research design	7
2.1 Research question	7
2.2 Research objectives	7
2.3 Method	8
2.4 Modeling code	8
2.5 Data	9
3 Case study	16
3.1 Midlothian Coalfield	17
3.2 Dawdon-Horden Mining Block	23
4 Conceptual models of mines	24
4.1 Hydrology of mine aquifers	24
4.2 Thermal system	25
5 Chapter 1 : Heat extraction Model	32
5.1 Background	32
5.2 Research Gaps	35
5.3 Aims and methods	35
5.4 Research Question	36
5.5 Hypothesis	36
5.6 Preliminary results	36
5.7 Conclusion and research outputs	48
6 Chapter 2: Thermal state of the mine	52
6.1 Background	52
6.2 Research Gaps	53
6.3 Aims and methods	53
6.4 Research questions	53
6.5 Hypothesis	54

6.6 Preliminary results	54
6.7 Results and research outputs	56
7 Chapter 3: Recharge potential of the Midlothian and Dawdon-Horden coalfields: an investigation of the key features for thermal modeling of flooded coal mines	60
7.1 Background	60
7.2 Research Gaps	63
7.3 Aims and methods	63
7.4 Research questions	64
7.5 Hypothesis	64
7.6 Preliminary results	65
7.7 Conclusion and research outputs	66
8 Data management plan	67
8.1 Data repositories	67
8.2 Version control management plan	67
9 Time plan	69
10 Supervisory arrangements	71
11 Resources and Training	72
11.1 Training need analysis	72
11.2 Teaching experience	72
11.3 Resources available	72
11.4 Resources needed	73
11.5 Conferences	74
12 Ethical and Health and safety considerations	75
13 Take home message	76
A Appendix	77
A.1 Equations	77
A.2 Figures from Chapter 1	80
A.3 Rock properties	81
A.4 Scripts	83
References	92

1 Context

1.1 Background

Heat demand for domestic and commercial space heating and hot water heating accounts for more than 1/3 of the energy consumption in the UK, and for more than 50% in Scotland. Most of the heat consumption is currently covered by natural gas, accounting for a large proportion of the Greenhouse Gas emissions in the country. Through the 2019 UK's Climate Change Act, both the UK Government and Scotland agreed to reach neutral carbon emissions by 2050 and 2045, respectively (Stark, 2019).

To achieve this goal, the decarbonization of residential heat became one of the main preoccupation of both governments. Scotland targets to replace all gas boilers by low-carbon heating systems in all new homes by 2025 (*Clean Growth - Transforming Heating* 2018). By 2032, the objective is to supply 35% of cool/heat for domestic heating and 70% for non-domestic heating, from low-carbon energy sources, against only 7.7% in 2017. Using mine-water as a heat energy source has therefore been of growing interest as it could partly contribute to this ambitious project (Banks et al., 2004). Todd et al., 2019 showed that about 7% of Scotland's heat requirement could indeed be sourced from abandoned flooded mine workings, lying just below populated areas.

1.2 Abandoned mines geothermal resources

Abandoned flooded mines constitute potential low-temperature geothermal reservoirs that can be used for energy storage and production (Adams and Younger, 2001). Coal has been mined in Scotland since the 12th century, but only emerged during the 16th Century and significantly increased in number during the 17th Century. In the early times of mining, coal was mostly extracted from shallow mines using the pillar-and-stall method. In the early 18th, the invention of the Newcomen steam engine enabled pumping water more efficiently, allowing the access to deeper part of the mines. This engine was first installed in the UK at Dudley Castle in Staffordshire in 1712. From the 1950's, longwall mining was the main method of extraction of coal in deep mines, and many areas initially mined by the room-and-pillar method were latterly reworked using this method (Atkinson, 1966). However, the commitment of the government to increase shares of oil and nuclear for electricity generation progressively led to a drop in the demand for coal. Hundreds of collieries closed between 1958 and 1959, and 23 additional mines closed following the 1984 miners' strike. Only 50 mines were still opened in 1992. The last underground coal mine, the Kellingley Colliery, closed in 2015.

After the closure of deep mine and the cessation of dewatering, water generally rebounds back to natural levels and fills the voids inherited from the mining activities (Robin et al., 2008). This interconnected network of open voids (i.e. mine workings, shafts and roadways) tends to form highly transmissive 'anthropogenic aquifers' (Adams and Younger 2001) from which important volume of water can be stored and extracted (Banks, 1997). A compilation of mine water temperatures in the Midland Valley of Scotland moreover showed that mine-waters are generally hotter than natural groundwater, which is generally around 10 to 12 °C in UK (Gillespie et al.,

2013; XXX). This can be explained by the existence of processes typically occurring in worked coal mines, such as pyrite oxidation, or heat advection through artificial large-scale transmissive pathway (Bailey et al. 2016).

Not only is mine-water heat attractive for its geothermal potential, but also for its proximity to the consumer and its broad accessibility (Ruhaak and Renz, 2010). Indeed, most of the mines are located near densely populated area, giving the opportunity to provide local population (i.e. both single household or district heating) with a low-carbon energy source for space heating or cooling (Farr et al., 2016). Energy can be extracted from mine-water using open loop or closed loop Ground Source Heat Pump (GSHP) systems (Małolepszy, 2003). Such system have already been implemented worldwide, such as Heerlen in the Netherlands (Ferket et al., 2011) or Mieres in Spain (Andrés et al., 2017; Loredo et al., 2017). In the UK, the first systems were implemented in Shotton and Lumphinnans in Scotland in 1999-2000, providing heat to 16 and 18 dwellings, respectively (Banks et al., 2009). The existence of infrastructures such as mine shafts moreover gives the opportunity to access mine-water while avoiding costs associated to the drilling of new boreholes, making of mine-water based heat systems cost-effective solutions relative to conventional GSHP systems (Ghoreishi Madiseh et al. 2012). In addition, to mitigate the discharge of contaminated mine water to the surface environment, the Coal Authority has been responsible for the implementation of mine water treatment systems across the UK (Younger, 2004). About 3000 L/s of mine water are pumped from more than 50 abandoned coal mines, representing about 100 MW of potential low enthalpy heat energy (Banks et al., 2009). Where pumping schemes are already implemented to maintain safe water level in the mine, using mine-water as a source of energy could therefore give the opportunity to decrease costs associated to the maintenance of water treatment systems by selling heating or cooling services (Loredo et al., 2016).

Finally, mine reservoirs also present potential for energy storage in addition to being viewed as a heat source. Industries, data centers or sport facilities are examples of buildings that have cooling demand which could be fulfilled by reversing the heat pump system. Heat pumps indeed provides the opportunity for seasonal and cyclical heating/cooling and can be used to inject and store excess heat from buildings into the ground, that could be extracted for future heating usage. Cyclical production has already been implemented worldwide (i.e. Mijnwater Heerlen' project, Verhoeven 2017) and has been proved to increase the overall efficiency and sustainability of mine-water based heat pump systems, by balancing heat recharge and discharge (Banks 2008).

1.3 Knowledge gap and research area

The geothermal potential of flooded mines depends both on the temperature of the mine-water and the rate at which that water can be extracted without significantly depleting the resource (Watzlaf and Ackman 2006). Previous publications about geothermal resources assessment in abandoned coal mines have used either numerical or analytical models to estimate the sustainability of heat extraction from flooded mine workings. Despite the existence of diverse worldwide studies, no standard procedure has emerged yet in mine modeling. This has been mostly attributed to the high complexity and potentially highly case-specific hydraulic characters of such system. In addition, it appears that there is no clear understanding of the main heat sources and key heat transfer mechanisms in mines, and of their contribution on the heat recharge rate. Most of the studies indeed only considered the local geothermal gradient as the main contributor to the thermal state of the mines, but only a few of them investigated the impact of previous mining activities on the geothermal gradient.

To promote the development of heat extraction schemes, the Coal Authority however wish to get a better understanding of the geothermal resources in mines, including their storage capacity and the sustainability of heat extraction. Knowing the lateral extent of the area affected by heat extraction around a production well and the recovery rate (i.e. time for a mine system to recover its initial temperature when production stops) is also of primary interest as it could support the development of a methodology to guide the licensing of heat (Ian Watson, Coal Authority, Pers. Com. 2019).

The present study therefore aims at getting a better understanding of the contribution from different heat sources on the heat recharge rate in mines and key heat transfer processes controlling the mine water temperatures. We will investigate the amplitude/direction of the heat fluxes induced by heat extraction from the mine and during recovery, but also the temperature distribution resulting from its complex production and flooding history. All those elements are critical to assess realistically the heat resource in mines, their renewability and long-term energy balances, and thus the sustainability of heat extraction from mine. This project finally aims at developing a reproducible strategy for mine modeling while simplifying the geometrical and hydraulic complexity of mines, and create a tool able to guide the licensing of heat.

2 Research design

2.1 Research question

The topic of this PhD can be defined as the "conceptualization of mine water temperatures", aiming at answering the general question: "why do different mines have different temperatures?". The aim of the research project is to get a better understanding of the key factors controlling the mine-water temperature as well as the temperature distribution in flooded abandoned mines, with a focus on UK coal mines.

To achieve this goal, the project has been divided in three main objectives that will be used to answer the following key research questions:

- What are the key heat recharge mechanisms and heat sources controlling the water temperature in flooded coal mines?
- What is the impact of past mining activities on the thermal state and temperature distribution in mines?
- What are the key mine features allowing to assess the sustainable heat potential of coal mines at the scale of a mine?

2.2 Research objectives

To answer those questions, the first objective is to create hydrological/thermal conceptual model(s) of flooded coal mines to identify the main controls on mines temperatures. We also want to develop a numerical approaches able to discriminate between the contribution from different types of heat fluxes induced by heat extraction and heat/water recovery.

The second objective is to determine the thermal state of a mine after a period of mining and flooding. The objective is to assess the initial temperature distribution within a mine to evaluate its initial heat potential.

The third objective is to assess the key features in mine plans having significant impact on the heat depletion and rate of energy recharge at the scale of a mine or network of interconnected mines. An approach to create representative but simplified model of mine workings will be developed in order to assess the potential of mines, in terms of energy storage/heat capacity. This analysis will be based on a comparative study between mines of different structures in two different coalfields: the Midlothian Coalfield in Scotland and the Horden-Dawdon Coalfield in NE England. Based on the knowledge acquired from previous research axis, this will be used to define the extent of the area impacted by heat extraction around the production well, depending on the mine structure. The ultimate goal of the PhD is to develop an analytical or numerical tool able to predict the long-term temperature change of the mine-water extracted for geothermal utilization.

2.3 Method

The research project will be divided in two part. The first part will be focused on developing modelling approaches, studying general processes and perform sensitivity analysis using simple conceptual representations of mine workings. In a second phase, we will implement and verify the findings and hypothesis based on available data from two study areas.

First, hydrogeological conceptual model(s) will be created considering different heat sources (i.e. natural heat flow, solar/surface heat, radiogenic heat production, pyrite oxidation, groundwater inflow from depth) and heat transfer mechanisms (i.e. heat convection / diffusion) depending on the geological context (i.e. horizontal layers, dipping layers, syncline). Numerical models will subsequently be used to assess the relative contribution of those heat sources on the heat recharge rates in mines (i.e. sensitivity analysis) and calculate energy balances. Of particular interest will be to identify the nature of the fluxes induced by water and/or heat extraction from flooded mine workings and their evolution throughout a production and recovery period. This will be done using 1D models of heat extraction and 2D models representing mines of simple geometries with different thermal/hydraulic boundary conditions and heat source/sinks. Results will be validated against analytical solutions.

Then, special attention will be paid to the perturbations caused by mining activities on the geothermal gradient, through long-term simulations of water extraction and recovery. A series of 2D finite-element models of mine workings with different geometries, boundary conditions and/or material properties will be developed to assess the impact of long-term water extraction and rebound on the resulting thermal state of a mine and expected heat recovery time (i.e. return to initial undisturbed temperature equilibrium). Results will be calibrated and validated using existing temperature profiles and recovery data.

Findings related both to the main heat sources/recharge mechanisms and key geometrical features will finally be applied to the selected case studies. A method will be developed to extract important geometrical features from the mine plans and create representative and computationally cost-effective mesh. After verifying the applicability of 2D models to simulate 3D mechanisms, an optimal mine modeling strategy will be developed using available geometrical/monitoring data in each area. A comprehensive comparative study between those two mining areas will be performed based on numerical simulations of flooding, heat extraction and heat recovery. Results will be used to estimate the area impacted by the extraction of heat, the time necessary for recovery, but also to assess their overall heat capacity. Based on the local energy demand, those elements will be used to predict the changes in the production temperature with time and evaluate the long-term sustainable heat recovery/storage potential of the mine reservoir.

2.4 Modeling code

Previous researches on the geothermal potential of flooded coal mines used modeling approach to predict both the absolute thermal capacity of mines and the temperature changes of the extracted fluid over time (Renz et al., 2009). Different methods have been used in the literature to solve for heat transfers and fluid flow equations in mine systems, going from analytical models (Pruess and Bovardsson, 1983), (Rodríguez and Díaz, 2009) to 1D/2D/3D numerical models (Loredo et al., 2016), or using a combination of both (Renz et al., 2009; Ferket et al., 2011).

Analytical models solve for the exact mathematical solutions of flow and heat transport by considering homogeneous systems, and therefore require geometrical simplifications (Banks et al., 2009; Loredo et al., 2017). They have been described as a useful tool at an early stage of a feasibility study to get a first insight into heat transfers and the sustainability of heat abstraction from geothermal systems (Banks, 2009; Loredo et al., 2017). Numerical codes used to model heat and flow transport processes in mines include Finite Difference simulators (FDM) such as SHEMAT (Ferket et al., 2011), Finite Element modeling software (FEM) such as TOUGH2 (Malolepszy, 2003; Guo et al., XXX), FEFLOW (Renz et al. 2009; Diersh, 2005, Andres et al.,), HydroGeosphere (Raymond and Therrien, 2008), or Finite Volume algorithm (FVM), such as MARTHE, FLUENT (Hamm and Bazargan Sabet 2010), THEMUT (Ghoreishi Madiseh et al., 2012) or OpenFOAM (Bao and Liu, 2018). Numerical models allow creating more realistic representations of mining scenarios but require more data and computational time. In addition, such complex model might be subjected to numerical instabilities, limiting their reliability (Renz et al., 2009). Numerical approaches are developed in more details in Chapter 6. Here we use OpenGeoSys, an open-source FEM modeling code which was developed to solve for coupled thermo-hydro-geomechanical-chemical (THMC) processes in porous and fractured media (Kolditz et al., 2012).

2.5 Data

Available data from diverse sources will be used to build and verify both conceptual and numerical models of mines. The data includes information from in situ sensors acquired by the Coal Authority, legacy data available in various archives (i.e. historical temperature data from Burley et al., 1984, pumping data from former private Coal Mining Companies), geological data from the British Geological Survey (BGS) database... The Glasgow Geothermal Energy Research Field Site and related published papers moreover constitute since 2018 an additional source of data (i.e. stratigraphy, rock properties, flow rate, temperatures), specifically acquired to improve the understanding of the geothermal potential of abandoned flooded mine workings below Glasgow. An inventory of the data available from the Coal authority has been made in January 2020 and is subjected to the academic license. Those data include:

- Monitoring data, including manual logging, continuous logging from temperature and water logger, punctual surveys, pumping tests... Depending on the nature of the site (i.e. naturally gravity-driven discharge area, pumped shaft/borehole, pumped discharge), different data set can be available.
 - Time series of pumping rate/discharge rate and/or groundwater levels (i.e. flooding rate) in shafts
 - Time series of temperature change in the shafts (at the logger depth)
 - Temperature and conductivity profiles with location of the seams intersected by the shafts
- GIS data
 - Mine data: shaft location, underground workings (deep, shallow and probable workings), roadway, contours of mining blocks, seam levels, location of outcrops, geological disturbances... Mine plans for the Dawdon-Horden area located under the sea have not been digitalised below the see, therefore no GIS shapefiles are available for under-water areas.

- Monitoring sites, discharge site, temperature sites
- Water data: Contour of minewater block, rivers
- Mine abandonment Plans, containing more details on the mine architecture. Those are used to identify the location and interconnections between the mine workings, roadways and shafts, that represent the main flow path in such systems. In the UK, the record of mine abandonment only started with the 1870 Mines Inspection and Regulation Act (NRA, 1994), while the acquisition of accurate mine plans only became mandatory in 1872. Even though, data often showed only the extent of the workings, but not their depth or any geological information. The acquisition of reliable data and maps only started with the nationalization of the coal industry in 1947, hence most of shallow early workings are unknown and unmapped (Henton, 1974; Richardson, 1983). However, mine plans do generally not inform on the current state of the mines and some information such as areas of extensive collapse are generally not known (Harrison and Scott, 1987).

Tables 2.1 and 2.2 summarizes the data available for the two study areas, described in the following chapter, that will be used for the calibration and validation of the models.

Name	Location type	Data Type	Hydro		Thermal	
			Calibration	Validation	Calibration	Validation
Bilston Glen	shaft	T-EC profile			2012 profiles	2016 and 2019 profiles
Bilston Glen	monitoring point	Water level, temperature TS	2000 - 2018	2019 -2023	-	-
Easthouse	shaft	T-EC profile			2016 profile	2019 profile
Easthouse	monitoring point	Water level, temperature TS	2013 - 2018	2019 -2023	2016 - 2018	2019 -2023
Junckie's discharge	monitoring point	Flow, temperature TS	2015 - 2018	2019 -2023	2016 - 2019	2020-2023
Elginhaugh discharge	monitoring point	Flow	(1996 - 2011)	-	-	-
Elginhaugh discharge	monitoring point	On-site temperature	-	-	-	-

Figure 2.1: Data available for model calibration and validation in the Midlothian Coalfield (Bilston Glen and Esthouses mines)

Name	Location type	Data Type	Hydro		Thermal	
			Calibration	Validation	Calibration	Validation
Hawthorn	shaft	T-EC profile			2000, 2003 profiles	2005, 2006, 2008 profiles
Hawthorn	monitoring point	Water level, temperature TS	2016-2018	2019 -2023	2016-2018	?
Dawdon	shaft	T-EC profile			2000, 2003, 2004 profiles	2005, 2006, 2008 profiles
Dawdon	monitoring point	Water level, temperature TS	2016 - 2018	2019 -2023	2016 - 2018	2019 -2023
Easington	shaft	T-EC profile			2000 profile	2005, 2006, 2008 profiles
Easington	monitoring point	Water level, temperature TS	2016-2018	2019 -2023	2016-2018	2019 -2023
Horden	shaft	T-EC profile			2003, 2004 profiles	2005, 2006, 2008 profiles
Horden	monitoring point	Water level, temperature TS	2016-2018	2019 -2023	2016-2018	2019 -2023

Figure 2.2: Data available for model calibration and validation in the Dawdon-Horden Coalfields

Figures 2.3 to 2.5 and Figures 2.7 to 2.8 are maps showing the available data for the Midlothian Coalfield and Dawdon-Horden mining blocks, respectively.

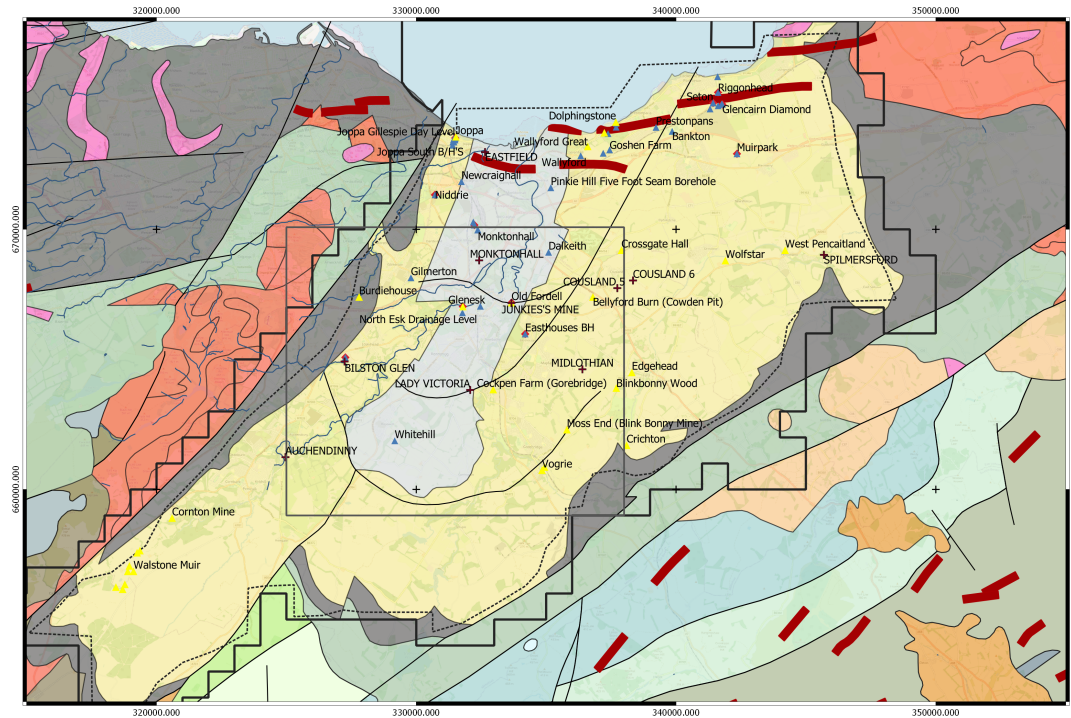


Figure 2.3: Geological map of the Midlothian Coalfield

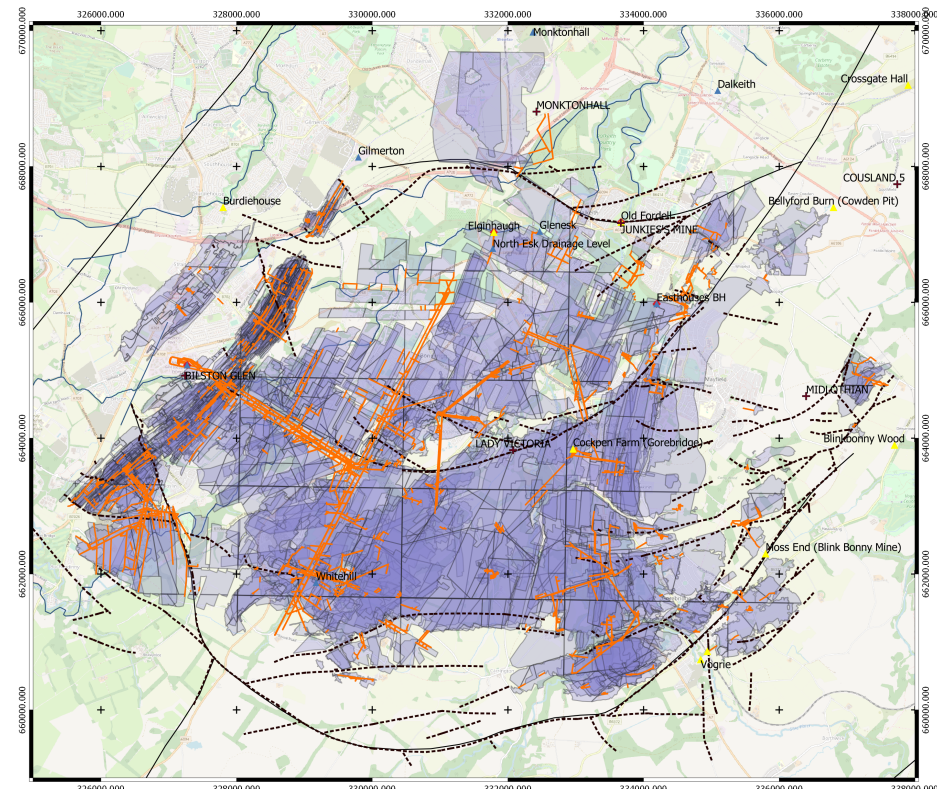


Figure 2.4: Underground mine workings and roadways in the Midlothian Coalfield

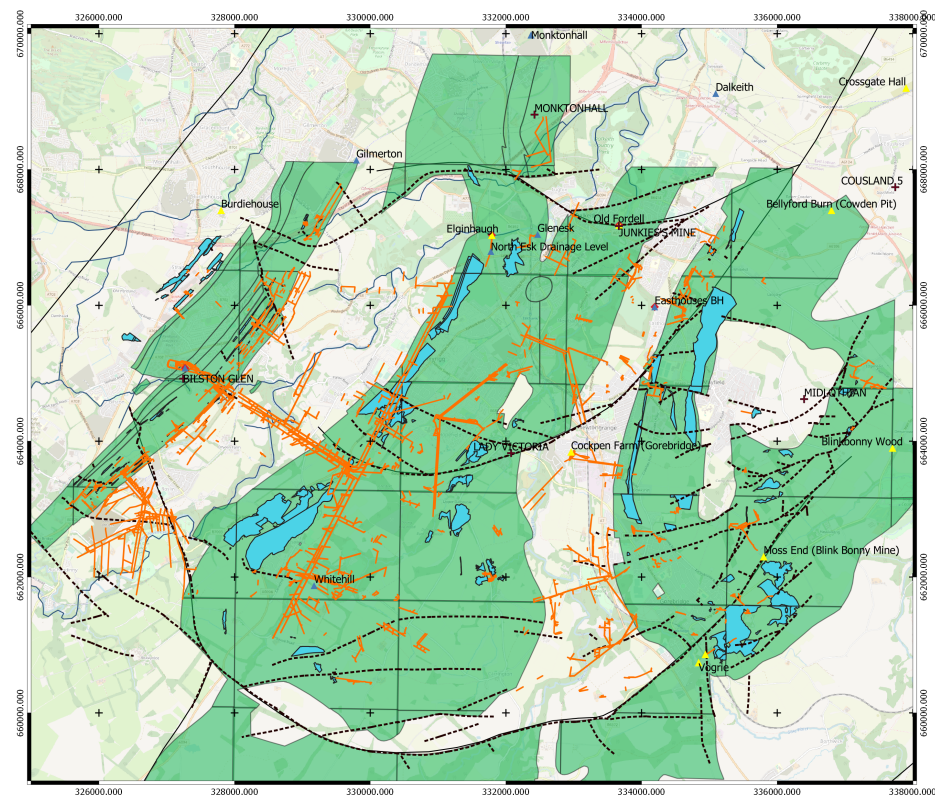
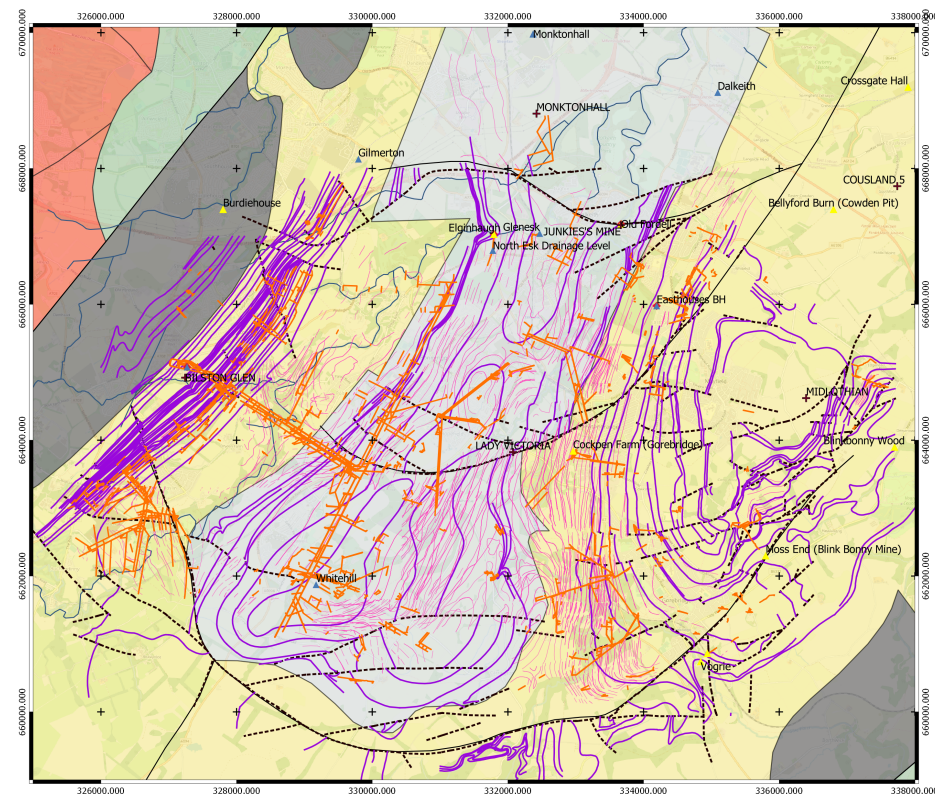


Figure 2.5: Probable and shallow mine workings in the Midlothian Coalfield



Legend

Sites	Faults
+	Boreholes
▲	Discharges
△	Monitoring site
◆	Temperature sites
Mine Data	
— Spine Roadway	Bedrock Geology Midlothian
— Outcrops	Clackmannan Group
— In Seam Level Contours	Scottish Coal Measures Group
— Geological Disturbances	Crawford Group
— Shallow Working	Gala Group
— Probable Working	Inverclyde Group
— Underground Working	Kirkcolm Group
— Waterways	Lanark Group
Water Data	Portpatrick Formation
— Water Blocks 2019	Reston Group (Lower Old Red Sandstone)
— Coalfield Consultation Area	Stratheden Group (Old Red Sandstone)
Geology	Shinnel Formation
— Dykes	Silurian rocks
	Strathclyde Group
	Tappins Group
	Extrusive rocks 1
	Extrusive rocks 2
	Igneous intrusions

Figure 2.6: Outcrop of coal seams in the Midlothian Coalfield

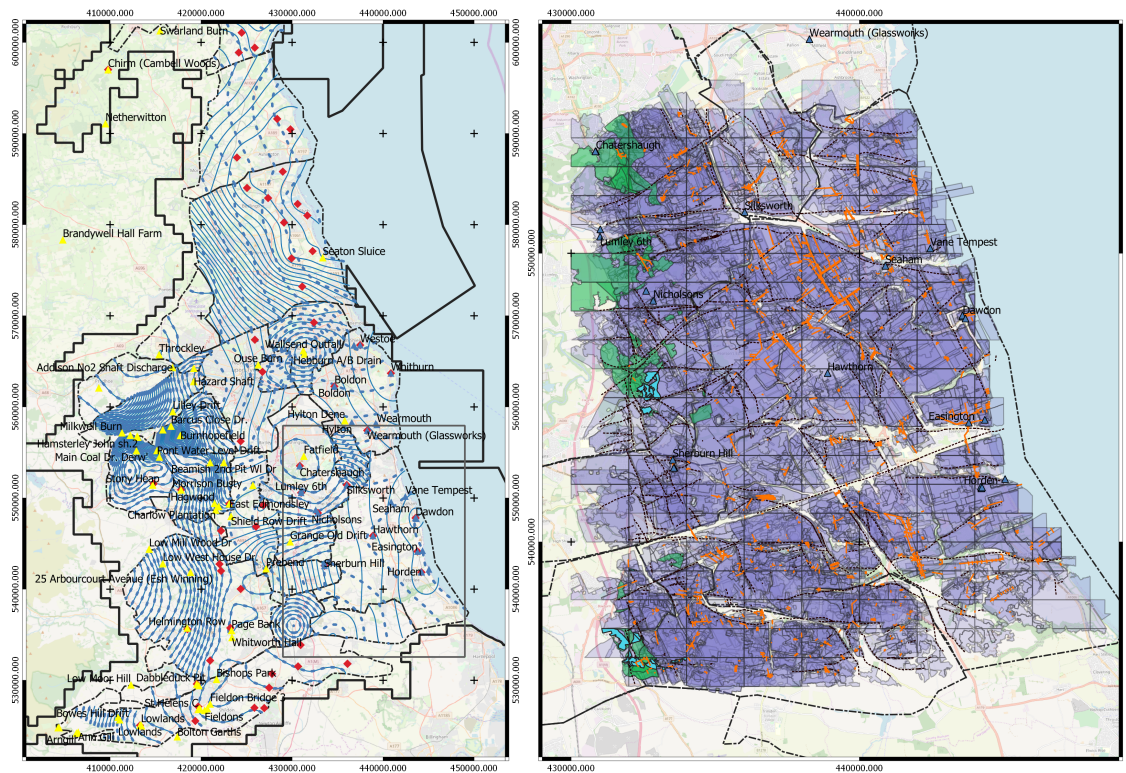
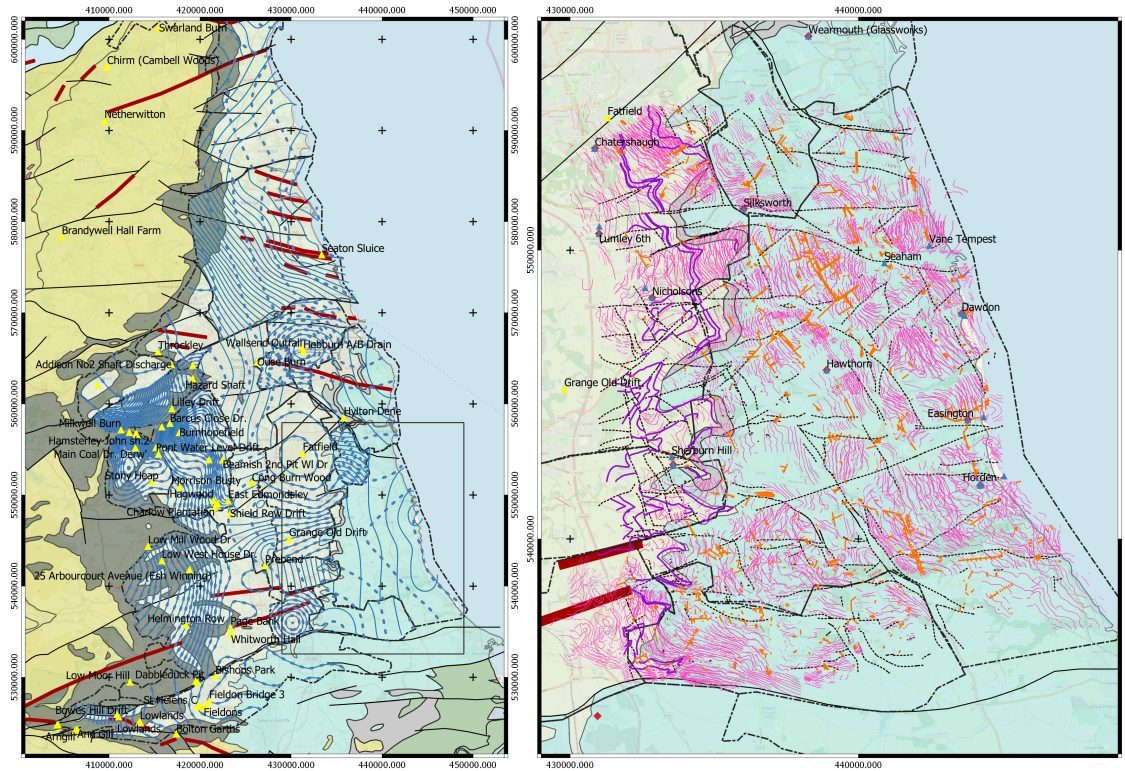


Figure 2.7: a) Water level data and location for monitoring sites, and b) Onshore underground, probable and shallow mine workings and roadways in the Horden-Dawdon mining block



Legend North East England

Sites		Current contours
+	Boreholes	Water Blocks 2019
▲	Discharges	Coalfield Consultation Area
△	Monitoring site	
◆	Temperature sites	
Mine Data		Geology
Orange line	Spine Roadway	Dykes
Purple line	Outcrops	Faults
Pink line	In Seam Level Contours	North East Bedrock Geology
Dash-dot line	Geological Disturbances	Pennine Lower Coal Measures
Cyan line	Shallow Working	Pennine Middle Coal Measures
Green line	Probable Working	Pennine Upper Coal Measures
Light purple line	Underground Working	Permian rocks
		Yoredale Group
		Zeichstein Group
Water Data		
- - -	Future contours	

Figure 2.8: a) Geological map, and b) Seam levels with location of outcrops in the Horden-Dawdon mining block

3 Case study

The Bilston Glen area, situated in the Midlothian Coalfield in Scotland, and the Dawdon-Horden Mining Block, situated in NE-England have been selected as case studies for the PhD research work, as both coalfields are or could be of geothermal interest for the authorities (3.1). While the Scottish coalfield is still at a post-mining water recovery stage, the Dawdon-Horden Coalfield is being pumped to avoid surface discharge since 2004 (source: The Coal Authority). For both area, the significant quantity and variability of the data type available (i.e. temperature and water level time series, depth-profiles) will therefore allow a proper calibration and validation of the numerical models. Moreover, the Midlothian Coalfield is located in a syncline structure, while the Dawdon-Horden Coalfield lies within slightly dipping layers extending under the sea, which would allow performing a comparative study based on the geometry of the mine workings. The present chapter consists of a literature review of the geological context and structure of the mines for both coalfields.

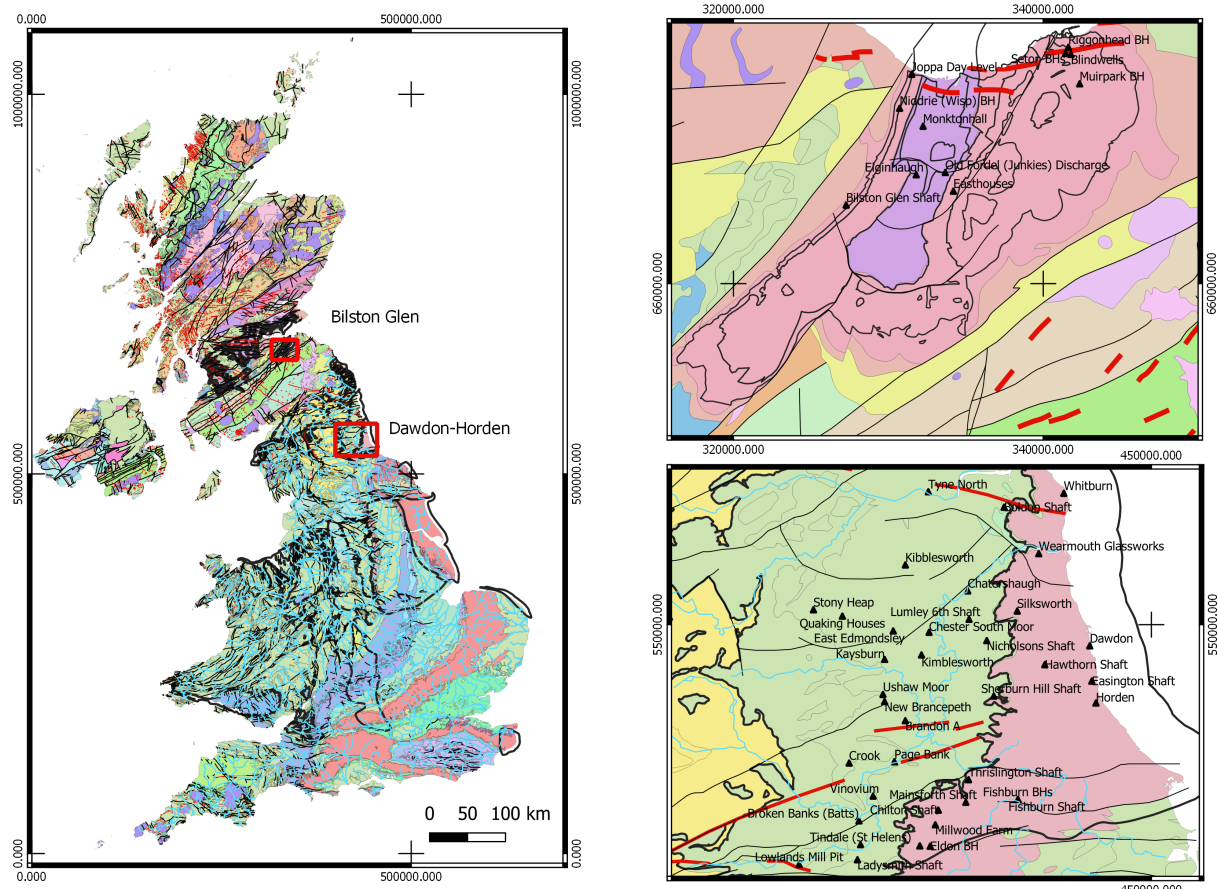


Figure 3.1: Location of the study areas

3.1 Midlothian Coalfield

The Midlothian Coalfield is located in the south east of the Midland Valley of Scotland (MVS), a 80 km wide, 150 km long WSW-ENE trending Carboniferous graben that developed on the eroded and deformed remnant of the Caledonian Mountains in Scotland (Cameron and Stephenson, 1985; Underhill, 1998; Read et al., 2002). It is located within the Midlothian-Leven Syncline, bounded on the north by the reverse NE-trending Pentland Fault and on the south by the Dunbar-Gifford and the Lammermuir faults (3.2).

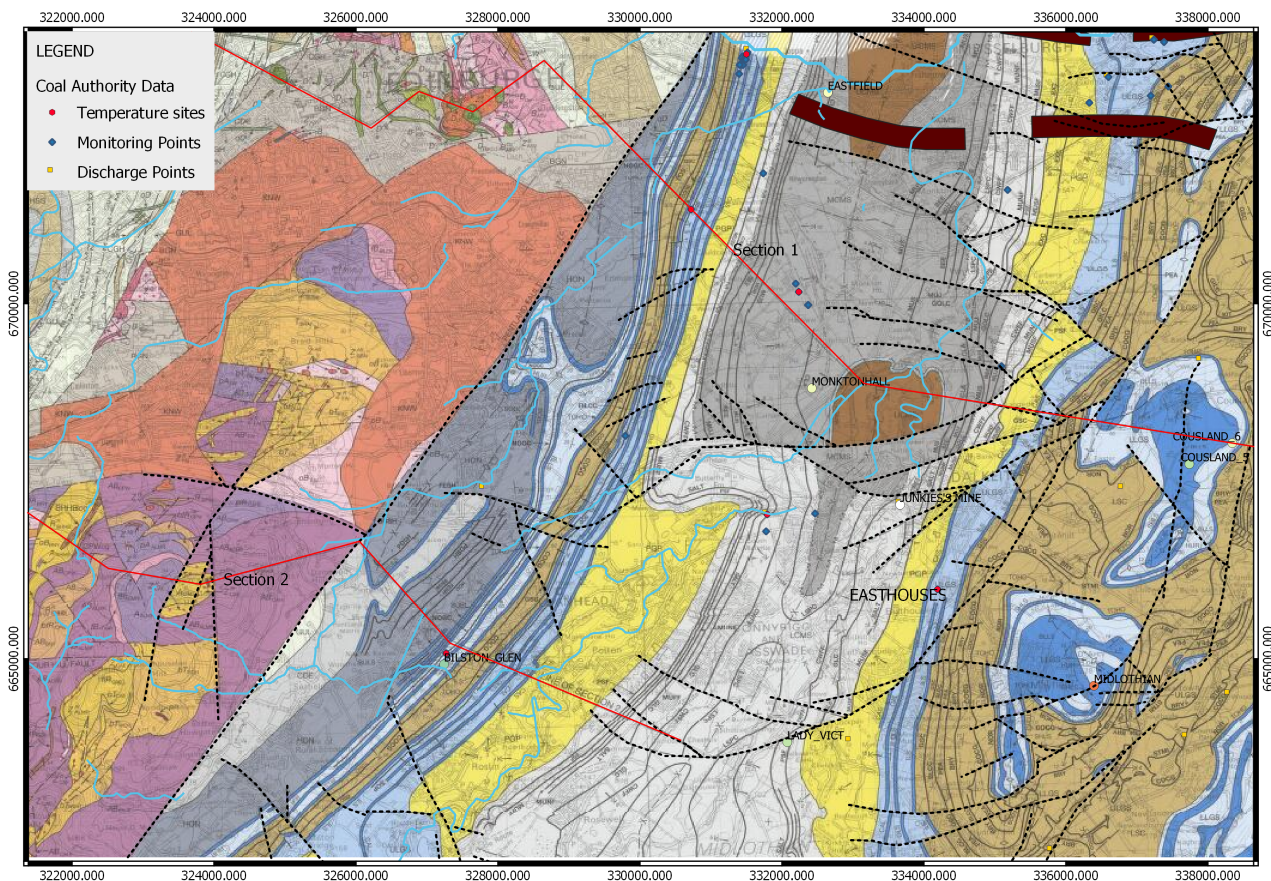


Figure 3.2: Geological map of the Midlothian Coalfield area (source: BGS database), with location of monitoring points (source: The Coal Authority)

The Midlothian-Leven Syncline is suggested to have been formed by syn-sedimentary growth during the Early Carboniferous followed by a Late Carboniferous fold tightening and reverse faulting that affected rocks from the Coal Measures Group (Underhill et al., 2008). While most of the faults became inactive after the early Carboniferous, the truncation of some structures by E-W striking Latest Carboniferous-Early Permian normal faults, quartz-dolerite dyke swarms and extensional fractures indicated that their formation was only completed by the end of the Carboniferous (Rippon et al., 1996; Stephenson et al., 2003; Monaghan and Parrish, 2006). From the Paleogene, the underplating of a magmatic plume associated to the opening of the North Atlantic

resulted in an increasing amount of uplift of Scotland (Hillis et al. 1994, White 1988). This uplift might have reactivated the Pentland fault during the early Neogene (Anderson, 19851). It also led to the significant erosion of the Carboniferous and post-Carboniferous strata, especially at basin margins and between the Midlothian–Leven Syncline and Clackmannan Syncline (i.e. at the location of the D’Arcy-Cousland Anticline). Thermal modeling around the Midlothian–Leven Syncline suggested that up to 1.9 km of sediments would have been eroded (e.g. Vincent et al. 2010; Vincent and Rowley, 2004).

The sedimentary succession in the Coalfield is typical of the sequence found within the Midland Valley of Scotland (3.3). It consists of 10-m thick cycles of non-metamorphized sandstones, siltstones and mudstones with beds of limestone, coal, fireclay, ironstone and oil-shale, deposited in a basin environment during the Devonian-Carboniferous period (Cameron and Stephenson, 1985), and intersected by andesitic/basaltic lava flows and pyroclastic rocks. Magmatic activity in the MVS extended from the Carboniferous to Permian for a period of about 90 Ma (Upton et al. 2004), and is suggested to have led to an increase in the heat flow during the Carboniferous, especially in the active eastern region.

The sedimentary succession in the MVS is subdivided into the Inverclyde, Strathclyde, Clackmannan and the Scottish Coal Measures groups (Browne et al., 1999). The Clackmannan Group consists of:

- The Upper Limestone Formation (ULGS), characterized by cyclical sequences of limestone, mudstone, sandstone, siltstone, seatrock and coal. Depositional environments are interpreted to range from shallow seas to deltaic and alluvial plains (Hall et al., 1998).
- The Limestone Coal Formation (LSC), which comprises cycles of coal, mudstone, siltstone, sandstone, seatearth and coal with some thicker mudstone intervals, ironstone and limestone. Compared to the Lower and Upper Limestone formations, the Limestone Coal Formation characterizes a return to relatively non-marine conditions in which large quantities of coal have accumulated.
- The Lower Limestone Formation (LLGS), dominated by repeated upward-coarsening cycles of limestone, bedded mudstone, siltstone and sandstone with minor seatrock and thin coal and ironstone deposited in a quiet marine and non-marine backwater (Hall et al., 1998).

The Upper Limestone Coal Formation is separated from the overlying Coal Measures Group by the Passage Formation (PGP). This formation is dominated by relatively coarse-grained sandstone with mudstone, seatclay and fireclay, deposited in a dominantly fluvial system (Hall et al., 1998). The Scottish Coal Measures Group is the youngest observable set of sedimentary rocks in the eastern part of the basin, and are mostly preserved in the centre of the synclines. It is subdivided into the Lower (LCMS), Middle (MCMS) and Upper Coal Measures formations (UCMS), which consist of fluvio-deltaic sedimentary rocks deposited in cyclical sequences of mudstone, siltstone, seatearth, sandstone and coal, in a costal deltaic plain with frequent occurrence of coal swamp conditions. The figure below (Fig 3.3) shows the typical geological log for the Midlothian Coalfield area.

Most of the coal produced in the Midlothian coalfield originates from the LSC and the MCMS. The thickness of coal seams typically ranges between 1 m and 3 m, depending on the thickness of the sedimentary cycle, with some exceptional seams reaching 15 m (Rippon, 2002).

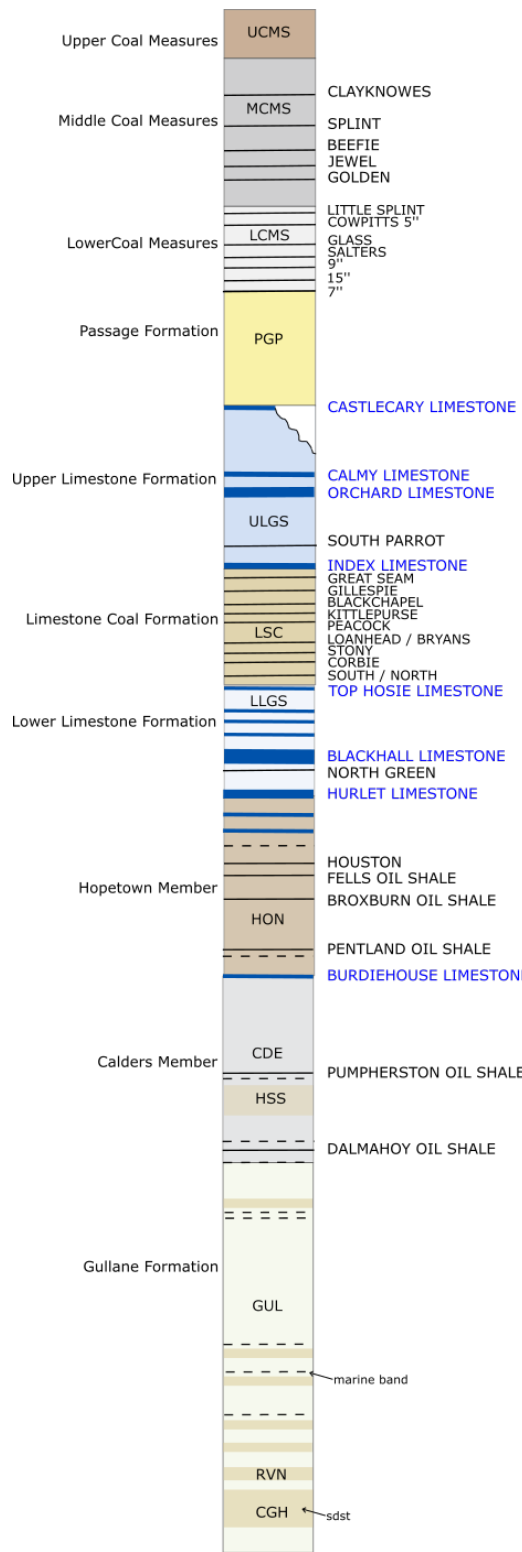


Figure 3.3: Geological log of the Midlothian coalfield area. In the Dalkeith area, the Coal Measures reach about 460 m. The maximum thickness for the UCMS, MCMS, LCMS is 1200, 350, 240 m, respectively, and averages 600, 550 and 240 m for the ULGS, LSC and LLGS, respectively.

3.1.1 Mining history

In the early stage of mining, shallow mines (i.e. the Polton and Whitehill collieries) extracted coal from the Coal Measures located in the central part of the Midlothian syncline, using the pillar-and-stall method. Coal beds from the Limestone Coal Formation have both been mined from shallow workings on the edge of the syncline where the formation outcrops (i.e. Roslin, Ramsay, Burghlee on the western limb and Lingerwood, Bryans, Newbattle, Arniston, etc... on the eastern limb), and later on by deep mines located in the deeper parts of the syncline (i.e. Bilston Glen, Lady Victoria, Easthouses). Most of the deep mines have been worked using longwall mining extraction methods. Some of the shallow and early mines were also reworked using this method.

Consultancy reports ordered by the Coal Authority have suggested that no hydraulic connections exist between the mines from the Coal Measures and the mines accessing the Limestone Coal Formation. While water has already filled the shallow workings, it is currently still rebounding in the deepest mines (XXX, XXX). Shallow mines located in the Limestone Coal Formation on the western side of the coalfield (i.e. Ramsay, Roslin, Burghlee) are interconnected, but no clear connections have been identified with the deep mines accessing the same coal beds (i.e. Bilston Glen). Old panels from the Burghlee mines are located about 40 m above Bilston Glen workings in the Great seam and are separated by 330 m in the Craigie seam. However, it has been suggested that the Roslin Colliery might drain into the Bilston Glen mine. Fig 3.4 shows a preliminary 2D conceptual model developed for the Midlothian Coalfield, based on a NW-SE cross-section through the syncline structure (see 3.2).

Similar rises in water level (i.e. about 20 m/yr) have been measured in the Bilston Glen and Easthouses shafts (Figs 3.5 and 3.6, respectively). Those mines, situated on both side of the Midlothian syncline, are connected by roadways and through the Great Seam at -502 m depth. On the eastern side of the syncline, the Easthouses, lady Victoria and Lingerwood mines, accessed by the Easthouses pumping pit, Bryan's pit and Easthouses inclines, are interconnected at different levels through shafts, roadways and goaf connections, mostly within the Great and Parrot/Splint seams. This includes roadway connection between Lingerwood Dicken's shaft and Lady Victoria shaft, incline connection between Easthouses Great Seam and Lady Victoria Splint Seam, goaf connection between Lady Victoria and Lingerwood Parrot Seam. In addition, the Eastwood pumping shaft connects the Parrot seam (i.e. base of the shaft) to the great seam from Easthouses, and the Eastwood Great seam connects to both the Lady Victoria Splint and Parrot seams by two steep drifts.

During mining activities, most of the workings located in the Limestone Coal Group were dewatered via shallow drainage adits. While shallow mine workings in the Coal Measures now drains from the Eldin Adit at Elginhaugh (i.e. Eldin Day Level at 48 m) to the river North Esk, discharge levels from deeper mines include the Old Fordel/Junckies Day Level portal (35-37 m AOD), Bryan's adit (50 m AOD) and the Burghlee Day Level (110 mAOD). First, the decant location for the Junckies Level is at about 44 m AOD in the Easthouses incline C, which access the interconnected Lingerwood, Lady Victoria, Easthouses and Bilston Glen mines via the deep Great seam. Recent reports suggested that the Junckies adit actually only drains the northern area and/or shallow workings of Easthouses-Lingerwood-Lady Victoria the in the Limestone Groups, and potentially of the Lower Coal Measures. Chemical analysis of the water discharged at Junckies indeed supported a shallow source and low residential time for this water. This might either be explained by rainwater infiltration into shallow workings of deeper Coal Measures or the drainage of water from workings separated from the Easthouses-Lingerwood-Lady Victoria workings located in the same Limestone Measures, at greater depth or to the South.

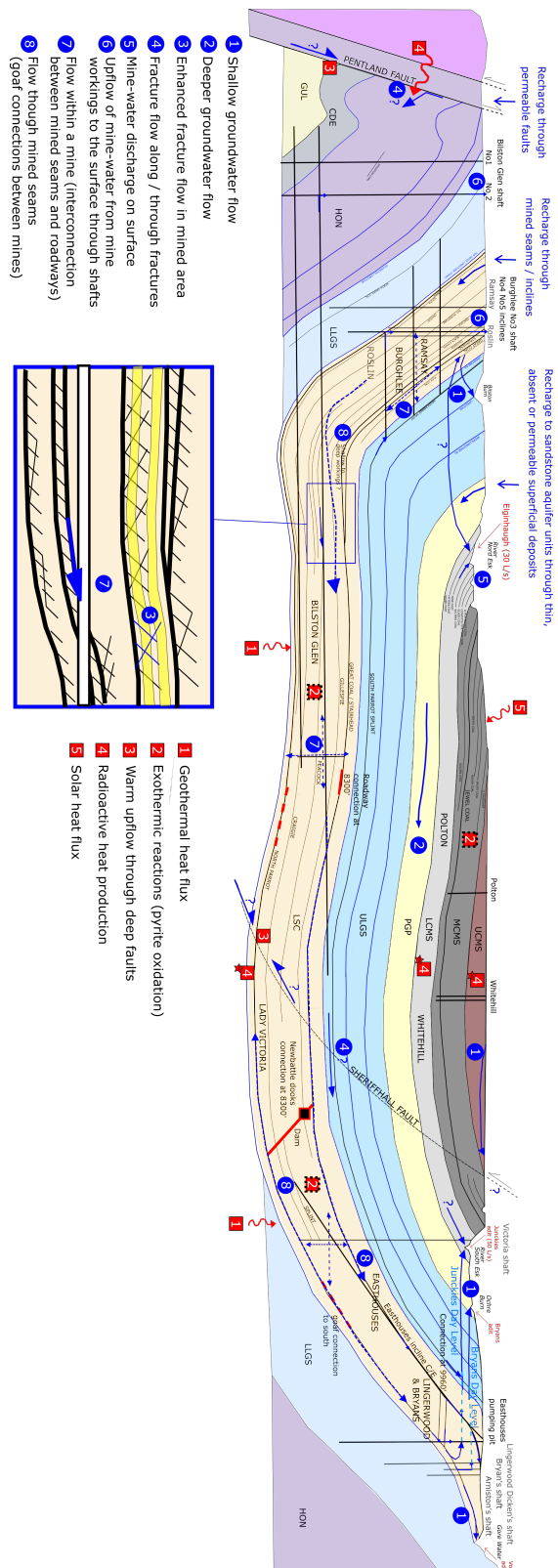


Figure 3.4: Conceptual model for the Midlothian Coalfield

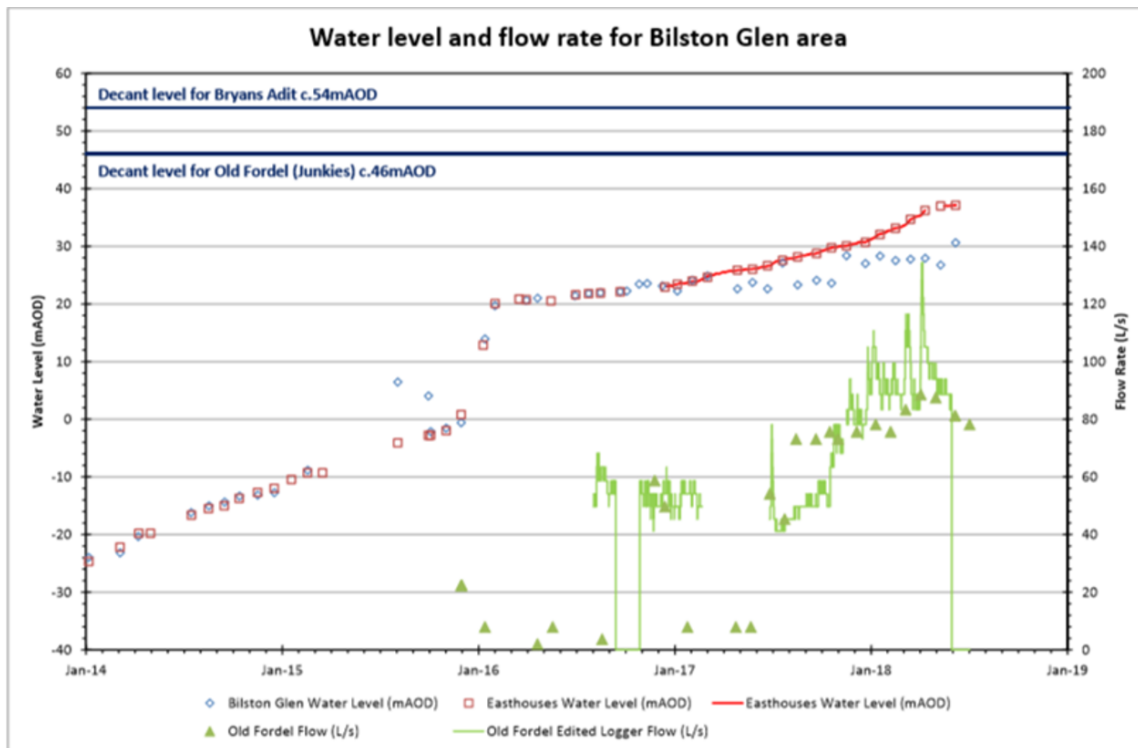


Figure 3.5: Change in water level measured in Bilston Glen shaft

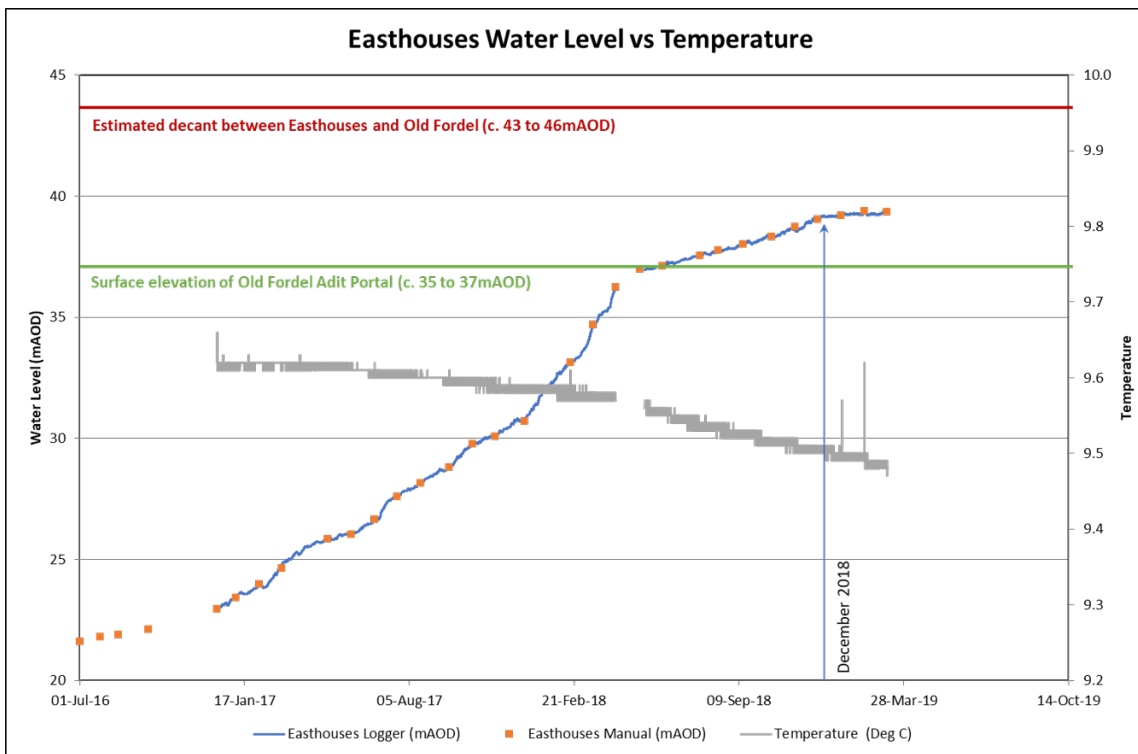


Figure 3.6: Change in water level measured in the Easthouses shaft

On the other side of the syncline, waters from the deep Coal Measures and Limestone Coal workings are drained by the Bilston Glen shaft to Elginhaugh. The increased CaCO₃ alkalinity (but low Mg/Ca content) at Elginhaugh compared to water at Junckies indicates a longer residential time in the deep limestone formations. The high sodium chloride content of the water at Bilston Glen was moreover suggested to characterise saline connate groundwater originating from the limestone deposition period. The Bryan's adit was finally designed to drain deep mining units of the Lady Victoria and Lingerwood via gravity draining of the shallow workings above, to the Ochre Burn. The decant level for the Bryans discharge is located in the Bryan's shaft (54.28 mAOD) that connects to Lingerwood Parrot seam and Easthouses Great seam. No discharge has occurred yet from the Bryan's adit, which is considered as a potential secondary discharge after Junkies's. Both the Burghlee's adit and Roslin's adit drains water from the shallow workings in the Limestone sequence on the west (reported as filled), to the Bilston Burn and Kill Burn watercourses, respectively. Water has been reported as stabilized in the Arniston mine, that connects to the Lingerwood mine through roadway in the Great seam, and discharge at Vogrie.

3.2 Dawdon-Horden Mining Block

The Dawdon mining area is located in North East England. There, 7 main seams have been worked using both pillar-and-stall and longwall mining. The coalfield consists of slightly dipping strata (1 - 5 °) extending below the sea toward the south east. The main seams are summarized in table XXX, together with their thickness.

Seam code	Ref letter	Name	thickness
NE120H	E	HIGH MAIN	1.8
NE140H	F	MAIN	1.2
NE170H	G	YARD	1.7
NE190H	H	MAUDLIN	1.1
NE210H	J	LOW MAIN	1.4 - 2.1
NE260H	L	HUTTON	1.5

Table 3.1: Main seams worked in the Dawdon area

Water pumping started in Dawdon in 2004. Since then, connections between the Dawdon, Easington and Horden mines have been identified, despite the presence of a E-W trending volcanic dyke between and of a dam between the mines that might be no longer active. Those are moreover connected with the Hawthorn mine, located further west. The Dawdon shaft is moreover interconnected with the Easington Colliery (roadways in seams J and F), Vane (connection in seam J) and Seaham (roadway in seam E) and with the general body of mine workings via Murton Colliery. A roadway might explain the interconnection between Horden, Easington and with the Blackhall Colliery. Potential roadway and goaf connection in Main seam and High Main might have been identified between Murton and Seaham, as well as a roadway connection between Shotton and Murton in Hutton seam. Finally, a roadway might link Easington and Murton in Main seam.

4 Conceptual models of mines

Geological systems are inherently complex and simplifications are therefore required to fully evaluate and understand the mechanisms that occur with them (Kruse and Younger 2009). In addition, mining activities are indeed likely to have caused perturbations of natural thermal regime of the mine systems (i.e. change in ground-water flow) and participated to the development of specific processes responsible for anomalous temperature distribution (Jessop 1995). In that view, constructing a comprehensive conceptual model of mine workings is the first step toward a good understanding on the heat sources and transfer processes in mines, and thus of the heat recharge potential of mine reservoirs. The present chapter aims at reviewing the current knowledge about mine reservoir systems in terms of geological and hydrological aspects.

4.1 Hydrology of mine aquifers

Mine aquifers are characterized by a triple-porosity composed of the primary rock porosity (i.e. unaffected rock), the mining voids (i.e. galleries, shafts, roads...) and mining-induced fractures (Wolkersdorfer, 2008). In mined strata, difficulties in predicting groundwater flow generally results from the complex geometry of interconnected open voids inherited from the mining history, not always well documented (XXX). Those tend to form high-permeability pathways in the mine, altering the natural groundwater flow within original aquifers. In the Midlothian Coalfield, the Carboniferous sedimentary sequence is composed of low permeability layers (mudstone) interbedded with higher permeability strata (sandstone, limestone) that tend to form complex multi-layered and moderately productive aquifers, with borehole yields in the range 5-15 l/s (MacDonald et al., 2004; Robins, 1990; Ball, 1999). The natural layering tends to create complex flow path, dominated by horizontal inter-granular flow and fracture flow. Lateral compartmentalization can also result from the intrusion of igneous rock (dykes, sills, plugs) or faults that can act either as permeable pathways or barriers to groundwater flow.

Despite the presence of coal seams adding more low-permeability layers between the sandstone aquifer units, the Carboniferous strata mined for coal generally have slightly higher productivity than the aquifers not mined for coal (Dochartaigh et al., 2015). Mining activities indeed resulted in an increase in permeability of the Carboniferous strata both by increasing the void space in zones where seams were mined out and through fracturing of competent horizons above the mined seams. The residual volume and geometry of mining voids will however depends both on the extraction method (i.e. pillar-and-stall, longwall mining), on the extent of induced fracturing, and on the amount of backfilling and subsidence. Despite many shafts, roadways or drifts might remain opened after the closure of a mine (Younger, 2001), some galleries might indeed be filled with collapsed roof material (i.e. the "goaf") while mining shafts might be backfilled before being capped (XXX, XXX). With time, ground subsidence also tends to reduce both the initially high volume of void created by mining, but also the transmissivity and storage capacity of mined strata (Younger and Robins, 2002).

Only a few aquifer properties data from pumping test are available for boreholes intercepting former mines. However, water extraction rate used for the dewatering of the workings during mining activities are assumed to

balance water inflow in mines and can therefore be used as a reference for estimated of the recharge rate. The following table summarizes typical extraction rates required in mines to maintain low water levels during mining (Table XXX).

Formation	Colliery	Flow rate
LCF	Prestongrange Colliery	40-75 l/s over 140 h/week at 165-225 m depth
	Kilsyth Colliery	150 l/s at 206 m depth
	Twechar Colliery	13 l/s for 12h/day ay 317m depth
	Monktonhall Colliery, Midlothian	35 l/s
MCMS	Bothwell Colliery	230 l/s at 396 m depth
LCMS	Polkemmet Colliery, West Lothian	75 l/s
	Frances Colliery, Fife	120 l/s
LCF / CM	Falkirk District	30-55 l/s
	Blindwells Colliery, East Lothian	315 l/s

Historical mine pumping rates (Gillespie et al., 2013). MCMS: Scottish Middle Coal Measures Formation; LCMS: Scottish Lower Coal Measures Formation; LCF: Limestone Coal formation; CM: Coal Measures

4.2 Thermal system

4.2.1 Geothermal heat flux

The geothermal gradient represents the rate of increase in the subsurface temperature with depth. It is determined by the geothermal heat flux and the thermal conductivity of the rocks (Busby et al., 2011). In theory, the average temperature gradient can be calculated from the mean annual ground surface temperature and an undisturbed, topography corrected temperature measured at a known depth (Rybäck and Sanner, 2000). In practice, measured temperatures will often differ from theoretical temperatures calculated from purely conductive geothermal gradients (Busby et al., 2011). Those anomalies can be explained by several reasons, such as the effects of groundwater circulation (i.e. convective flux), local internal heat production (i.e. decay of radioactive elements), inefficient heat transfer through low conductivity rocks (i.e. trapped heat), heat refraction processes (i.e. due to tilted layers) or the presence of anthropogenic heat sources, superimposing onto the conductive heat flow.

Heat flow and temperature measurements from onshore boreholes and mines in the UK have been collected in the BGS Catalogue of Geothermal Data for the UK (Burley et al., 1984; Rollin, 1987) or are available as Hard Copy temperature logs in BGS archives. Additional values were published by Downing and Gray (1986), Lee et al. (1987) and Barker et al. (2000), but no new data has been acquired since the 1980s (Gillespie et al., 2013). In 2013, Gillespie et al. used a compilation of 35 heat flow data reported from Burley et al. (1984) and Breton et al. (1988) to map the heat flow in Scotland. Most of the values were measured at depth < 400m in onshore boreholes, 13 of which are located in the MVS. Results indicated an average heat flow of 56 mW/m², with values ranging from 29 to 82 mW/m². Apparent ‘hot spots’ corresponding to granite intrusions were identified in the central part of the Midland Valley and in the East Grampians region, with heat flows of 60 mW/m² and 70 mW/m², respectively (Gillespie et al., 2013).

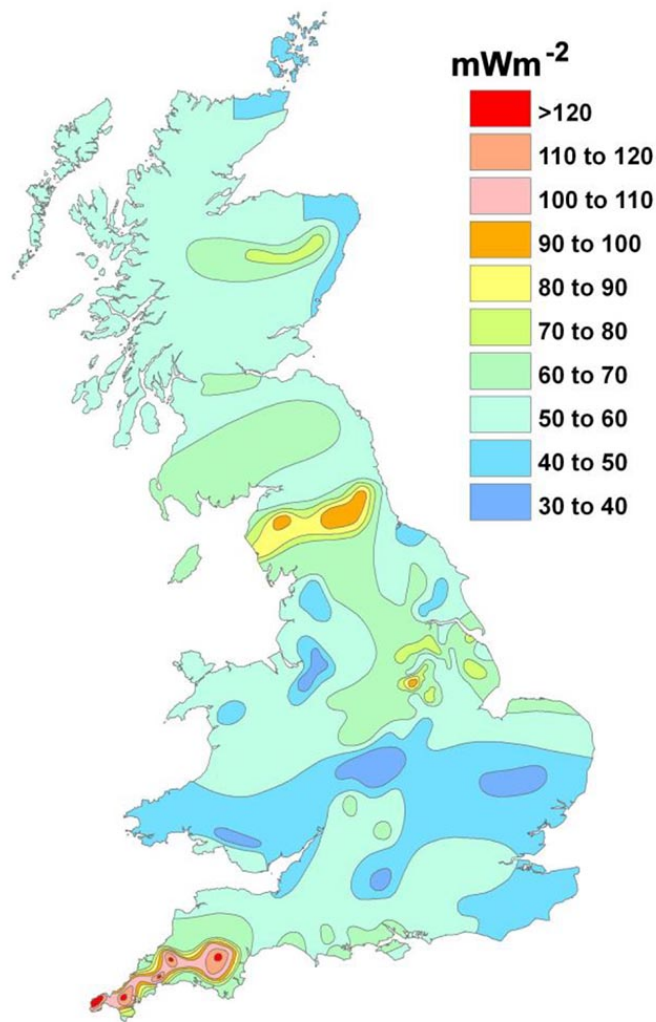


Figure 4.1: Heat flow map for the UK (Busby, 2011).

In borehole where no heat flow has been measured, geothermal gradients have been calculated based on the temperature measurements made at the bottom or near-bottom of 61 boreholes, down to 1300 m depth (Burley et al., 1984). The average temperature gradient for all boreholes ranges from 3.7 to 45 °C/km, with a mean of 22.5 °C/km and a median of 21.5 °C/km. Plotted together, the data indicate an average gradient of 30.5 °C/km which correlates throughout the entire depth range intersected by those boreholes. Using 133 BHT acquired from depth >1.5 km in 72 offshore wells in the North West Margin area (Gatliff et al., 1996), Gillespie et al. (2013) however noted the increase in the deep geothermal gradient from about 35.8 °C/km at 1 - 3.5 km to 46.7 °C/km at 3.5 - 5 km, relatively consistent across Scotland, and independent of the location (i.e. onshore or offshore) and the type of rock (i.e. sedimentary, crystalline basement) in which measurement were taken. Plotted together, onshore and offshore temperature measurements indicated an average geothermal gradient of 31.9 °C/km.

Despite temperature measured below 1.5 km depth are assumed to be only little affected by surface perturbations, Westaway and Younger (2013) suggested that near-surface temperatures in Scotland might have been disturbed by climate warming since the last prolonged glaciation, accounting for the lower geothermal gradient

near the surface. When extrapolated to the surface, the best-fit shallow geothermal gradient estimated from boreholes < 400 m depth indeed indicates a surface temperature of 4.0 °C, which is lower than the current yearly average surface temperature in Scotland of about 9°C by (Gillespie et al. 2013). Several studies already mentioned the importance of considering the effects of past climatic variations on the shallow geothermal gradient, especially at high latitudes (i.e. Birch, 1948; Carslaw and Jaeger, 1959; Gosnold et al., 2011; Majorowicz et al., 2012; Raymond et al., XXX; Baltrami et al., 2017). Paleo-climate signals have been described as a series of mean surface temperature change before present day, that propagates downward by conduction and tends to superimpose to the quasi-steady state thermal field associated to the Earth's internal heat (Baltrami et al., 2017). While the extent of the perturbations mainly depends on the magnitude and time scale of the past variations, the amplitude of the temperature change due to surface disturbances will tend to decrease exponentially with depth depending on the thermal conductivity of the ground, and with a time lag since the onset of the perturbation at the surface (Westaway and Younger, 2013; Busby et al., 2015, Beamish and Busby, 2016). In the UK, Wheildon and Rollin (1986) suggested that boreholes < 100 m depth are sensitive to surface temperature variations over the past 500 years, while Baltrami et al. (2017) showed that past climatic signals > 1000 years B.P are still contributing to the thermal state of the subsurface down to 500 m depth. Using individual temperature measurements from shallow depth (< 400m) would therefore tend to underestimate the true "steady-state" background geothermal gradient and thus the extent of tgeothermal resource at depth. New interests in re-evaluating the heat flow including paleo-climate corrections have recently grown in the UK. Westaway and Younger (2013) suggested that heat fluxes measured in shallow boreholes in Scotland would need to be increased by 18 mW/m² to account for the effects of palaeo-climate. The correction would be reduced to 8.8-13.5 mW/m² for 1 km deep boreholes and 0.2-9.1 mW/m² for 1.5 km deep boreholes.

4.2.2 Radiogenic heat production

The Earth's natural heat flow is generally attributed to a primordial heat (i.e. inherited from the formation of Earth) and to up to 45% to a contribution from the natural decay of radioactive isotopes of uranium (²³⁸U, ²³⁵U), Thorium (²³²Th) and potassium (⁴⁰K) (Pollack and Chapman, 1977). Radiogenic heat production from rocks A (uW/m³) can be calculated as the sum of the contribution from those four elements using the following relationship (Rybäck, 1988; Vila et al., 2010; O Neil, 2016):

$$A = 10^{-5} \rho \times (9.52[U] + 2.56[Th] + 3.48[K])$$

with ρ the average rock density (kg/m³) and [U], [Th] and [K] the concentrations of Uranium (ppm), Thorium (ppm) and Potassium (wt%), respectively. Due to geochemical differentiation, partial melting and magma crystallization processes, the upper crust is enriched in heat producing elements (HPEs) compared to lower levels (Beamish and Busby, 2016), and U, Th and K can be found in minerals in most crustal lithologies. Measurements of RHP in continental rocks has shown that acidic rocks have the highest heat production rate (i.e granites), followed by basic and ultrabasic rocks (Rybäck, 1986; Cermak et al., 1990; Brown and Musset, 1995).

Scotland is located on a geologically stable part of Earth's crust, where only granite intrusions would contain sufficient concentration of K,T and U element to generate radiogenic heat at significant levels and thus represent an additional source of in-situ heat (Gillespie et al., 2013). In Scotland, the largest and greatest concentration

of intrusions is located in the block of crystalline rocks bounded by the Highland Boundary Fault and the Great Glen Fault. Some granite intrusions can be found south of Inverness and near Aberdeen, but only have small heat producing (HP) values (0.6–2.2 uW/m³), in the Grampian Highlands and in the Northern Highlands (with HG of 2.2 to 7.3 uW/m³). Two large intrusions (Fleet and Criffel), with HP values of 3 and 2.2 uW/m³ were emplaced in Southern Scotland, at the end of the Caledonian Orogeny (410–390 Ma). Only one intrusion of significant size, the Distinkhorn intrusion, can be found in the MVS and consists of diorite and granodiorite with relatively low HP capacity (2.0 uW/m³).

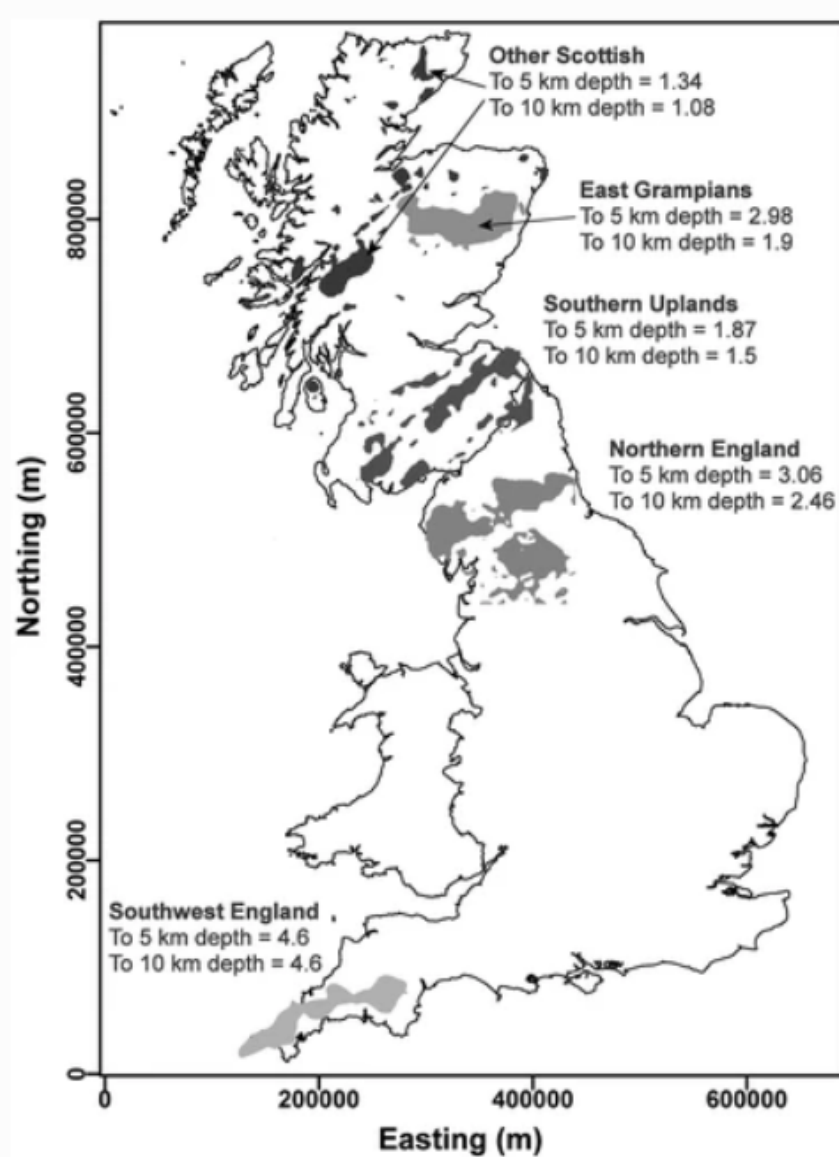


Figure 4.2: Locations in Great Britain with significant quantities of heat producing granites within the upper crust. Quantitative figures of average heat production in, uW/m³ (Busby, 2017)

Table XXX summarizes representative RHP values for the main lithological groups that compose the lithosphere.

lithology	density	mean	std	25th	Median	75th
granite	2650	2.827	2.176	1.741	2.429	3.233
granodiorite*	2718	1.838	2.401	0.938	1.501	2.214
basalt	2750	0.358	0.394	0.077	0.214	0.533
alkalic basalt*	2957	0.69	0.355	0.342	0.543	0.801
Andesite*	2811	1.059	1.203	0.452	0.817	1.246
rhyolite*	2674	3.084	5.975	1.72	2.546	3.732
mudrock	2400	1.392	0.702	0.968	1.442	1.657
wacke	2400	0.984	0.535	0.548	0.993	1.212
sandstone	2400	0.896	0.468	0.536	0.819	1.206
carbonate	2400	0.477	0.356	0.216	0.416	0.618
limestone*	2789	2.066	24.568	0.387	0.777	1.632

Table 4.1: RHP values for different lithological groups in uW/m3 (Vila et al., 2010. *Hasterok et al., 2018). Mudrocks include fine-grained consolidated or unconsolidated sedimentary rocks such as mud/mudstone, silt/siltstone, clay/shale, argillite, lutite.

According to Vila et al. (2010), density plays a important role for radioactive heat production (RHP) in sedimentary rocks due to compaction effects. Their RHP appears to be relatively low (<1.5 uW/m3), except for organic, K-rich sediments and K-rich evaporites that have values exceeding 3 uW/m3. While U and Th are negligible in major minerals, K indeed contributes the most to radioactive heat generation and occurs in major silicates (i.e. feldspar, micas) (Webb et al., 1987).

RHP is moreover highly correlated to grain size in detritic rocks, with the higher the grain size and the lower the RHP. In the sandstone group, arkoses have the highest values (about 1.25 uW/m3). Hasterok et al., (2018), suggested that aluminous shales are generally high heat producing (2.9 uW/m3) while iron shales are low heat producing (1.7 uW/m3). The weathering of (K-rich) feldspars and mica, that can be found in higher concentration in felsic rocks (i.e SiO₂ rich) tends to form K-rich clays such as illite that are therefore good heat producers (Hasterok et al., 2018). Evaporites (except KCl-rich rocks) and non-detritic siliceous and Fe-MN-rich rocks have values <0.5 uW/m3 (Hasterok et al., 2018). Carbonate-rich rocks and pure quartzite generally have lower HPE than detritic sedimentary rocks, with values ranging between 0.2 and 1 uW/m3. Rybach (1986) proposed values of 0.57 and 0.34 uW/m3 for limestone and dolostone, respectively. In crystalline rocks, andesite and tholeiitic basalts have mean RHP of 0.82 and 0.05 uW/m3, respectively (Hasterok et al., 2018). RHP from granite is very variable and generally depends on their petrogenesis. Finally, Hasterok et al., (2018) nfinally showed that metamorphic rocks tend to have similar heat producing capacities as their protoliths.

The distribution of radiogenic HPEs therefore provides an important control on the temperature distribution within the earth lithosphere (Sandiford and McLaren, 2006). Where the heat flow is not disturbed by heat convection, it can therefore be used together with a determination in the radiogenic heat production (RHP) to constrain the thermal field within the crust (Jaupart and Mareshal, 2003).

4.2.3 Mine-water temperature

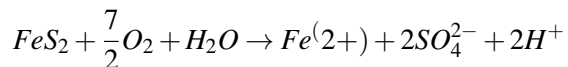
While rock temperature in deep mines is expected to be mostly controlled by the geothermal gradient (Anderson and De Souza, XXX), Burnside et al. (2019) suggested that the heat flow in flooded workings is actually controlled by heat advection. Analysis of temperature in mines in the UK showed that there are significant variations in the temperature of mine waters measured down to about 1500 m depth in shafts (Gillespie et al., 2013). In the Midland Valley of Scotland, temperatures measured from nine boreholes range from 12 to 21 °C, with a mean and median of 17 °C (Burley et al., 1984). Mine-water temperature is typically higher than the typical natural groundwater temperature from Carboniferous aquifers in the MVS. However, no clear correlation has here been found between the measured temperature from mines and the depth of the measurements. This suggested that other factors might contribute to the definition of the mine-water temperature. However, predict the temperature of water pumped from former mine shaft can be difficult, as water of different temperature might enter the borehole at different depths (Gillespie et al., 2013).

Additional data collected as part of the Scotland Baseline Project in 2008, indicate temperatures of 19.2 °C for mine-water pumped from the Polkemmet mine shaft, and temperature of 9.8 °C for gravity-driven discharged mine-water. Farr et al. (2016) suggested that measured temperatures are highly dependent on the location of the logger relative to the surface features and influences by 1) cold recharge entering the drainage system (i.e. shallow logger in gravity driven adit, highly correlated with air temperature), 2) localized recharge events such as period of intense rainfall (i.e. adits with transfer pumps with more stable yearly temperature) or 3) the absence of connection with surface recharge (i.e. deep warm water with constant temperature throughout the year).

The subsections below aim at getting an overview of the different processes that might be responsible for anomalous temperatures in mines.

Exothermic reactions

Mine waters generally contain a high concentration of iron that result from the oxidation of sulphide minerals (i.e. pyrite, marcasite, sphalerite, galena) contained within the coal deposits. As most of the geochemical reactions occurring in mines, oxidation reactions are exothermic and therefore contribute to the overall temperature in mines. The oxidation of crystalline pyrite to ferrous iron can be expressed as (Sherwood, 1987;farr et al., 2016):



Banks et al. estimated that 1400-1500 kJ/mol of heat energy can be released through pyrite oxidation, which generally occurs when water is lowered by pumping and enter in contact with oxygen. Using discharge value at Ynysarwed with a total iron concentration of 0.001377 mol/L (Langmuir, 1997; Atkins and Paula, 2006), Farr et al. (2016) moreover estimated that pyrite oxidation is able to generate a temperature increase of 0.5 K/L of water.

Heat convection

Anomalous temperatures i.e. where the water temperature is greater than the rock temperature, have been observed in abandoned mines. Those were partly explained by the existence of free 'natural' convection of water flowing from different mined levels into open vertical shafts (Krig, 1939) and by recharge from greater depth

through faults. Large mining voids (i.e. shafts, roadways) indeed create highly transmissive flow pathway across large areas and depths by connecting both laterally and vertically formerly separated groundwater flow systems. Those tend to promote convective heat transport within aquifers of poor natural transmissivity, adding more complexity to the groundwater flow. Faults can also have substantial impact on subsurface temperatures due to their influence on rock permeability. They can either act as a barrier or as a highly conductive flow pathways, allowing water recharge from surface and/or depth or from the coast, such as i.e. Highland Boundary Fault (Browne et al., 1987).

In large mining voids, water bodies tend to form density-related stratification resulting from the mixing of cold meteoric water and warmer saline water originating from depth (Nuttall and Younger, 2004). Hamm et al. (2010) showed using numerical models that efficient intra-well mixing induced by water density differences (i.e. free convection) tends to fix the temperature along the shaft close to the average of the temperatures at the top and bottom, when no pumping is performed. The presence of several galleries intersecting the shaft at different levels induces local water mixing and allows the establishment of higher temperatures at the bottom of the shaft. Pumping water from mine generally encourage turbulent water mixing, which can destroy density-related stratification in wells and reduce the water quality (Hamm et al., 2010; Burnside et al., 2019).

Turbulent flow is particularly prominent in large open voids such as roadways, which favor high velocities. This contrasts with low velocities and laminar flow observed in the less permeable porous rock mass and in the backfilled part of goaf materials, drivings and caverns, that represent the highest volume of void in mines (Renz et al., 2009).

Blanketing effects

In mines in the Carboniferous succession of the MVS, the presence of many low-conductivity horizontal rock layers such as mudstone or coal are finally likely to form “cap” rocks, creating situations where the inflow of geothermal heat from below might be trapped, forming positive heat anomalies. Such blanketing effects has been described by Busby et al. (2011) for the NE England, where low conductivity Carboniferous rocks are present above the Weardale granite, which has a high heat production (Downing and Gray, 1986a,b).

5 Chapter 1 : Heat extraction Model

5.1 Background

With the growing interest in geothermal energy for domestic heating and cooling, borehole heat exchanger (BHEs) coupled ground source heat pump (GSHP) systems have been increasingly used worldwide (Chen et al., 2019). Analytical and numerical approaches have been developed to assess the system performances and the sustainability of heat extraction through the study of its thermal response over time (i.e. Rybach and Eugster. Signorelli et al., ; Lazzaru et al., ; Zanchini et al., ; Chen et al., 2019; Lyu et al., 2017, Zhang et al., 2016, Stylianou et al., 2017). Studies showed that the energy performance of GSHPs strongly depends on the heat transfer process between the BHEs and the ground. In a purely diffusive medium, it mainly depends in the long term on the thermal conductivity of the ground (i.e. Florides et al, Choi and Ooka, Stylianou et al., 2017; Chen et al., 2019). The presence of groundwater was suggested to improve the long-term performance of BHE both by increasing the heat exchange rate during production (Zanchini et al., Stylianou et al., 2017; Wang et al.) and by favoring heat recovery (Hein et al. 2016, Erol et al., 2015). In medium with groundwater circulation, analysis showed that soil heat capacity and thermal conductivity only have minor impact on the sustainability of a GSHP system and that dispersion tends to increase the area of impact of heat extraction.

5.1.1 Analytical solutions

Many analytical solutions have been developed to understand heat transfer processes in porous media for scenarios with different boundary conditions. Analytical solutions are necessary to benchmarks linear or quasi-linear problems, and are required to verify and validate numerical methods that will be used to solve for problems with greater geometrical complexity.

The problem of heat diffusion in a porous media due to heat extraction/injection from BHE has first been described using the Infinite Line Source (ILS) model (Carlslaw and Jaeger, 1959). The ILS model considers an homogeneous and isotropic medium with constant thermal properties and a uniform initial temperature (T_0) that remains the far field temperature during the simulation. The temperature field around the line source with constant injection rate q (W/m) can be written as a function depending on the time t and the radial distance r (m) from the line source as followed:

$$\Delta T = \frac{q_0}{4\pi\lambda} E_1 \frac{r^2}{4\alpha t}$$

with $r^2 = x^2 + y^2$, ΔT the temperature difference between the measured temperature and the background temperature at time t , λ the ground thermal conductivity and E_1 the exponential integral function. This function can be approximated by $\ln(\frac{4\alpha t}{r^2}) - \theta$ for large values of $\frac{4\alpha t}{r^2}$, with θ the Euler's constant = 0.5772 and α the thermal diffusivity of the subsurface. In BHE models, a thermal resistance factor R_b is generally added to the ILS source solution in order to faithfully characterise the heat transfers between the borehole walls the circulating fluid, and better assess the evolution of the fluid temperature (i.e. Monzo et al., 2011; Zeng et al., 2002).

However, heat dissipation in an aquifer can be described as a coupled process of heat conduction through the solid matrix and the water in its pores and heat advection within advancing groundwater (Su et al., 2004). Recent studies attempted to include the effects of groundwater flow into BHEs modelling to evaluate the impact of heat convection on the performances of the system, based on the Moving Infinite Line Source model (Sutton et al. XXX, Diao et al. XXX; Hecht-Mendez et al, Fujii et al., Brunetti et al., 2017; Biglarian et al., 2017; Gordon et al., 2017). The analytical solution for the application of an instantaneous line source of heat along the z-axis in an isotropic medium with groundwater advection in the x direction is given by Marshall (1958):

$$\Delta T = \frac{Q}{4\pi\alpha t} \exp\left(-\frac{(x - V_h t)^2 + y^2}{4\alpha t}\right)$$

with V_h the thermal velocity of the water (m/s). One of the main limitation of this model is the that water temperature is not impacted by temperature at the boundary conduction (Rivera et al., 2015). Advection transport instantaneously the heat fluxes induced by the BHE over the porous fluid and solid matrix and thus, advancing thermal plume delineates the domain where reservoir exhaustion takes place (Rivera et al., 2015). In real systems, temperature drawdown in the matrix is expected to stimulate net heat influx from advection $q_w = \rho_w c_w \frac{dT}{dx}$.

To account for the relative contribution from reservoir exhaustion or groundwater advection in the overall power balance, Rivera et al. (2015) therefore developed a new analytical approach that quantify both vertical and horizontal transient heat flux regime stimulated by BHE, including uniform horizontal groundwater flow and heat exchange with the atmosphere. Study the relative contribution of conductive and convective heat transfers processes in porous systems requires the use of dimensionless parameters such as the Peclet number $Pe = \frac{v_T h}{\alpha}$ and the Fourier number $Fo = \frac{\alpha t}{h^2}$ (Molina-Giraldo et al., 2011; Rivera et al., 2015; Biglarian et al., 2017; Tye-Gingras and Gosselin, 2014). Those allow eliminating the dependency of the results on the i.e.borehole length h , medium thermal diffusivity α , operation length t or effective thermal velocity of convective heat transport $v_T = u_x \frac{(\rho c)_f}{\rho c} = \frac{u_x}{R_T}$ (Molina Giraldo et al., 2011), with u_x the Darcy velocity, $\rho c = \phi \rho_w c_w + (1 - \phi) \rho_s c_s$ the volumetric heat capacity of the saturated media and $(\rho c)_f$ the volumetric heat capacity of the water. R_T is a retardation factor that expresses the delay of the heat front with regards to the true pore waterfront. It is explained by the energy required to heat up or cool down the matrix (Barends et al. 2010).

5.1.2 Sustainability issue

Most of the studies aiming to assess the performances of BHE focused on the temperature evolution within the system throughout the production time. However, sustainable heat production from BHE can be achieved if the heat load extracted is balanced by the rate of heat recovery in the subsurface. In the early stage of production, heat extraction from the ground is expected to create a zone of depressed temperature around the borehole, leading to radial conduction of the heat stored in surrounding rocks toward the BHE (Banks, 2008). According to Banks (2008), the cooling of the area might induce an increasing heat flow of solar energy from the surface that will eventually balance the heat abstracted. In Chen et al. (2019), the authors showed that using a specific heat extraction rate of 100 W/m, quasi steady-state equilibrium outflow temperature could be reached after 20 years of production from a BHE in China, considering a geothermal gradient of 0.03 °C/m . Other studies showed that another way to achieve sustainable heat extraction is to perform cyclic production or through artificial heat recharge (XXX). Being able to discriminate between the energy sources through a detailed understanding of the

heat fluxes induced during heat extraction (both axial and radial) is therefore essential to get a better insight on the sustainability of heat extraction (i.e. Rivera et al., 2015).

Extensions of the standard Moving Infinite Line Source model have therefore been made to better study the fluxes induced by heat extraction/injection whilst accounting for axial (Molina-Giraldo et al., 2011) and seasonal/cyclical effects (i.e. Rivera et al., 2015; Erol et al., 2015; Biglarian et al., 2017; Salah Saadi et al., 2017). In a system without groundwater flow, Zhao et al. (2020) showed that radial heat conduction tends to dominate during operation, while vertical heat flux dominates during recovery. Sufficient thermal recovery period after each heat extraction cycle allows the elimination of coldness accumulation near the borehole and a quasi-total heat recovery of the ground (Zhao et al., 2020). In a system with groundwater, Rivera et al. (XXX) showed that horizontal advective transport tends to enhance vertical conductive heat fluxes, but the relative power source from groundwater and storage varies over time. In the early stage of production, energy is mainly extracted from storage. Local depletion then enhances the vertical fluxes. While the relative contribution from the bottom reaching a limit of 24% of the total power demand, the contribution from the surface becoming dominant for $Fo > 0.13$. Study of heat recovery after a production period showed that in terms of power, quasi-steady state might be reached within a much longer time period compared to results from recovery based on temperature analysis (i.e. Rybach and Eugster, XXX; Signorelli et al, XXX). Further analysis showed that axial heat fluxes tend to accelerate recovery and that the ground surface provides up to 2/3 of the power over the full life-cycle of the system, meaning that for shallow BHE (less than 100 m depth), heat from the earth's interior is not the main source of heat.

5.1.3 Surface boundary condition

The majority of studies of heat transfers around BHE implied isothermal boundary conditions, both in the far field and at the upper/bottom boundary (i.e. Zhao et al., 2020). The importance of considering heat flux boundary condition has however been underlined by Salah Saadi et al. (2017). During production, the temperature distribution around BHE is not equal to the undisturbed ground temperature from the surface to the bottom, and axial effects become important at both ends of a BHE (Erol et al., 2015). Therefore, considering a heat flux boundary conditions instead of an imposed undisturbed temperature at the surface appear to be more valid to avoid overestimating the available recharge. Furthermore, using heat flux boundary conditions makes possible the simulation of temperature change at the surface, especially when extraction of heat is made at shallow depth and for long operation periods. In Saadi et al. (2017), surface heat flux boundary condition also permitted to treat seasonal effects as a physical balance between convective heat transfer between the ambient air temperature and the soil surface, and the solar radiations (source term).

Heat conduction through the ground surface is the results of the combination of convective heat transfer between the atmosphere and the ground surface, which depends on the solar radiations absorbed by the ground surface (SR), the longwave thermal radiations emitted from the ground (LR), related to the emissivity of soil ($\varepsilon\Delta R$), the latent heat related to evapo-transpiration process (ET) and the convective heat flux due to wind velocity (CE):

$$q = SR - LR - ET - CE$$

Based on this relationship, Singh and Sharma (2017) expressed the variations in the effective ground surface temperature as a time-variant first type boundary condition calculated from a general convective heat transfer coefficient, depending on the ambient air temperature and solar radiation. This allowed to realistically assess the contributions of the surface boundary on the energy recharge to the ground, considering seasonal variations.

The effect of daily/annual air temperature variation on the ground sub-surface temperature has been well studies. Analysis showed that annual variations in surface temperature/solar radiations generally only reach about 20m depth. At that depth, the ground temperature equals the mean annual air temperature and below, it follows the local geothermal gradient. Daily soil temperature variations are relatively difficult to model due to short term weather variations, seasonal variations, moisture content of soil, and heterogeneous thermal conductivities (Ozgener et al., 2013). In this study, daily variations are however not of interests as they impact only reach a few cm depth (about 20 cm).

5.2 Research Gaps

Despite the performances and sustainability aspects of BHE have been well studied using both analytical and 1D to 3D numerical studies, a few of them assessed the area of the ground impacted by heat extraction to provide the necessary energy o consumers. Some studies gave an insight of the direction of the conductive flux induced during production and recovery, allowing to express the thermal impacts in terms of energy balance rather than absolute temperature. However, there is still a lack of investigation regarding the extent recharge provided by solar input, heat storage from surrounded rocks, deep geothermal flux or groundwater recharge, for deeper systems, including mine reservoirs. From Rivera et al. (2015) in which the model considered uniform temperature distribution along the BHE, we suggest that further analysis would be require to evaluate the relative contribution from the geothermal gradient and geothermal heat flux for deeper borehole. The current state of knowledge for advective-diffusive heat transfers induced by BHE-GSHP systems will moreover here be used to study the heat exchange processes in porous layers to get an insight of what might happen in mines coal seams.

5.3 Aims and methods

The aim of this chapter is therefore to get a better understanding of the heat fluxes and heat transfer mechanisms in the subsurface through energy balances. We will need to describe 1) the relative contribution of surface/bottom recharge during heat extraction and recharge, using 1D model, 2) lateral recharge using 3D diffusion model, 3) the relative contribution from heat convection and conduction through the porous medium, using 2D advection-diffusion models (i.e. with groundwater flow). Analytical solutions will be develop to assess what is the proportion of heat absorbed/released by the porous media from/to the circulating fluid.

We also want to evaluate the extent of heat depletion caused by a constant heat load extraction from simple mine systems and evaluate the key parameters to reach a steady state production temperature. To achieve this, energy balance calculations will be made based on the estimations of how much heat is produced and diffused from surrounding rocks. We will attempt to estimate the footprint area of heat extraction for a single house in the UK, and compare it to the available recharge to assess the sustainability of BHE-GSHP systems from the heat resource perspective.

5.4 Research Question

What are the key heat recharge mechanisms and heat sources controlling the water temperature in flooded coal mines?

- What are the main heat sources in coal mines ?
- Can thermal steady state (energy balance between heat extracted and heat recharge) be reached?
 - What is the nature of the heat fluxes and the relative contribution from heat diffusion and advection during production (i.e. heat/water extraction) and heat recovery/flooding ?
 - What is the rate of heat exchange between the recharge mine-water and the surrounding host rock in mined areas (i.e. goaf) and tunnels (i.e. depending on the origin/temperature of recharge water, on its flow rate, on the flow path length, on the properties of the host rock)
- What is the footprint area of heat extraction?

5.5 Hypothesis

- Heat sources in deep mine systems include radiogenic heat production, pyrite oxidation, the geothermal heat flux and advective warm water from depth.
- Thermal steady state can be reached for low extraction rate
 - H0: During production, heat is mainly sourced from advective groundwater in tunnel and the heat depletion from surrounding rock (i.e. vertical conductive heat flux) is limited.
 - H1: During production, horizontal conductive heat flux are dominant in goaf materials.
 - H2: During recharge, vertical heat flux are dominant, with a 50/50 contribution from solar and geothermal heat flux
 - H3: During recharge, heat recovery is promoted by advection from deep warm water.
- The footprint area is mainly dependent on the hydraulic gradient

5.6 Preliminary results

5.6.1 Heat generation in mine

Fig. 5.1 shows a conceptual model for a mine of simple geometry composed of 3 seams of coal. The uppermost one is unmined, the middle one is mined according to the longwall method (i.e. collapsed goaf material) and the lower most is mined according to the pillar-and-stall method.

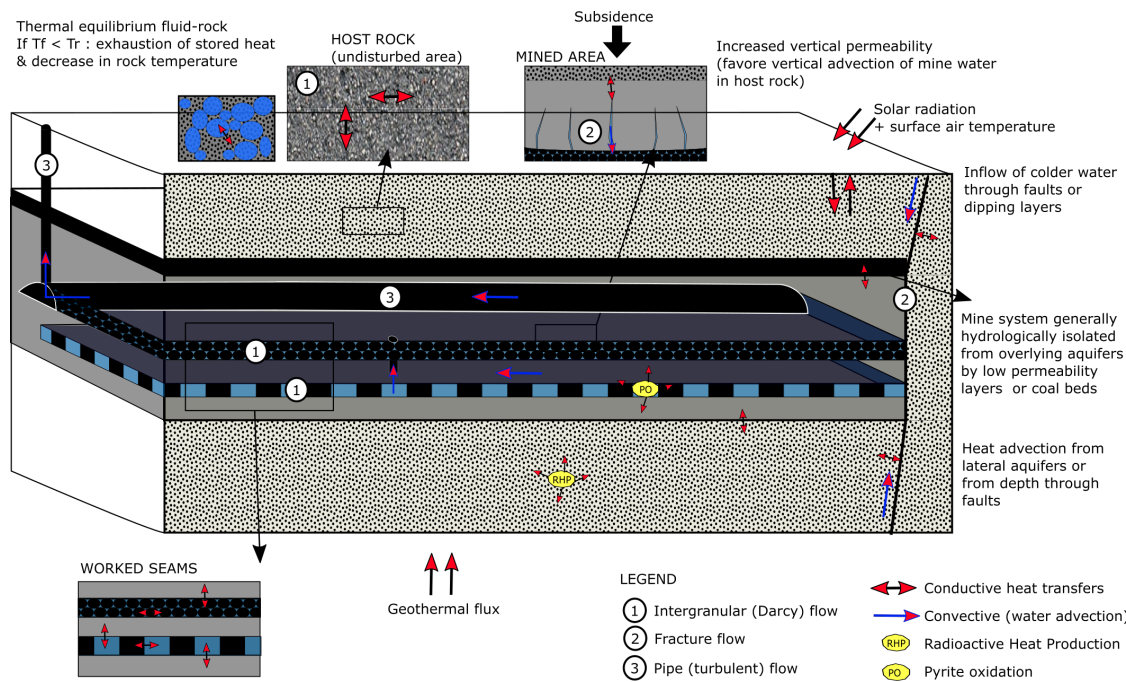


Figure 5.1: Conceptual model of mines showing the potential hydrological, thermal and geometrical aspects in mines. See legend for more details.

Radioactive heat production

We evaluate the impact of radioactive heat production from different lithologies on the undisturbed geothermal gradient using a fictive vertical column of rocks (Fig 5.2). Initial temperature distribution within the model was first determined from steady state and transient simulations using purely diffusive heat transfers (Fig. 5.3). The model consists of a 1 dimensional finite-element mesh composed of 4000 line elements.

The steady state temperature profile is determined from surface and bottom temperatures of 9 ° and 40° at 1 km depth, respectively (see dotted black line in Fig. 5.3). In the transient simulation, and initial gradient of 40 °C/km is used, allowing visualizing the effects of long term surface warming (i.e. 1000 years) on the shallow temperature gradient (orange line in Fig. 5.3). The significant difference in the profiles obtained from steady state and transient simulation show that for $\Delta T = 9^\circ\text{C}$ on surface, 1000 years is not sufficient for the gradient to reach its undisturbed steady state, with perturbations visible down to 180 m depth. Based on the harmonic mean of the thermal conductivity of the different lithologies composing the rock column (2.145 W/°C/m), we then calculate the geothermal heat flux necessary to conserve the average steady-state gradient of 0.031 °C/km. Calculations indicate an average flux of 66.5W/m² across the rock column, which is confirmed after running a 1000 years steady-state simulation based on heat-flux boundary conditions (i.e. no change in gradient).

RHP source terms are then added to the steady state temperature profile to evaluate their contribution on the geothermal gradient, using both flux and constant temperature at the upper and bottom boundaries. Results for a 100 years long simulation are shown in Fig. 5.3 (green line and dashed black lines) and show a consistent increase in temperature along the trend of the geothermal gradient that might indicate that radiogenic heat production has been overestimated.

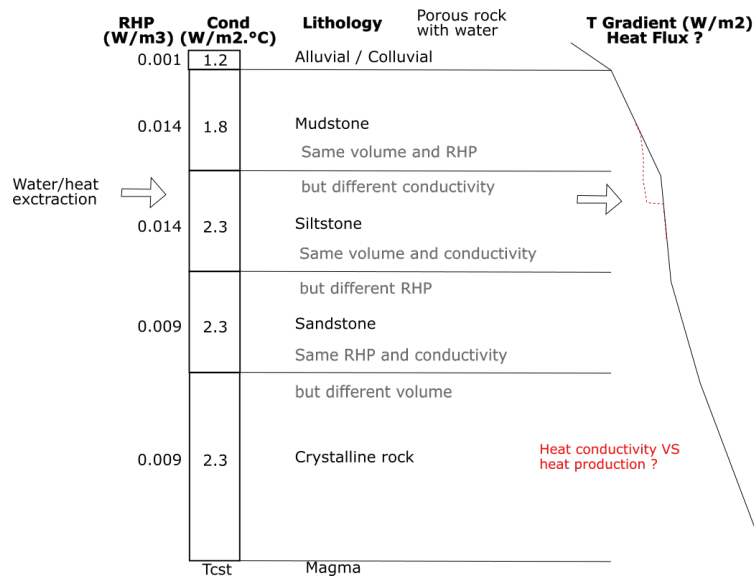


Figure 5.2: Radioactive heat production rate (RHP), thickness and conductivity values for a fictive column composed of different lithologies used to estimate the contribution from radiogenic HPEs on the geothermal gradient

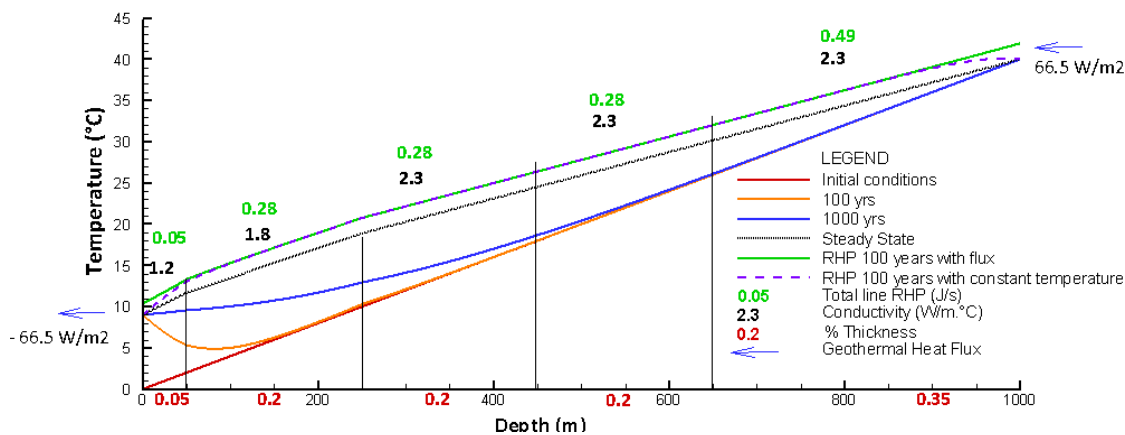


Figure 5.3: Geothermal gradients obtained for steady-state, unsteady-state and RHP with constant heat flux and/or constant temperature boundary conditions

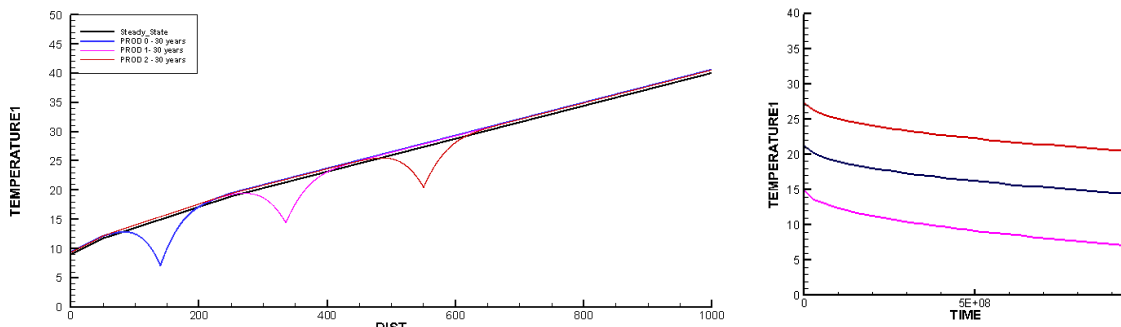


Figure 5.4: Results from RHP simulations

Finally, we add source terms aiming to simulate heat extraction at a rate of 15 J/s (W) at 140 m (in the mudstone section), 335 m (in the siltstone section) and 550 m depth (in the sandstone section), in three different 30-year long simulations. Temperature profiles after 30 years of extraction are plotted together in Fig. 5.4.

Further work is required to estimate the relative contribution of RHP production versus rock thermal conductivity and of the geothermal heat flux on the undisturbed geothermal gradient in the UK. Data from geological logs of the Carrington-1 well (Monaghan and Brown, 2014) have been used as a reference to assess the thickness of each formation in the Carboniferous succession of the Midlothian Coalfield and the proportion of the different lithologies in each formation. Based on data from the literature, we made a rough estimation of the radiogenic heat production and average thermal conductivity for each formation (see appendix XXX).

5.6.2 Heat extraction model

Mathematical approach

The average energy consumption for a single house in the UK is 12 400 kWh per year, with a maximum of 18 000 kWh in winter and 8 000 kWh in summer. To satisfy this yearly demand, a heat pump would need to deliver an average heat load of 1415 W by extracting heat from the underground. This represents a total energy of $4.47 \times 10^{10} J$ over a year. In reality, the total heat load H delivered by a heat pump corresponds to the sum of the heat extracted from the ground G and the electric heat E required for air compression (Banks, 2008).

$$H = G + E$$

The coefficient of performances (COP) of GSHP is generally used to characterize the efficiency of the system. It can be used to calculate the total heat delivered by the heat pump H as a function of the electrical power E provided.

$$COP = \frac{H}{E}$$

Using an average COP of 3.4, the average heat that would need to be extracted from the ground to satisfy a heat demand of 1415 W is therefore:

$$G = H(1 - \frac{1}{COP}) = 1000W$$

This corresponds to a total energy of $3.15 \times 10^{10} J$ over a year. Considering a 40 m long borehole heat exchanger, the specific heat absorption from the rock (as defined in Banks, 2008) would here be 25 W/m. GSHP are however generally designed to cover 60 % of the peak heat demand. Assuming that a 3000 W heat pump is used to cover for the peak heat demand of a single 90 m² house, which generally averages 5000 W (i.e. energy flux of 56 W.m⁻²), the actual specific thermal output for a 40 m long borehole would be 75 W/m. Using a COP = 3.4, the specific peak heat absorption from the rock, calculated using equation XXX, would instead equals 53 W/m (Banks, 2008).

The total heat content of a rock mass can be estimated using the Eq. XXX.

$$Q = \rho_r V c \Delta T$$

with ρ_r the rock density, V the volume of the rock mass, c the specific heat capacity and ΔT the temperature change across the heat exchanger. Assuming $\rho_r = 2650 \text{ Kg.m}^{-3}$, $c = 950 \text{ J.(kg.K)}^{-1}$ and $\Delta T = 5^\circ\text{C}$, the volume of rock required to provide a total heat load $Q = 4.47 \times 10^{10} \text{ J}$ (i.e. energy for one year) is about 3700 m^3 . Assuming that the heat is extracted radially from a borehole with a length $h = 40 \text{ m}$ situated in the center of a cylindrical volume, the radius of the cylinder would be about 5 m , corresponding to a surface area of 93 m^2 . For $Q = 3.15 \times 10^{10} \text{ J}$, the required volume is about 2500 m^3 , which corresponds to an area of about 63 m^2 (i.e. cylinder radius of 4.5 m). 

Alternatively, we can calculate the surface area that would be required to provide heat recharge to the BHE system. We first assume that the heat is extracted from a vertical one-dimensional BHE and that recharge occurs from above (i.e. heat flux generated from solar energy) and below (i.e. geothermal heat flux). Where ground temperature has not been disturbed by heat production, heat conduction from or toward the surface depends on the effective surface temperature relative to the sub-surface temperature. In the shallow sub-surface, ground temperature is generally assumed to be equal to the mean annual air temperature. During winter, the ground temperature is higher than the average air temperature, and thus, the heat flux is directed from the ground toward the surface. In summer, the ground is colder than the air temperature and thus the heat flux is reversed, recharging the ground with heat.

The effective surface temperature depends on a complex combination of several factors, such as the amount of solar shortwave radiations, longwave radiations emitted from the ground or wind speed (i.e. convective heat flux from the air to the ground surface), that will impact daily/yearly heat recharge from the surface. In Edinburgh, the average annual rate of insulation is in the order of 94 W/m^2 , with a minimum of 13 W/m^2 in December and 181 W/m^2 in July (Whitlock et al., 200). Due to the low diffusivity of soil (i.e. low thermal conductivity but high specific heat capacity), the refraction of solar radiation and the emission of long-wave radiation by the ground, the net incoming shortwave radiation into the ground only equals 10s of W/m^2 and solar radiations only heat up the upper meters of the ground. Despite heat transfers to the ground can be affected by precipitation, water infiltration and evapo-transpiration processes, Fig 5.5 shows that shallow subsurface temperature tends to roughly follow the trend of the air temperature on a daily basis. Annual variations of the air temperature generally propagate down to about 20 m depth only. Below that depth, the ground temperature is no longer influenced by the yearly changes in surface temperature and equals the annual average surface temperature, before following the local geothermal gradient at greater depth.

If we assume a geothermal heat flux of 0.06 W.m^2 and a solar heat flux allowing a recharge of 6 W.m^2 (XXX) half of the year, the area required to provide the necessary recharge to the BHE is about 330 m^2 (see Eq. XXX).

$$\text{Area} = \frac{1000 \text{ W}}{0.06 + 6 \times \frac{1}{2} \text{ W.m}^{-2}} = 330 \text{ m}^2$$

We then assume that heat extraction from BHE induces lateral heat flow from surrounding rock (i.e. Heat mining). Based on the estimated 63 m^2 footprint area required for heat consumption for one year, the geothermal heat flux and solar heat flux would contribute up to $0.06 \times 63 = 4 \text{ W}$ and $6 \times \frac{1}{2} \times 63 = 190 \text{ W}$ to the total heat recharge, respectively. That means that about 800 W will be mined from surrounding rocks. Assuming a borehole length of 40 m and a perimeter of 28 m ($2\pi r$ with $r=4.5\text{m}$), the lateral heat flux would be in the order of 0.7 W.m^{-2} 5.6.

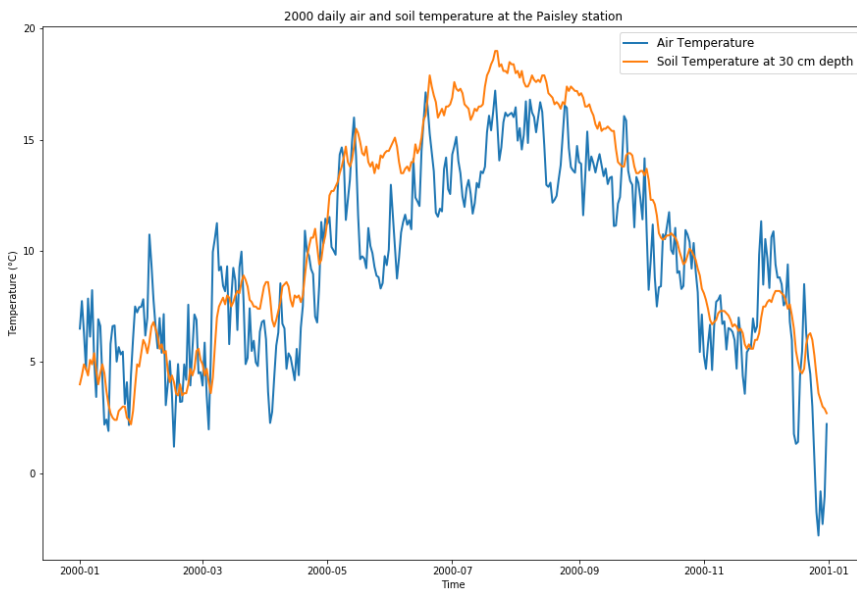


Figure 5.5: Daily air temperature and soil temperature measured at 30 cm depth at the Paisley station, Glasgow area, in 2000

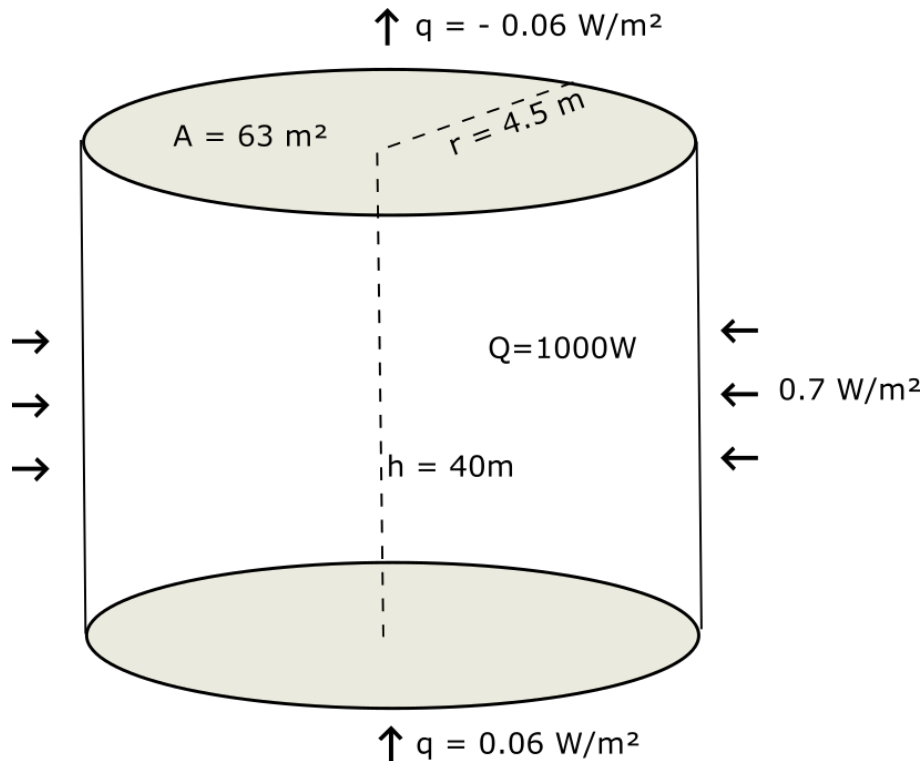


Figure 5.6: Conceptual model for the BHE with induced heat flux

Numerical results for heat extraction with diffusion only

We use the OpenGeosys finite element modelling software to simulate the change in temperature within a volume under heat extraction and evaluate the impact of the recharge rate/parameters and available surface area on the temperature decline (i.e. Kolditz et al., 2012; Chen and Shao et al). We consider the borehole heat exchanger as a one-dimensional finite-element model consisting of a vertical line source composed of 4000 elements of 0.1 m in length. The BHE is treated as a homogeneous porous medium with a thermal expansion of $1 \times 10^{-5} \text{ }^{\circ}\text{C}^{-1}$, specific heat capacity of 950 J/Kg.K and thermal conductivity of 3.0 W/m.K. The initial temperature distribution through the vertical line is defined by a geothermal gradient of 0.02 $\text{ }^{\circ}\text{C}/\text{m}$, corresponding to a surface temperature $T_0 = 7 \text{ }^{\circ}\text{C}$ and a bottom temperature $T_z = 15 \text{ }^{\circ}\text{C}$ at $z = 400 \text{ m}$ depth. Natural steady state conditions are calculated using constant top and bottom heat flux boundaries of -0.06 and 0.06 W/m², respectively. Those are assumed to represent the geothermal heat flux entering the model from below, flowing through the BHE and coming out at the surface. They were defined accordingly to the geothermal gradient and the thermal conductivity, using Eq. XXX.

$$q = K \frac{dh}{dx}$$

In the long term, it is assumed that the flux coming in is equal to the flux coming out of the system through purely conductive heat transfers. A first simulation was run to ensure that the geothermal gradient within the model remains stable over a total duration of 30 years, using the constant heat flux boundaries.

We then use a series of transient simulations to determine the amplitude of the variations in the surface heat flux required to reproduce the change in surface temperature observed in Scotland. The average yearly temperature change in east Scotland is calculated from the data available on the UK Meteorological Office website. The mean annual temperature over the 1910-2019 period is 7 $\text{ }^{\circ}\text{C}$, with a mean winter temperature of 2 $\text{ }^{\circ}\text{C}$ and a mean summer temperatures of 12 $\text{ }^{\circ}\text{C}$. Simulations are run using a series of different heat flux variations at the upper boundary. The yearly fluctuations in the surface heat flux are approximated using equation XXX,

$$Q = -A \sin(2\pi * \frac{\Delta t}{t}) - q$$

with A the amplitude of the variations, Δt the time increment (days), t the total duration (365 days x 30 years) and q = 0.06 W/m² the geothermal flux from below.

Using amplitudes of A ranging from 0.01 to 10 W/m², we find that the expected yearly surface temperature changes can be simulated for A = 6 W/m² (Fig. 5.7.a). The change in the subsurface temperature under the effect of the fluctuating heat flux is simulated for a period of 20 years. Following a slight increase in the yearly average surface temperature, a fluctuating steady-state temperature is reached at the surface after a period of about 9 years (Fig. 5.7.b). From there, it is assumed that the temperature profile is stable and no longer affected by the initial conditions. Thus, the output temperature profile from this simulation is used as initial conditions for the subsequent simulations.

Temperature profiles displayed in Fig 5.8 shows that the impact of fluctuating surface heat flux does not extent further down to 27 m deep, where the average temperature is 7.4 $\text{ }^{\circ}\text{C}$ all year long.

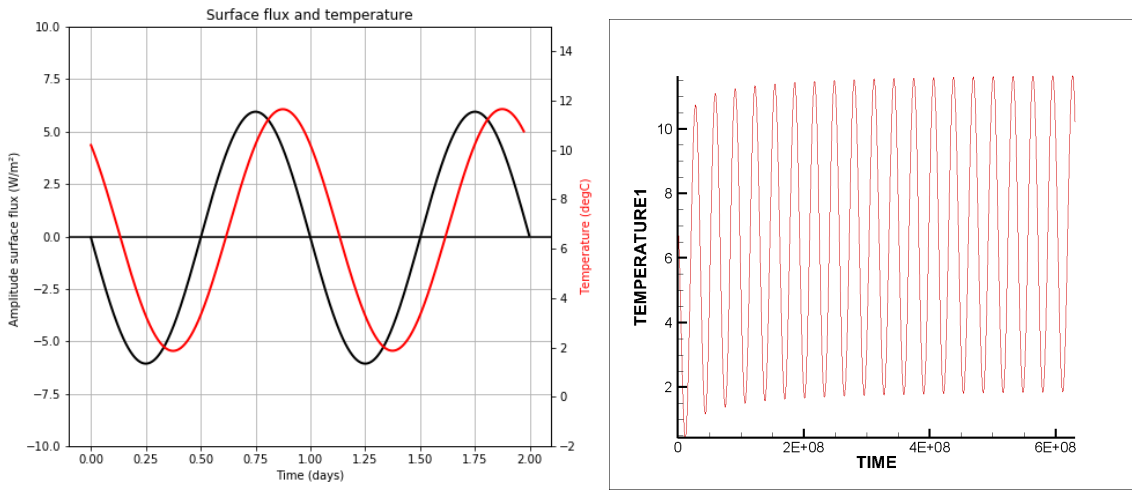


Figure 5.7: a) Surface heat flux input and resulting surface temperature change. The negative flux indicate flux from the ground to the surface (winter) and positive flux from the surface to the ground (summer) b) Temperature variation at the surface due to variation in the surface flux for 20 years

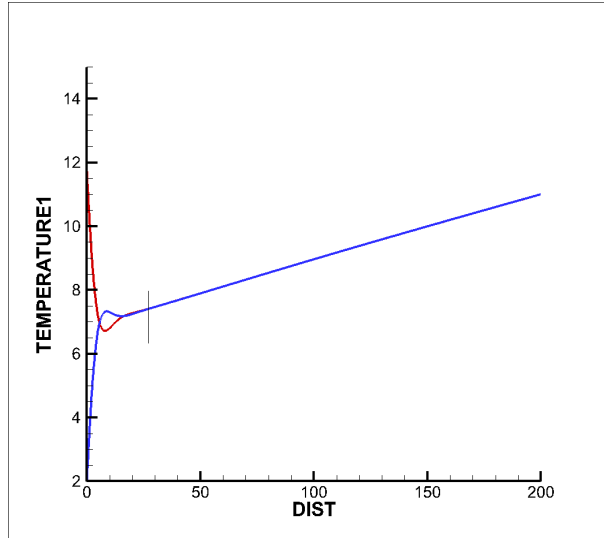


Figure 5.8: a. Winter (blue) and summer (red) temperature profiles

We then simulate the change in temperature in the rock mass over time due to heat extraction, using purely diffusive heat transfers within a porous media. Heat is extracted from a BHE situated between 80 and 120 m depth. Two heat extraction scenarios that satisfy the thermal load of a single house are compared. The first scenario assumes constant heat extraction of -1000W along the BHE. The second scenario considers seasonal heat extractions, which corresponds to a fluctuating source term, with a minimum of -1294 W in winter and a maximum of -706 W in summer, distributed along the 40m long BHE. The total heat load is calculated using Eq. XXX, with $A = 294$ W, the amplitude of the variations and $q = 1000$ W the average year heat load extraction. After 30 years of production using fluctuating and constant heat extraction rates, similar temperature profiles are obtained, indicating that average yearly extraction rate is representative of a fluctuating extraction rate around this average (Fig. 5.9).

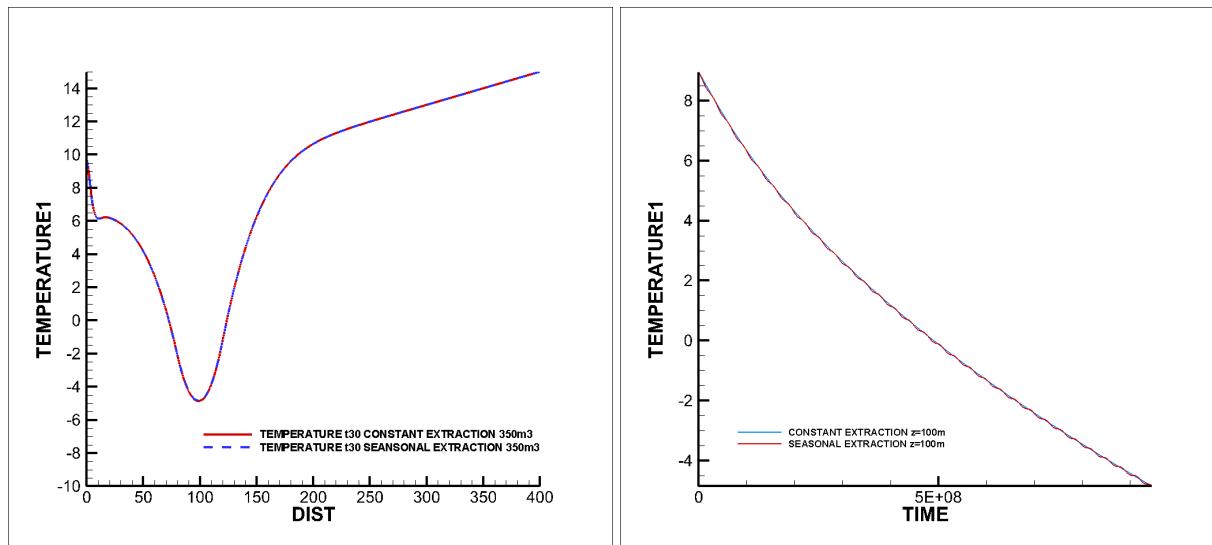


Figure 5.9: a) Temperature profiles and b) temperature changes at 100 m depth, after 30 years under constant and seasonal extraction (350 m² line source)

Temperature profiles after 1 year and 30 years of production are therefore shown for a constant extraction rate in Fig. 5.10. Specific line source areas of 200, 350 and 600 m² are defined to evaluate the impact of the available stored energy on the temperature decrease in the system. For each case, the solar and geothermal heat flux are scaled up appropriately and simulations are performed for constant and fluctuating extraction rates. In those vertical 1D models, recharge is assumed to occur only from the surface (half of the year, when the extraction rate is the lowest) and from below (all year long). However, as no lateral heat flux is allowed, no recharge occurs from neighboring areas. Thus, 1D models tend to overestimate the temperature decline and represent a most pessimist case. Results need to be compared against numerical model.

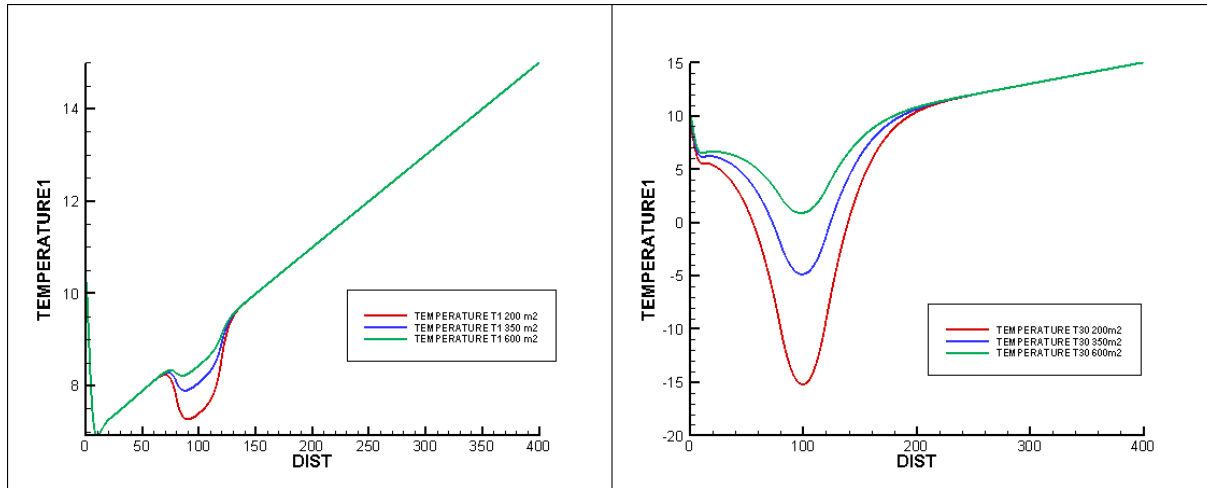


Figure 5.10: Temperature profiles after a) 1 year and b) 30 years, for a constant extraction rate of -1000 W

Additional simulations are made in order to assess the impact of different boundary conditions on the final temperature profile, using a constant surface and bottom temperature of 7 and 15 C, respectively, a constant

flux of -0.06 W/m² and the seasonally fluctuating surface heat flux. Fig. 5.11 shows the temperature profiles for each scenario using a line source area of 350 m², after a production period of 30 years, together with the temperature time series at a depth of 0 and 100m. As the BHE is located below the depth of influence of yearly solar variations, the temperature change at 100 m is not impacted by the surface boundary conditions. However, in the simulations based on heat flux boundary conditions, the ground surface temperature starts to decrease after about 15 years due to the extension of the thickness of rock depleted in heat.

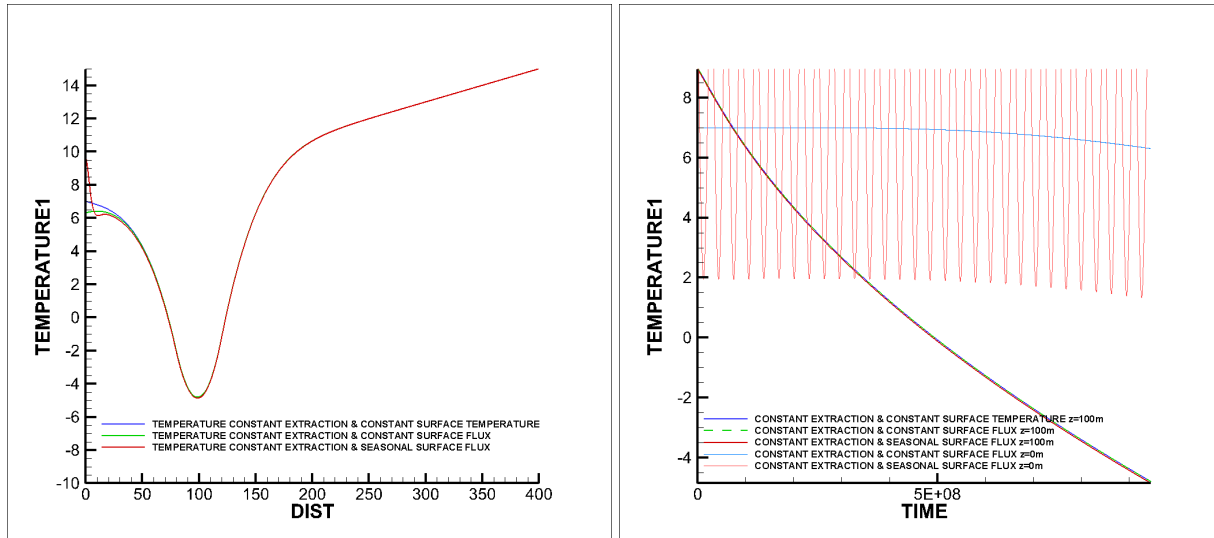


Figure 5.11: a. Temperature profiles and b. Temperature change at 0 and 100m depth for or different boundary conditions.

We finally assess the impact of the length of the BHE on the final temperature and the temperature distribution within the line source. By dividing the borehole size by two (i.e. extends from 80 to 100 m depth), the specific specific heat absorption of the BHE is increased by two (increases from 25 to 50 W/m). Simulations for a constant and seasonal extraction rates are done for a constant surface heat flux and results are displayed in Fig. 5.12. Results show that reducing the BHE length tends to increase the temperature decrease of the rock mass while maintaining the same thickness of rock affected after 30 years.

Next step would be to have a 3D model able to represent the transient heat transfers laterally and vertically.

5.6.3 2D heat diffusion-advection

Benchmarking

Diffusive and advective heat transfer contributions are assessed through the analysis of the propagation of a heat pulse injected for 1 second and of continuous heat injection within 1D and 2D plane homogeneous incompressible porous media. The porous media have a density of 2500 kg/m³, a thermal expansion of 1×10^{-5} , a thermal capacity of 1280 J/kg °C, and a conductivity of 2.78 W/°C.m. The circulating fluid has a specific heat capacity of 4068 J/kg °C and a heat conductivity of 0.63 W/°C.m.

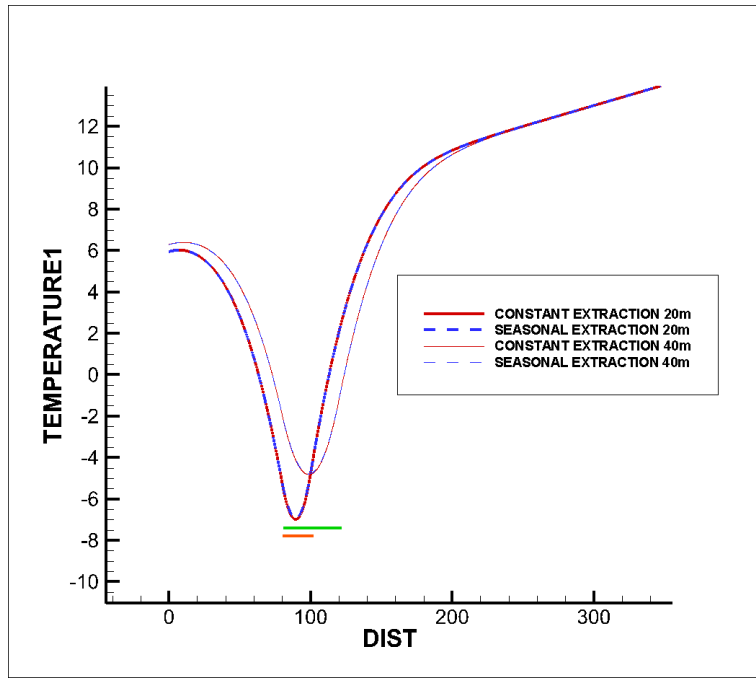


Figure 5.12: Temperature profile for a constant and seasonal extraction rate for 20m (orange) and 40m (green) long BHE after 30 years of production.

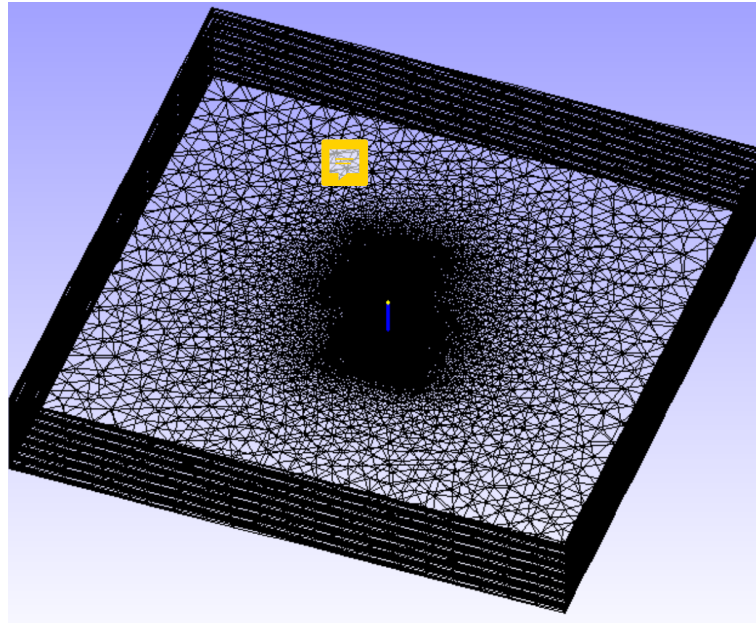


Figure 5.13: 3D FEM mesh for BHE

A head gradient of 20000 Pa allows groundwater to flow eastward at a Darcy velocity of $v = 2.5 \times 10^{-3} m/s$, considering a permeability of $k = 2.184 \times 10^{-13} m^2$ and fluid viscosity $u = 1.8 \times 10^{-5} \text{ Pa.s}$, according to the following equation:

$$v = k \frac{\Delta P}{\Delta x} \frac{1}{u}$$

The propagation of the heat pulse at $t = 0$ s and the constant heat injection within the model of initial temperature $T_0 = 0$ °C are first solved numerically for a 1D line model. The heat source corresponds to a point/line source with fixed temperature $T_1 = 100$ °C situated on the left boundary of the model. For each model, we evaluate the impact of the mesh size (1 and 8 mm line elements) and of the material porosity (0.1 and 0.5) on the final temperature distribution (at $t = 1000$ s). Results are then compared for a 2D domain composed of 480 quadratic elements for the 8mm mesh and 34560 elements for the 1 mm mesh, and for different dispersivity values (0 or 0.1 m²). Figure XXX in appendix XXX show the results for the benchmark analysis together with final temperature distribution in 2D domains, together with temperature profiles and temperature time-series for both pulse and continuous injections.

An attempt to validate numerical results against the corresponding analytical solution has moreover been made. Comparing numerical results with analytical solutions is a first step toward a better discrimination of the heat transfers processes taking place throughout space and time, when groundwater circulation is involved. While the analytical and numerical solutions fit well (5.14), the appropriate analytical solution for a heat pulse has not been found yet (see script in appendix XXX). The analytical solution for the continuous heat injection is based on the solution described in Barends et al. (2010). This solution is based on the Lauwerier concept (1955) and was developed to explore the complete heat storage and transfer processes, including convection by pore fluid flow, conduction, dispersion and thermal bleeding in a homogeneous reservoir with plane uniform steady groundwater flow. In this model, water of temperature T_1 is injected at a rate $Q(\text{m}^3/\text{s})$ at $x=0$ and $t=0$. No hydraulic and no thermal flows are set to the lower boundary and the upper boundary is defined as impermeable but can conduct heat through thermal bleeding in an overlying rock strata. Result from their analysis showed that despite the effected zone in the overburden is rather limited, thermal bleeding has a large effect on the temperature pattern in a reservoir.

The solution used here for the temperature distribution along the line for continuous injection is the one derived for $z=0$ (no heat diffusion in the overburden) and represents the temperature distribution in the reservoir when there is no heat diffusion in the overburden (Abramowitz and Stegun, 1968; Ogata and Banks, 1961):

$$\Delta T = \frac{T_1 - T_0}{2} \left(\operatorname{erfc}\left(\frac{(x - V_h t)^2}{4\alpha t}\right) + \exp\left(\frac{xv}{\alpha}\right) + \operatorname{erfc}\left(\frac{(x + V_h t)^2}{4\alpha t}\right) \right)$$

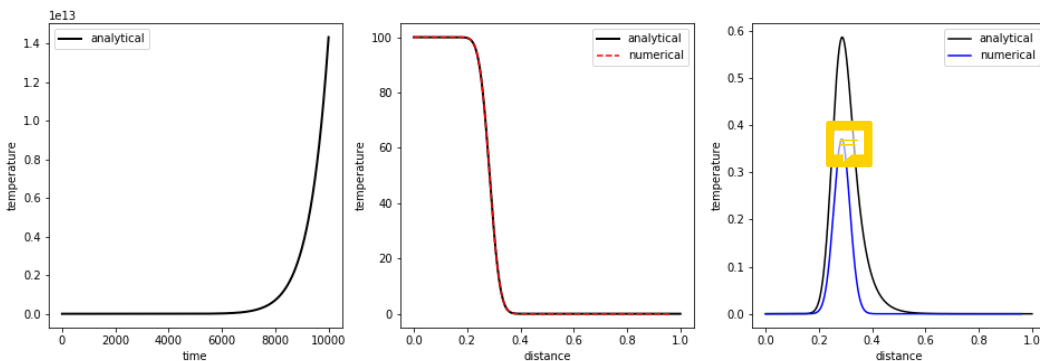


Figure 5.14: Comparison of the analytical and numerical solutions for continuous heat and heat pulse injections

Assessment of the potential geometrical simplifications for mine system modeling

We explore the possibility of creating a stack of highly permeable layer (i.e. mined coal seams) versus host rock to evaluate the impact of reservoir geometry on overall temperature change and timing of heat depletion in terms of thermal energy content. To do this, we first extended the initial model to evaluate the effect of various rock properties and the contribution from thin layers ($h = 0.1$ m or 0.2 m) situated above and below the original 0.36 m thick layer on the final heat distribution. Results are developed in appendix XXX.

Then a complex model is created, composed of 3 porous coal seams (0.02 m thick) in between 4 layers of host rocks of (0.05 m thick), and two impermeable layers of 0.01 m, resulting in a total model thickness of 0.28 m. In the "sandwich model" (term used by V. Hamm for modelling of the Dogger Aquifer, France, XXX), the stacked permeable coal beds (0.06 m thick) are embedded between two 0.1 m thick layers of host rock. In a first set of simulations (V1), rock properties similar to those used in the previous analysis are attributed to the different layers (see Fig. 5.15). In a second set of simulations, rock properties are defined accordingly to properties likely to be found in mine systems. Four different classes of materials have been used in the literature to describe the mine. It includes the unaltered rock (i.e. quasi-impermeable, homogeneous, isotropic and unconfined porous medium, with 0.1% porosity, $K = 1 \times 10^{-7}$ m/s, i.e. Fandos et al., 2004), the mined volume (i.e. altered material in the zone between galleries, with various porosity range $2-22\%$ and $K = 2 \times 10^{-4}$, i.e. Andres et al., 2017), the open voids (i.e. galleries with rectangular cross sections and circular shafts, with 100% porosity, $K = 1$ to 5 m/s, i.e. Renz et al., XXX) and the overlying strata ($K = 1 \times 10^{-4}$, i.e. Zhai et al., XXX). The permeability used as input parameter in the model, is calculated from the hydraulic conductivity K , the fluid viscosity μ and the fluid density as followed:

$$k = Ku/\rho g$$

The resulting temperature distribution, vertical/horonzontal temperature profiles and temperature time series are displayed in figures 5.16, 5.17 and 5.18, respectively. In addition, we calculated the integrated temperature change within the model over each time steps in order to get an insight on the overall change in energy stored in the system depending on the modeling approaches. Results are displayed in Fig. 5.18 and suggest that the sandwich model tends to highly underestimate the overall temperature change  within the model. A code, shown in Appendix XXX is finally being developed to visualize the final heat distribution in term of net heat flux (5.19), but improvements need to be done to be able to make the distinctions between convective/diffusive flux.

5.7 Conclusion and research outputs

Sensitivity analysis will be required to better understand how the permeability contrasts between the different layers, their porosity, thermal conductivity and geometrical arrangement impact the heat fluxes during production and contribute to the overall temperature change over time. We will also study the results through steady-state simulations and determine the time necessary for the systems to reach equilibrium, based on the modeling approach. From this, energy balance calculations will be made and the area of influence determines.

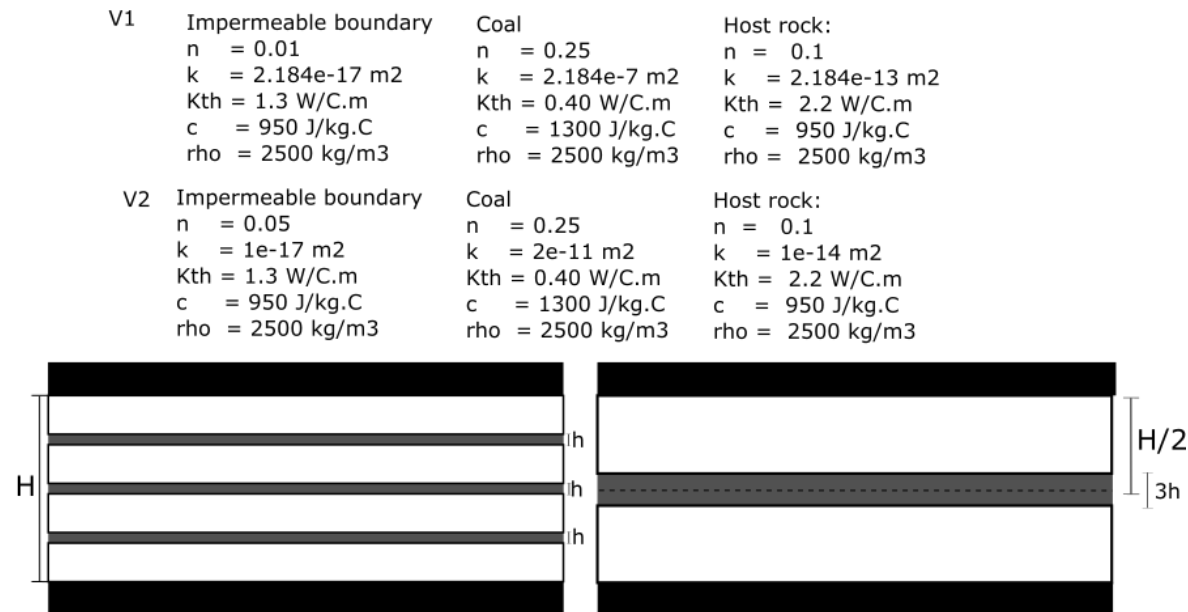


Figure 5.15: Rock properties for model complex and simplified "sandwich" model

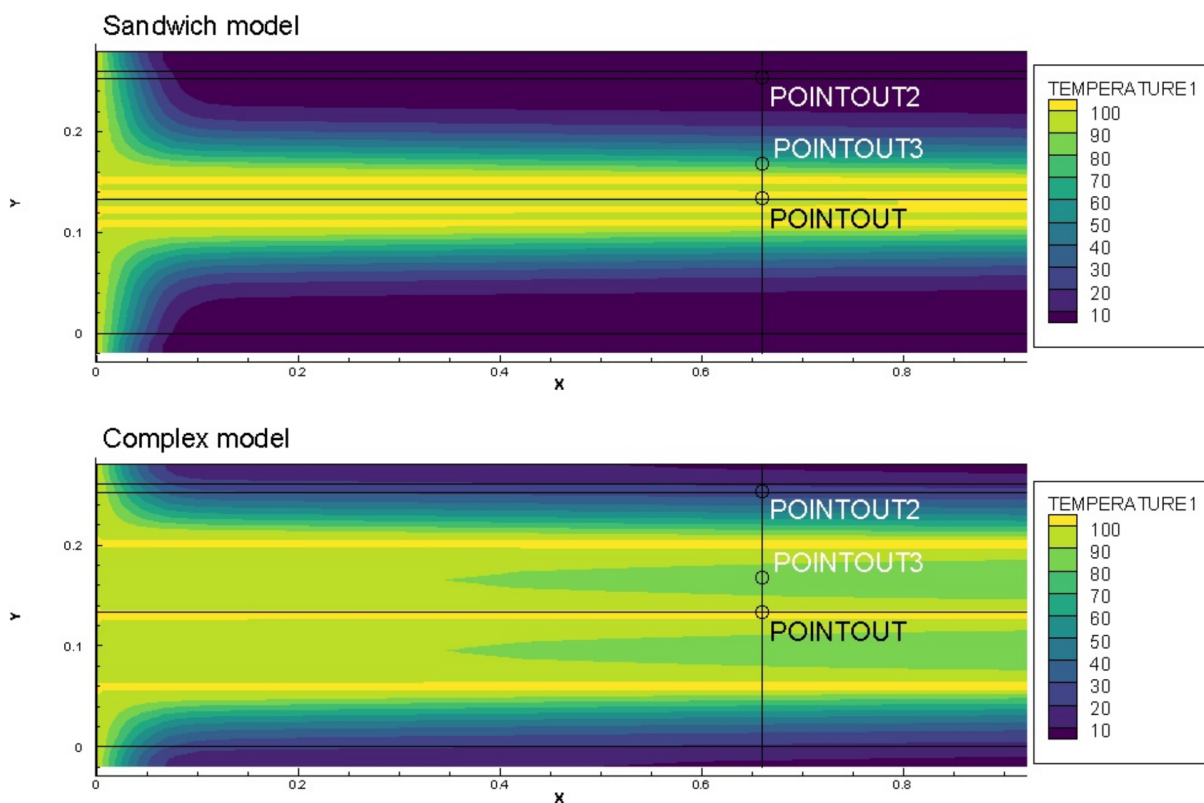


Figure 5.16: Temperature distribution within the model complex and simplified "sandwich" model at t=1000s

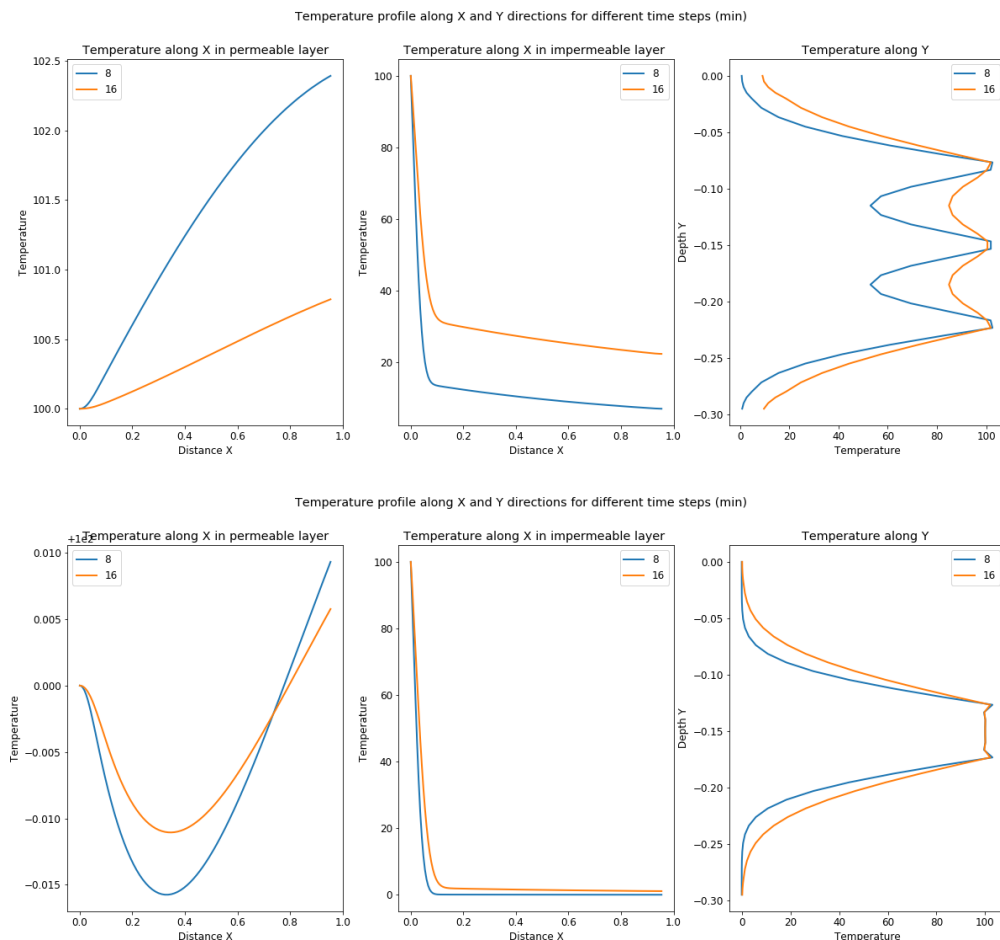


Figure 5.17: Temperature profiles within the model complex and simplified "sandwich" model at $t=1000s$

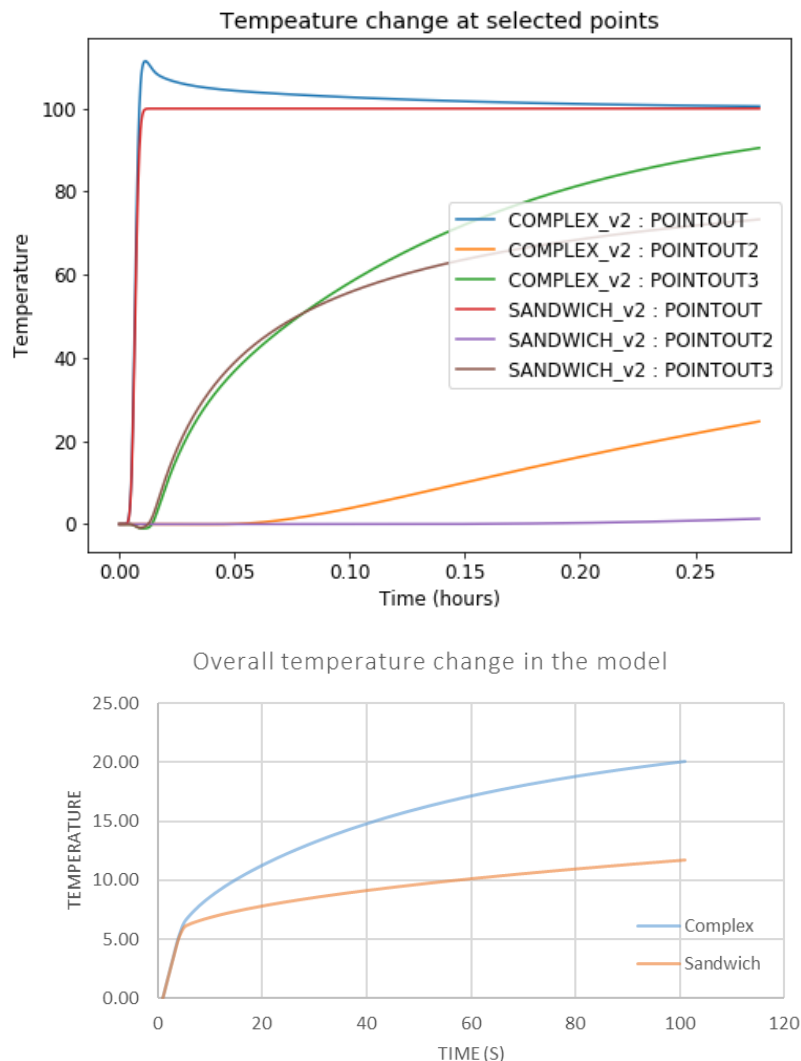


Figure 5.18: a) Temperature change at the points shown in Fig. XXX over time and b)Integrated temperature change over time for both models

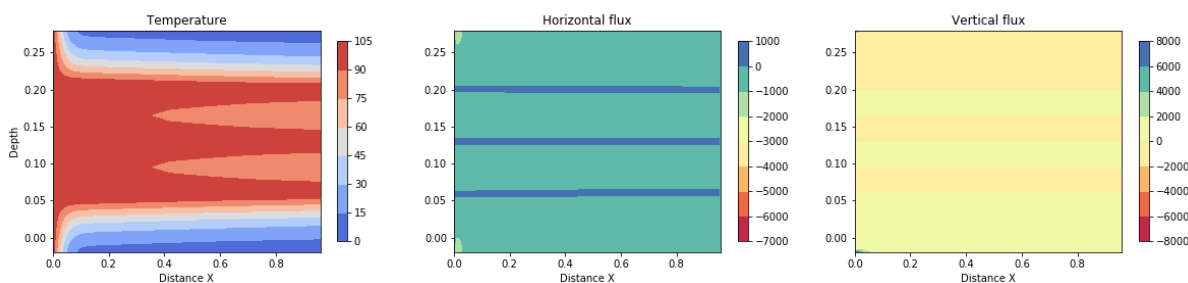


Figure 5.19: Vertical and horizontal net heat fluxed within the complex model and temperature distribution at t=1000s

6 Chapter 2: Thermal state of the mine

6.1 Background

Until the 1990's, most of mine modeling studies aimed at predicting water rebound in mines after the cessation of the mining activities and the stop of dewatering. In those studies (i.e. XXX), the authors developed strategies to create realistic but simplified representation of mine workings and of the hydraulic problem. More recently, the growing interest in evaluating the geothermal potential of flooded coal mines worldwide increased the complexity of mine modelling through the addition of the heat transfer problem.

In mine modeling, initial temperature distribution and surface/bottom boundary conditions are generally set up accordingly to the local geothermal gradient, with the mine water temperature being in thermal equilibrium with the rock mass. Constant heat flux and constant or variable temperature conditions (i.e Andrés et al. 2017) are commonly attributed to the bottom and surface boundaries, respectively.

In the UK, Gillespie et al. (2013) however pointed out the lack of correlation between the temperature of the mine-water measured in mine shafts and the depth of measurements. It was therefore suggested that other parameters are controlling the mine water temperature in addition to the geothermal gradient or that temperature gradients in mines may therefore not represent purely conductive heat flows (Beamish and Busby, 2016). Another possibility is that the geothermal gradient in mines does not follow the regional gradient. During mining activities, water is indeed pumped to allow access to deep part of the mine and air-ventilation is installed to guarantee the removal of gas and dust in the underground mine, minimize the stresses on the equipment and ensure safe conditions for the miners (Anderson and De Souza, 2015; Malolepszy, 2015). The inflow of cold air in the pumped sections of the mine is therefore expected to decrease temperature in the galleries. On the other hands the remains of highly conductive mining voids after the flooding of the mine tends to create large-scale interconnections between different parts of the mines or between aquifers previously isolated. Such hydraulic perturbations might favor advection of heat and explain the perturbations of the geothermal gradient in mines.

Despite it is well known that extensive periods of mining activities would have disturbed temperatures in mines and affected virgin rock temperatures (Tammemagi and Wheildon, 1974), only a few studies considered the effect of early mining activities on the thermal state of flooded mines before the start of geothermal production. Malolepszy (2003) estimated the rate of cooling of the rock mass resulting from ventilation in the Nowa Ruda mine in Poland, using measurements of rock temperatures taken during periods of mining. In the vertical 2D model representing a geological cross-section preserving the dips and thickness of the rock beds, the authors calculated the natural-state conditions in the mine by simulating the conditions under mining activity (assuming a cooling of 8 °C) and the temperature recovery in the working after the stop of the mining activities. After a period of mining of over 200 years and a subsequent flooding period of 5 years, the authors showed that about 10 years would be required for the rock of the to heat up back to its initial temperature of 23 °C at 890 m depth.

6.2 Research Gaps

Despite many mine modeling studies have been performed to estimate the geothermal potential of worldwide mines as well as the sustainability of heat production, only one considered to our knowledge the effects of past mining activities and flooding on initial temperature distribution within the mines. Knowing the time for the mine to return to its undisturbed thermal state (i.e. equilibrium with regional gradient) and the temperature distribution before geothermal production is however essential to assess the initial heat capacity of the mine and understand the heat fluxes that might participate to heat recharge.

6.3 Aims and methods

The study aims at understanding the temperature distribution in deep coal mines before production start, and the effect of the duration of the mining and flooding periods. We will attempt to quantify the cooling induced by air and cold water infiltration during mining and the time required for heat recovery during water rebound, to understand the perturbations of the geothermal gradient induced by mining activities. Available mining and post-mining data (i.e. water level, temperature time series and profiles, timing and location of mining activities, volume of residual voids) will be used to verify our analysis and evaluate the potential impact of mining activities on the current hydraulic and thermal state of the mines, depending on their current state (i.e. flooded, in current recovery...) and geological context.

We will moreover assess the influence of the hydraulic lateral and bottom boundary conditions on temperature distribution within the mines using simple 2D numerical model. In the literature, hydraulic boundaries to model are generally set as no flow boundaries, and away from the mine system to limit their influence on the results (i.e. Raymond and Therrien, 2008; Ghoreishi Madeish et al., 2012). This assumes that mines are hydraulically isolated from other systems.

6.4 Research questions

What is the impact of past mining activities on the thermal state and temperature distribution in mines?

- Does the geothermal gradient in mines follow the undisturbed regional geothermal gradient ?
 - Does dewatering and ventilation during mining affect the rock temperature?
 - How long does it take for rock temperature do re-equilibrate with the regional gradient after a mining period subsequent flooding?
 - What is the effect of water advection in large voids on the heat distribution in mines?
- Are the mine waters at equilibrium with the host rock temperature?
 - How long does it take for the water volume in tunnels to heat up to the surrounding rock temperature?
 - What defines the temperature profiles within the shaft during periods without production and with production (i.e. number / depth of intersected coal seams, inflow temperature...)?

6.5 Hypothesis

- The geothermal gradient reaches a state of "partial equilibrium" in the flooded mine, with dominant conductive heat flux in the host rock and isothermal conditions in tunnels and shafts.
- The water is initially at equilibrium with the host rock.
- Return to undisturbed conditions is completed within 10-20 years after flooding is completed, depending on the depth of the mine and source of recharging water.

6.6 Preliminary results

6.6.1 Model set up

The two-dimensional vertical model consists of three horizontal coal seams embedded in an homogeneous host rock. A stapple shaft is connecting the seams on the western side of the model and a deep shaft is connecting the seams from the surface on the eastern side. The seams are 3 m thick and the main and stapple shafts are 6 and 3 m in diameter, respectively. Each element (i.e. host rock, seams, shaft) are assumed to be porous materials with different solid, hydraulic and thermal properties.

6.6.2 Initial and boundary conditions

We simulate change in head and temperature over time, during mining, after mining (i.e. water rebound), and during pumping for geothermal utilization purpose, using different boundary conditions. Initial steady state conditions are first calculated during an initial run, depending on the different scenarios. Those are summarized below and include:

- Thermal boundary conditions: geothermal gradient of 0.027 °C
 - Constant temperatures of 9.5 °C and 18.2 °C at the top and bottom, respectively.
 - Constant vertical flux of 0.06 W/m² in and out of the model.
- Hydraulic boundary conditions
 - Fixed head boundary conditions of 0 m on both west and east boundaries, with a constant head of 0 m across the model.
 - Fixed head boundary conditions of 0 and -100 m on the west and east BC, respectively, with a head gradient from west to east.
 - Horizontal flux of 4e-6 m³/s from west to east (corresponding to the 100 m head difference).
 - Inflow of 4e-6 m³/s from west (initial head of 100 m) with constant head of 0 m on the east.
 - Outflow of -2e-6 m³/s on the east (initial head of -100 m) with constant head of -50 m on the west (unsaturated system with initial head difference of 50 m).

For each scenarios, initial conditions were calculated from Dirichlet-type boundary conditions in a steady-state simulation without extraction of mine water or precipitation (i.e. undisturbed situation. In scenarios where hydraulic and thermal fluxes are used, undisturbed conditions are then simulated using the corresponding Neumann-type boundary conditions to ensure stable initial conditions before simulating flows under mining conditions. The equivalences between Dirichlet boundary conditions (i.e. constant head or constant temperature) and Neumann boundary conditions (i.e. thermal / hydraulic fluxes) are calculated according to Eq. XXX.

$$q = K \frac{dh}{dx}$$

We assume that the model is saturated with water with a density of 1000 kg/m³, a viscosity of 1e-3 Pa.s, a specific heat capacity of 4680 J/Kg.K and heat conductivity of 0.6 W/m.K.

6.6.3 Material properties

The initial undisturbed temperature and head distributions are determined for a uniform porous aquifer interbedded with three coal seams. During simulations under mining and flooding conditions, different hydraulic property values (i.e. porosity, hydraulic conductivity and storage coefficient values) are assigned to the mined area, shafts and coal beds to account for the changes induced by mining activities. Those were attributed based on existing data for the Carboniferous strata in the UK and on previous hydraulic modelling studies in mines, and are summarized in Table XXX.

Zone	Host rock		Mined area		Seams		Shaft	
Simulation	1	2	1	2	1	2	1	2
Porosity (%)	0.1	0.1	0.1	0.15	0.05	0.25	0.1	1
Hydraulic Conductivity K (m/s)	1e-7	1e-7	1e-7	1e-5	0.5e-7	1e-2	1e-7	1
Storage Coefficient S	1e-5	1e-5	1e-5	1e-5	1e-5	2e-4	1e-5	1

Table 6.1: Summary of the hydraulic properties for each material/elements used in (1) steady-state and (2) mining/flooding/production simulations. Values of storage for the workings area and host rock are based on Raymond and Therrien (2009). In their study, the authors suggested values of Hydraulic conductivity of 2.30E-02 and 4.50E-05 m/s and porosities of 0.25 and 0.05 for the workings and host rock, respectively.

Thermal properties for the Carboniferous rocks of the Midland Valley of Scotland are summarized in Table XXX (Appendix XXX). Average matrix thermal conductivity of 0.31 W/m.K and 1.7 W/m.K have been reported for coal and goaf (i.e. unconsolidated roof material), respectively, in Herrin and Deming (1996). Due to fracturing and partial filling of the coal with water, its bulk thermal conductivity has however been suggested to raise up to a value of 0.4 W/m.K (Herrin and Deming, 1996). Here, thermal properties are kept constant for all simulations and scenarios. For the host rock, we assume a thermal conductivity k and thermal capacity c of 3.14 W/m.K and 950 J/Kg.K, respectively. The seams have values of k = 0.31 W/m.K and c = 1380 J/Kg.K. All elements are attributed a thermal expansion coefficient of 1e-5. In Guo et al. (2018), different densities are attributed

to the mining area to account for the difference between the intact and the fractured rock due to mining. We here assume that the host rock and the seams have densities of 2650 kg/m³ and 1500 kg/m³, respectively, for all simulations. We finally assume an isotropic heat dispersion coefficient of 0.5 m to account for the size of the mesh in the wells.

6.6.4 Water extraction

For all scenarios, water extraction during mining activities (i.e. dewatering) is simulated for a period of 30 years using an extraction rate of -0.01, -0.08 or -1e-4 m³/s. We then simulate water recovery for a period of 50 years in order to evaluate the time necessary for the geothermal gradient to re-equilibrate within the mined area. Finally, we simulate pumping for geothermal utilization purpose for a period of 30 years following the flooding of the mine. For each scenario, we moreover compare the evolution of the temperature profile with cases where surface inflow (i.e. precipitation) is added. To evaluate the impact of the pumping depth on the temperature profile in the shaft, we finally perform a series of simulation in mining or production conditions using three different pumping depth: between 50-70 m, between 110-130 m and between 150-170m. For each situation, the chosen flow is divided accordingly between the nodes intersecting the borehole line.

6.7 Results and research outputs

Preliminary analysis showed that the use of different material properties in the dewatering simulation relative to those used for the initial undisturbed conditions simulations tend to create instabilities in the beginning of the simulation. The significance of the choice of different boundary conditions will be used to determine the main processes and rate of heat recharge. The objective will be to improve those preliminary models to produce similar temperature profiles than the ones measured in shafts of the study areas. Conductivity profiles could moreover be used as an additional data source for the model calibration, both as hydraulic constraints (i.e. define the origin of water depending on its temperature/salinity) or thermal constraint (i.e. density relative free-convection in open voids). This would imply the addition of a mass transport term in the numerical simulations. Examples of temperature/conductivity logs in the Bilston Glen shafts and Dawdon Victoria shaft are shown in Fig. 6.4 and Fig. 6.5.

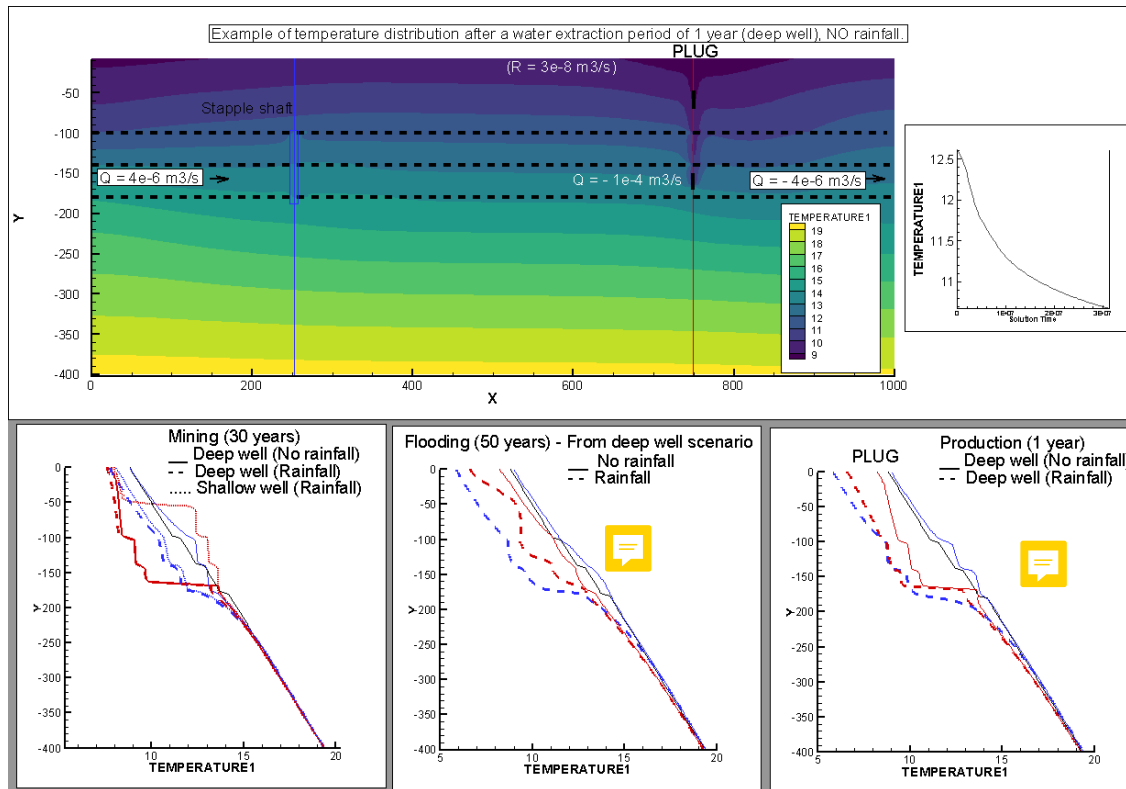


Figure 6.1: Results using hydraulic flux across the model

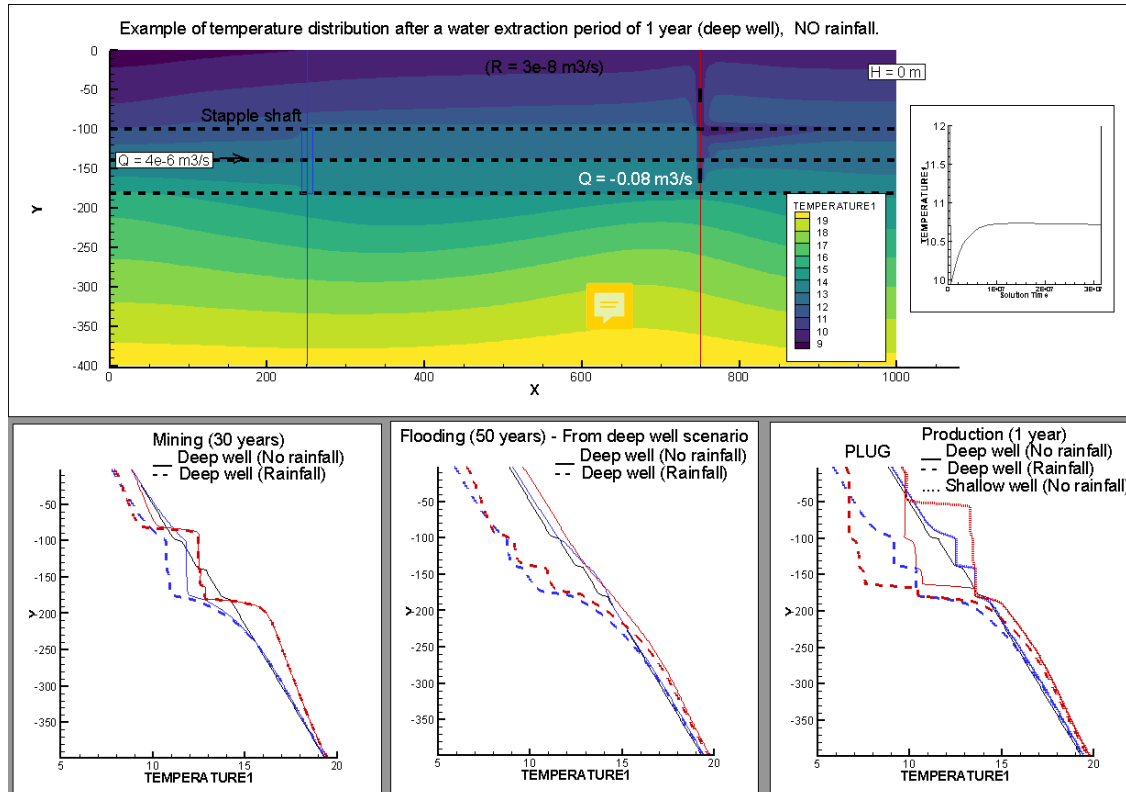


Figure 6.2: Results using entering flux on the west and fixed head on the east

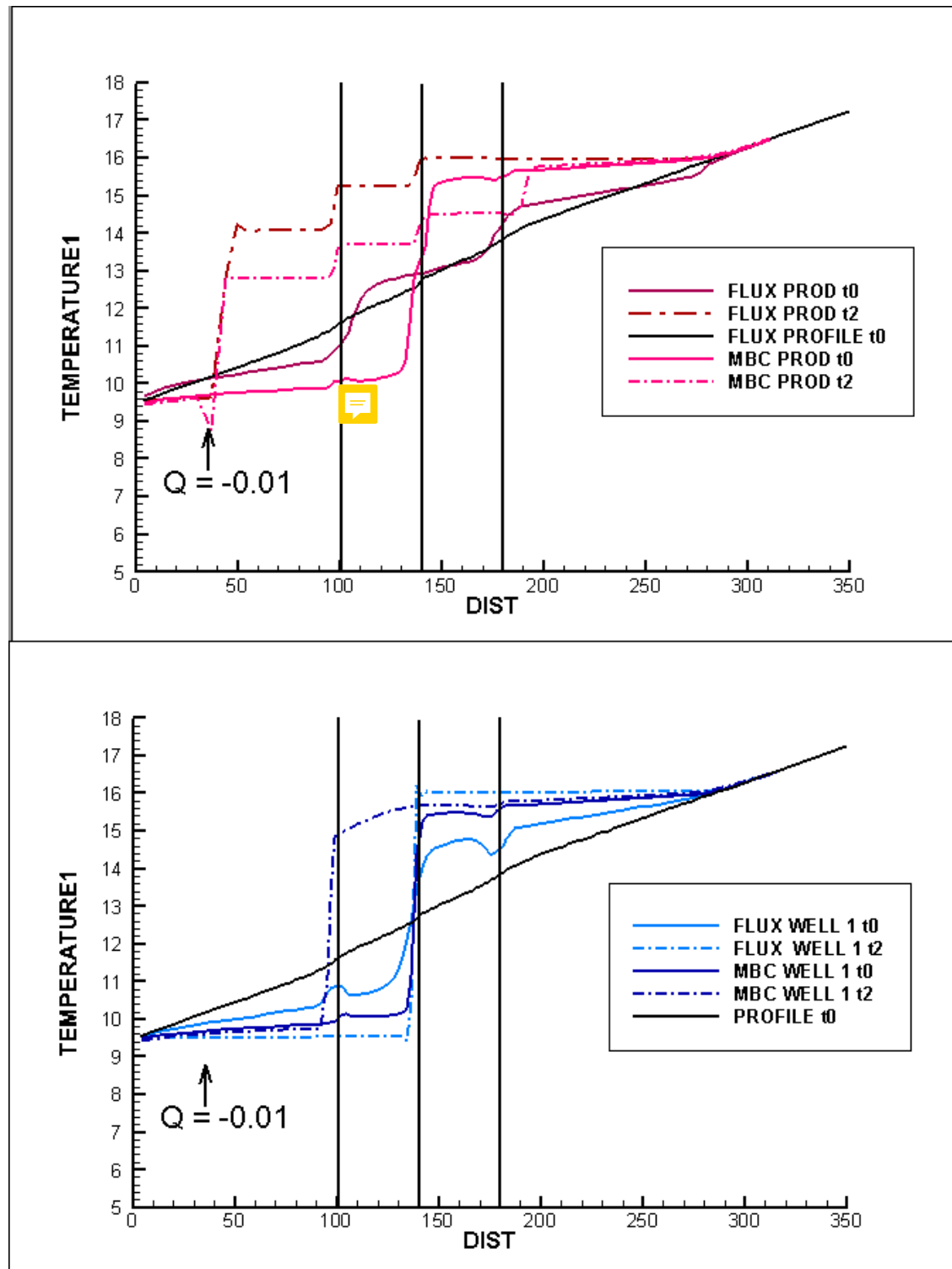


Figure 6.3: Results using closer well distance (shallow water extraction from undisturbed situation)

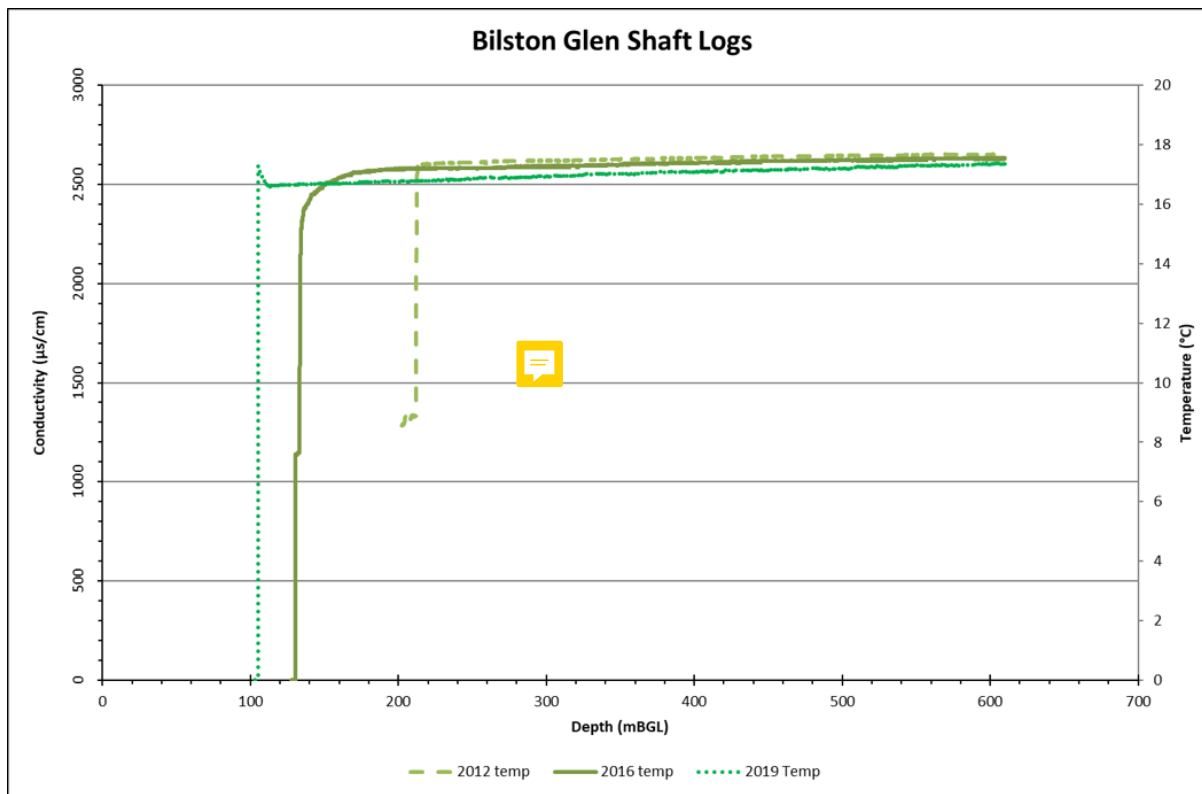


Figure 6.4: Bilston Glen a shaft logs

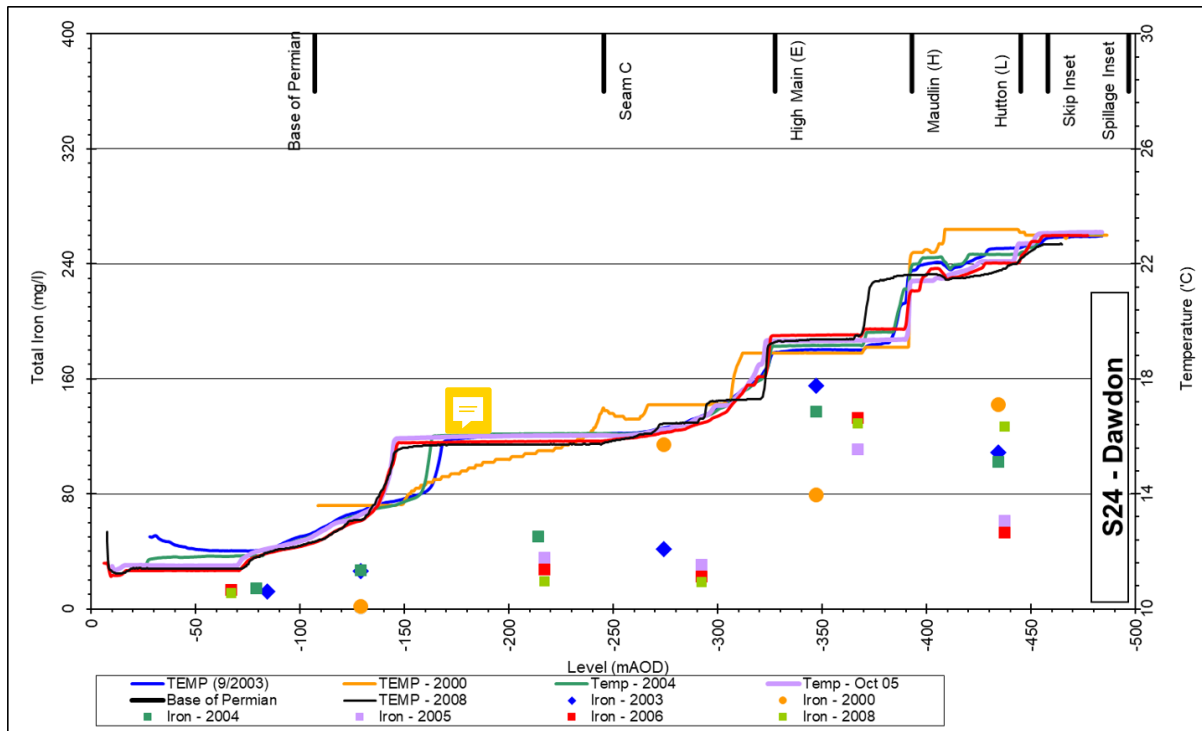


Figure 6.5: Dawdon shaft logs

7 Chapter 3: Recharge potential of the Midlothian and Dawdon-Horden coalfields: an investigation of the key features for thermal modeling of flooded coal mines

7.1 Background

7.1.1 Numerical approaches for mine systems

Past researches involving modeling of abandoned flooded coal mines have been faces to the important difficulties arising from the complex geometry of the mine workings. In most of the studies, abandoned coal mine reservoirs have been described as a dual-porosity medium, composed of two main domains:

- The mine open voids, that are assimilated to tunnels of simple geometries. There, the heat transfer problem can be view in a similar way to heat exchanger, allowing to solve for simple 1D heat transfer equations using either semi-empirical method, analytical or numerical model (see equations in previous Chapter).
- The mined areas, that corresponds to the volume surrounding the open mine voids. This area can be composed of different type of materials (i.e. "goaf", fractured rock) with secondary porosity that is closely related to the mining method and the roof conditions.

In mine reservoir modeling, the main difficulty arises from the necessity to solve simultaneously for heat transfer and mass flow within a porous matrix (i.e. undisturbed rock, galleries, "goaf", caverns and drivings), open pipes (i.e. shafts, roadways, tunnels) or fractures (Ferket et al., 2011; Renz et al., 2009). Different approaches have been used in the literature to represent mining voids (Renz et al., 2009) whilst avoiding numerical instabilities caused by the permeability contrasts between the open mining voids (i.e. dominantly turbulent flow) and the porous aquifers (i.e. dominated by laminar flow). This ranges from the combination of 2D/3D porous media approaches with 1-D pipe flow (Adams and Parkin 2002; Raymond and Therrien 2008) to the assimilation of the mine as a porous media with different hydraulic conductivities (i.e. host rock and mining voids) dominated by Darcy flows (i.e. Malolespsy, 2003).

For complex real-case mine modeling studies, Raymond and Therrien (2008) and Andrés et al., (2017) suggested to model the pipe network (i.e. shafts and roadways) as 1D elements embedded within a 3D mesh representing the porous mine aquifer. Despite 1D elements cannot model turbulent flows, interactions between the intact strata of the mine aquifer and the conduits in mined out areas have been successfully modelled using this approach. Renz et al. (2009) combined the Darcy equation to solve for laminar flow in the porous rock mass (e.g. Diersch, 2005), the Hagen–Poiseuille equations (i.e. slow-moving laminar pipe flow), and the Manning–Strickler

equation for 1D pipe/channel turbulent flow (e.g. Diersch, 2005). Similarly, Ferket et al. (2011) used coupled analytical models of heat transfer in mine void and discrete ‘pipe network’ hydraulic models based on semi-empirical approach (Rodriguez et al., 2009) to determine the heat capacity of the Asturias mine in Spain. This model was able to simulate both heat transfers between water and pipe walls and advective flow within a system of complex geometry, using a hybrid node-loop approach (Rossman, 2000).

7.1.2 Void volume estimates

Several methods have been deployed to derive estimates of the residual void volume in mines. Those methods imply taking into account the initial amount of void and scale it by a factor accounting for backfilling, subsidence and induced fracturing. Jossop (1999) suggested that this factor is in the order of 25%, both in longwall and pillar-and-stall mining areas, while Malolepszy (2015) considered that 5-40% of the initial volume of the mined space remains open depending on the mining method employed. In room and pillar mining method, pillars and open spaces are generally left in place, and only small and local convergence of the roof/floor is expected. Few debris resulting from roof falls are found on the floor and are assumed to be compensated by the creation of voids in the roof. For Younger et al. (2002), 50% of void mines are therefore likely to remain open if no collapse occurs. In contrast, the formation of goaf and the convergence of the workings roof/floor in longwall mining areas generally tend to fill the mined area, reducing the initial void volume in the workings. Gillespie (2013) suggested that about 20% of the mine voids remain after subsidence above longwall panels, while Younger and Adams (1999) attributed to goaf a porosity of 30% after subsidence and fracturing. Whiteworth (2002) considered that residual void volume in longwall mining area represent 10% of the extracted height in areas of total extraction. The initial void volume can generally be calculated from the volume of coal extracted. As this value is rarely known, Andres et al. (2017) derived the volume of coal extracted from the mass of coal extracted in the Asturias mine, available from coal production data, and from the mean density of the excavated rock. Other studies suggested to use pumping rate or water recovery data to derive the post-mining void volume.

7.1.3 Geothermal potential estimates

Several modeling strategies have been employed to assess the geothermal potential and sustainability of heat production from abandoned flooded mines. In Ghoreishi Madeish et al. (2012), the thermal breakthrough issue is addressed by assimilating the mine as a horizontal tunnel, in which cold water is injected at the entrance and produced at the other end after flowing through the tunnel. While conductive heat fluxes are generated along the axe of the tunnel, heat recharge to the water is here mainly attributed to radial conductive heat transfers from the surrounding rock mass, ignoring the effects of natural convection inside the rock mass (i.e. heat advection). On the other hands, Guo et al. (2018) studied the effects of secondary porosity within the fracture zone that generally develops above mined-out area was using a FDM approach. There, the mine was considered as a dual-porosity medium composed of a homogeneous caved zone (i.e. isotropic goaf material) and an overlying fracture zone (i.e. anisotropic medium with regular vertical fractures), surrounded by a large continuous media.

Analytical solutions for heat transport, although necessary to validate numerical models, generally express single processes at the time and does not give an overall understanding of the heat fluxes and recharge potential. Heat transfers in complex system therefore need to be solved through numerical approximations. Numerical

models of existing worldwide coal mines includes the Gaspe Mines in Quebec (Therrien et al., 2004), the Nowa Ruda coal mine in Poland (Malolspiszy, 2015), the Asturias mine in Spain (Andrés et al., 2017; Renz et al., 2009) or mines in France (Hamm and Bazargan Sabet, 2010). The main conclusions resulting from those studies are summarized below:

- The sustainability of heat production from mines highly depends on the relative contribution of advective/conductive heat transfers, the impact of induced flow circuits, the time required to recover thermal equilibrium between the rock and the water after production.
- The sustainable rate of heat extraction from mine tunnels depends on the thermal conductivity of the surrounding rocks (Ghoreishi Madeish et al., 2012). The dimensions of the tunnel tends to impact the total recoverable heat from the mine.
- Backfilled stopes have great potential for sustainable geothermal heat production, with the main heat transfer mechanism being conduction (Ghoreishi Madiseh and Abbasy, 2015)
- The geothermal potential of mines depends on the height of the fracture zone. The permeability of the roof is beneficial to heat transfer, while the fracture permeability in the fractured zone tends to decrease the production temperature (Guo et al., 2018).
- The heat extraction rate is related to the injection temperature (Guo et al., 2018)
- Seasonal heat extraction allow better heat recovery and sustainable heat extraction (Ghoreshi et al, 2012; Hall et al., 2011; Hamm and Bazargan Sabet, 2010).
- For hydraulic conductivity contrasts between the mine void K_{mine} and the rock $K_r < 1 \times 10^5 m/s$, the higher the K_{mine} , the smaller the decrease in extraction temperature. For higher contrasts, the higher the K_{mine} , the greater/quicker is the decrease in extraction temperature. From $K = 1 \times 10^4 m/s$, mixing of warm and cold water occur as a result of the establishment of free convection within the mine voids, leading to faster transport of cold water toward the extraction well (Renz et al., 2009).

7.1.4 2D vs 3D modeling approaches

Hamm and Bazargan Sabet (2010) suggested that a "equivalent porous media" assumption can be used for mine workings when large-scale modelling is considered. However, this approach could be improved by using a multi-layer models taking into account detailed digital maps of the mine's galleries/shafts, better describing the 3D geometrical and hydraulic connections in the mines. 2D models are suggested to be appropriate for initial sensitivity analysis of rock properties and for model parameter analysis. For some authors, they cannot be used to faithfully represent 3D geometries and the heat capacity of mines and thus, 3D models have generally been directly created or created subsequently to 2D models (i.e. Andrés et al., 2017). To deal with the fact that 2D models cannot realistically represent the high storage capacity of driving and caverns, whose extent is mainly in the orthogonal direction to 2D models, Renz et al. (2009) however used a "heat capacity equivalent" to represent the real behavior of heat and mass flow in these voids. Their results showed that 2D models cannot properly account for movement due to free convection when density-dependent simulations are performed compared to

3D porous media approach. However, the overall heat storage from large mining voids are better accounted for in the 1D/2D model.

7.2 Research Gaps

The geothermal potential of mine has been suggested to be highly dependent on their local hydraulic condition and geometrical structure. Thus, most of the authors developed their own modeling approach, based on the data available and the purpose of modeling, to estimate the geothermal potential of existing mines. Those attempts revealed that wanting to accurately represent the complex geometry of mines can be tedious, and simplifications are generally required (i.e. Raymond and Therrien, 2008; Hamm and Bazargan Sabet, 2010; Therrien et al., 2004 and Malolspszy, 2003, Andrés et al., 2017; Renz et al., 2009). Therefore, no standard mine modeling approaches have emerged yet at this stage and there is no general understanding of the mechanisms occurring in mines (Renz et al., 2009).

In addition, predictions of groundwater flow in the mines strata is generally limited by the lack of pre-mining or early-mining data and uncertainties about the volumetric capacities and lateral/vertical hydraulic connections within the mines. Indeed, mines plans are sometimes incomplete (i.e. old mine plans, not updated) or nonexistent, limiting the potential to set up reliable numerical models. This adds to uncertainties in the assumed parameters and boundary conditions (i.e. lack of pre-mining thermal and hydraulic properties, cyclic changes of precipitation/evaporation...). On the other hands, performing numerical calculations considering a whole complex mine system with detailed geometry would require extreme computing capabilities and amount of time.

7.3 Aims and methods

Because of the lack of data and the complexity of the geometry of mining voids, it is therefore essential to understand what elements really matter in modelling thermal processes and in the assessment geothermal potential, at the scale of the mine or interconnected mines. While large open voids in mine (i.e. shafts, tunnels) provide significant potential for heat exchange between the host rock and the mine-water over the whole depth range spanned by the worked coal seams (Banks et al., 2003), goaf and galleries (i.e. porous media) tends to represent the greatest proportion of the mine. This chapter therefore aims at assessing the important features to extract from existing mine plans for the estimation of the long-term heat capacity of mines. We want to investigate the validity of using 2D models to avoid constructing complex 3D models, through the definition of "equivalent porosity" and "equivalent heat capacity" factors. To achieve this, we will also develop a methodology and/or a tool able to convert GIS mine features into 2D finite-element mesh, or to use them to calculate input parameters for the models. Our study will be based on available data (i.e. both geometrical data for model construction and monitoring data for model calibration) for the Dawdon-Horden mining field and on the Midlothian Coalfield. The expected outputs from this analysis will be the assessment of the overall heat capacity, sustainable heat extraction rate (i.e. allowing balances heat extraction/recharge) and steady-state footprint area of heat extraction for those two areas, accordingly to knowledge acquired from previous chapters.

7.4 Research questions

What are the key mine features allowing to assess the sustainable heat potential of coal mines at the scale of a mine?

- Can 3D phenomenon (i.e. overall heat capacity and change in heat storage) can faithfully be scaled up in 2D?
 - What is the effect of lateral connectivity of roadways on the extent of the heat sink and on the heat exhaustion/recharge rate?
 - How does the density and/or absolute volume of mining void contribute to define the total energy content of the mine?
 - What is the footprint area of heat extraction for a typical single house energy consumption?
- Can homogeneous hydraulic and thermal properties accounting for both galleries and induced fractures be attributed to mining areas (i.e. excluding roadways and shaft)?
 - Does the geometry of the voids resulting from different mining approaches (i.e. pillar-and-stall, longwall mining) impact the heat exchange rate between the host rock and the mine-water and the recharge rate at the scale of the mine?
 - How does the relative permeability contrasts between roadway/tunnels, the mined area and unaffected host rock contribute to the overall change in energy content in the system and the rate of energy transfer?
 - Can we develop an “equivalent porosity-permeability” coefficient?
- How does the volume and inter-connectivity of roadway network and the coal seams distribution affect the lateral and vertical temperature distribution and the direction/amplitude of the induced heat fluxes during production/recovery?
 - Can we simulate the water recovery rate/temperature measured in shafts in the Midlothian coalfield ?
 - Is the extracted water temperature and the evolution of the temperature profiles within the shafts in Dawdon-Horden be reproduced?

7.5 Hypothesis

- An "equivalent porosity" and "equivalent heat capacity" parameter can be defined to scale up 3D processes in 2D models
- At the scale of the mine, the mining approach does not affect the long-term heat capacity of the mine
- The interconnection between tunnels and the model boundary conditions (i.e. source of hydraulic recharge) highly affect the long-term temperature change and production temperature.

7.6 Preliminary results

The two figures below are examples of mesh created, here manually, to investigate the impact of the coalfield geometry on the temperature distribution (7.1).

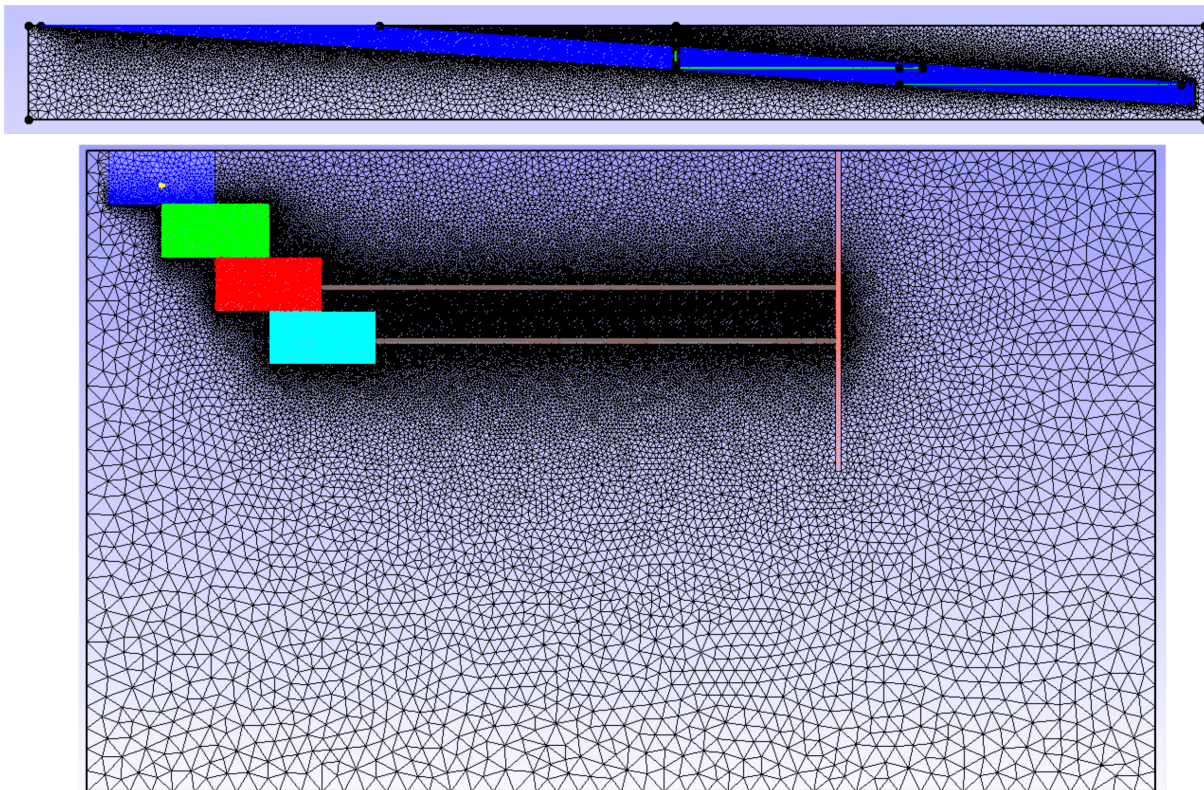


Figure 7.1: Example of mesh for equivalent porosity model for a) the Dawdon-Horden area and b) the Midlothian Coalfield

To attribute the different areas of the model with representative material properties, we first suggest to develop a factor representing the total proportion of void per depth interval, according to the following relation:

$$\Phi = \frac{V_{void}}{V_{minedvolume}}$$

with

$$V_{void} = \sum_{n=1}^n [A_{workedseams} \times h_{workedseams} \times f]$$

with n the number of workings in the considered min volume, A the working area and h the worked seam thickness.

For each "block", specific initial temperature and thermal/hydraulic properties (i.e. thermal conductivity, hydraulic conductivity) will be attributed according to the nature of the geological layer and initial undisturbed state. Appropriate thermal and hydraulic boundary conditions will be set. Each block will moreover be inter-connected through roadways (high conductivity pathway between mine volumes representing connections between different mines and/or mined parts of a same mine) accordingly to the information provided in the mine plans.

7.7 Conclusion and research outputs

8 Data management plan

8.1 Data repositories

File path	Usage	Description
C:	Desktop local space	Modelling and data processing
M:	Personal drive	General/administrative documents
R:	Research data store	GIS Data and projects, long-term storage of modeling results/analysis, Meeting reports and bibliography (i.e. scientific papers, reports, books)
GitHub	Online university account	Storage repository and version control for reports (i.e. confirmation report, literature review, meeting reports), scripts, figures and overall data storage
Google Drive	Personal drive	Administrative documents and temporary notes
Overleaf	Online university account	Document redaction (i.e. reports, PhD plan)

Table 8.1: Data management

The codes and meshing, modeling and visualization software used (OpenGeosys, gmsh, paraviw, Tecplot, QGIS) have been installed on the C: repository. Numerical model simulations are run on the C: repository and numerical output files are then transferred on the R: repository, which has a greater storage capacity.

8.2 Version control management plan

Version control for the data, reports and Python scripts is managed through the combined use of GitHub and GitHub Desktop on both personal and university computer. Overleaf is and will be used for report and future manuscript writing, to ensure safe version control, back-up and access from different places. This will also facilitate the exchanges and feedback with the supervisory team. All python scripts written as part of the PhD are currently stored on a personal GitHub repository and run from the Spyder application. Verified codes will be made available through GitHub website in the long-term.

For each modeling study undertaken as part of the PhD project, README files and Excel "Modeling-Data-Management" file has been developed and copied in each corresponding folder. The EXCEL file summarizes the name, input parameters (i.e. medium properties, boundary conditions, initial conditions...) for all models related to the study. It also includes a column for the objective of the model, the observation and the interpretation, that

are developed in more details in the README file. Each Excel file also contains an sheet for the calculation of the stability criteria of the models.

9 Time plan

The first year will involve the data collection of available data from the Coal Authority and other sources, the development of conceptual models and the investigation of the key controls on mine water temperature and recharge mechanisms. The second and third year will progress through the development of numerical modelling of temperature profiles and the interpretation of the results particularly with relevance to scoping out the size of the temperature resources available to use (see detailed timeline in Fig. 9.1).

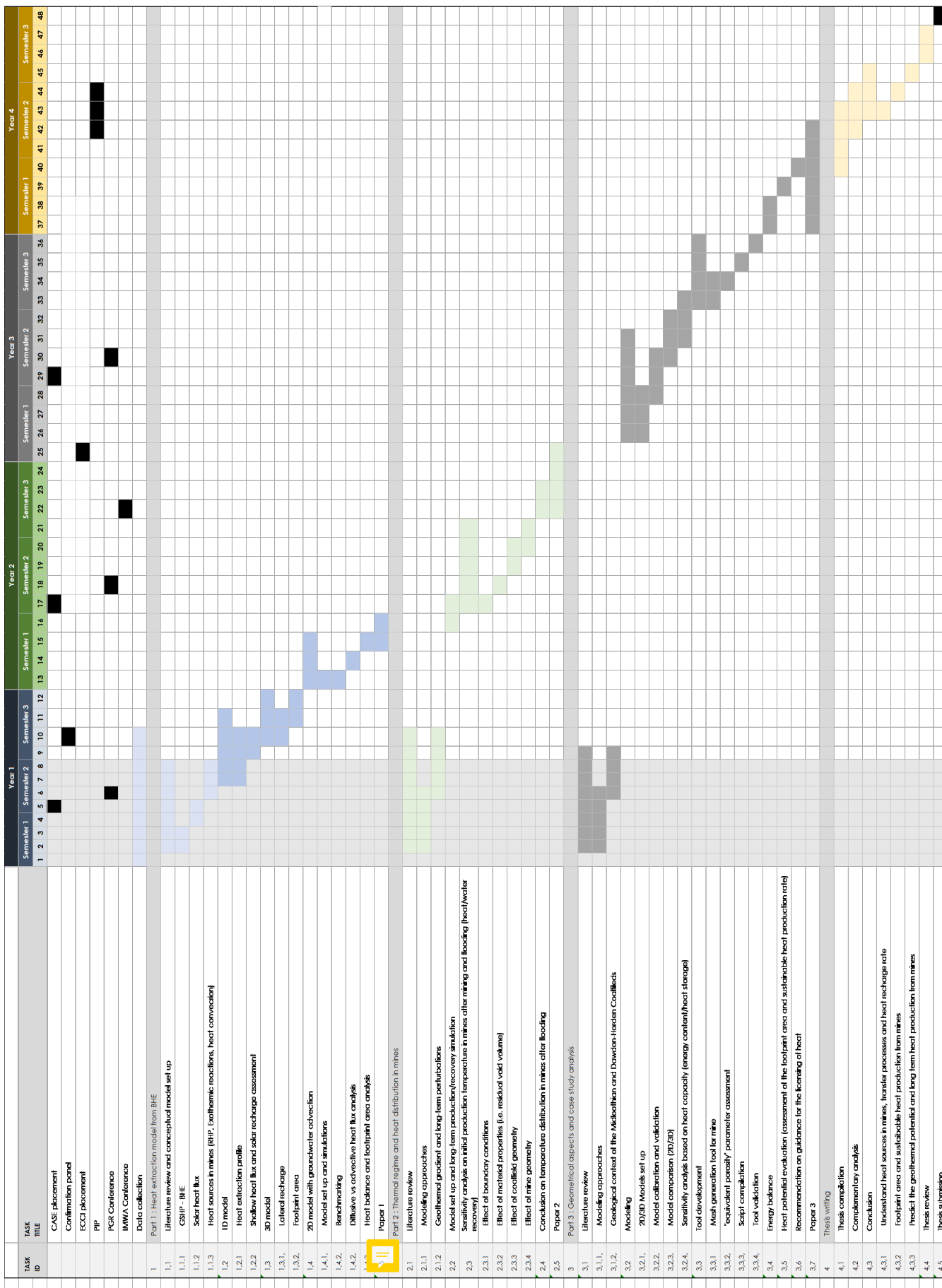


Figure 9.1: GANTT chart

10 Supervisory arrangements

- Principal supervisor : Christopher McDermott (University of Edinburgh)
- Co-supervisors (University of Edinburgh):
 - Stuart Gilfillan (geology, geochemistry)
 - Andrew Fraser-Harris (modeling expert)
- Advisor: Wyn Williams (University of Edinburgh)
- External Advisors:
 - Ian Watson (Coal Authority, CASE sponsor)
 - Andrew Gunning (RSK)
- External collaborators: David Banks (Holymoor Consultancy Ltd)

11 Resources and Training

11.1 Training need analysis

Skills / training required	Courses / resources identified
Couples TH modelling (OGS)	Hydrology 2 (self-directed learning)
Hydrodynamics / Geothermics in mines	Journal / books (self-directed learning)
Python coding	NMDM course (E4 DTP training, Datacamp courses)

Table 11.1: Skills and formations required

Other workshop attended are reported below:

The Writing Process: Getting Started (SCE/MVM)	IAD	29-Apr	3 hours
Top tips for writing an abstract	IAD	24-Apr	1 hour
Top Tips for Writing a Literature Review workshop	IAD	17-Apr	1 hour
E4 DTP Online PhD Training: Introduction to Career Pathways		28-Apr	3 hours
An Introduction to Copyright and Publishing workshop	IAD	22-Apr	2 hours
Beating Writers Block (SCE/MVM)		15-Apr	3 hours
Working productively at a distance	IAD	09-Apr	1,5 hours

Table 11.2: Courses attended

11.2 Teaching experience

- Hydrology 1 (Tutor, semester 1)
- Hydrology 2 (Tutor, semester 2)
- Earth Dynamics (Field demonstrator, Semester 1)
- Introduction to Geological Records (Demonstrator, Semester 2) and Lake District Field Trip (Field demonstrator, Semester 2, cancelled)

11.3 Resources available

Open-source software, including OpenGeoSys, QGIS, Tecplot as well as Python scripts are being used to conduct the PhD project. Modeling results are being visualized and post-processed using Tecplot, for which an extra-license has been provided. A renewal of the license will be required for the following years.

Source name	Total amount (£)	Comment
RTSG	3,450	NERC Research Training Support Grant
CASE funding	3,000	Coal Authority
Travel Grant	500	Estimated (application necessary)
TOTAL	7,000	Estimated

Table 11.3: Sources of income (total for 3 years)

11.4 Resources needed

Expenditure source	Amount (£)	Comment
Software license	540	Tecplot
Laptop	??	Need to be investigated
Visit Mining Museum	11.50	Museum + Guided visit
COAL Authority visits	74.40	Reimbursed drom CASE funding
UK 7th Geothermal Synopsium	150.59	TRansport + Conference
Coming conferences:	Estimates:	
WGC	380 + 200	
GeoTHERM	50 + 250	Conference fees +
GradSchool Conference	175 x 2	Transport
IMWA	250 + 100	
EGU	350 + 200	
SUB-TOTAL	3,000	
Open-source publishing licences	1,500	Estimations for 3 publications
Computing capacity/storage	1,500	Reserves
TOTAL	7,000	Include all income sources

Table 11.4: Resources required and potential expenses (NB: The total expenses ignore the expenses types, which might or might not be covered by all income sources. More detailed budget analysis is required to define which expense could be covered by which income source).

To date, no fieldwork has been planned or deemed required. All the data useful to calibrate or validate the model will be provided by the Coal Authority through the PhD lifetime, or acquired during CASE placement (no additional fees). Other external sources/private companies moreover offered to acquire and share additional temperature data that could be used for this study.

11.5 Conferences

Conferences attended and planned are summarized in Table XXX. All the conferences planned between April and August 2020 have been cancelled/postponed due to the Covid-19 Pandemic.

Conference name	Date	Organiser	Location
UK 7th Geothermal Synposium	Nov 2019	Geological Society London	London
Career and Industry Days	4 Dec 2019	Geological Society London	Edinburgh
GradSchool Conference 2020	7-9 Feb 2020	University of Edinburgh	Glasgow
PGR Conference (cancelled)	23-24 April 2020	University of Edinburgh	Edinburgh
WGC (postponed)	24-30 April 2020	International Geothermal Association	Reykjavik, Iceland
GeoTherm 2021	March 2021	European Geothermal Energy Council	Offenburg, Germany
GeoSciences PGR Conference	April 2021	University of Edinburgh	Edinburgh
IMWA Conference 2021	June/July 2021	International Mine Water Association	Cardiff, Wales, UK
EGU 2022	April 2022	European Geosciences Union	Vienna, Austria

Table 11.5: Conferences of interest

12 Ethical and Health and safety considerations

The research conducted through this PhD does not involve any subjects or fieldwork. All research will be exclusively conducted within the UK, either at the University of Edinburgh or at the Coal Authority Mansfield office, under the supervision of Ian Watson. All conditions regarding intellectual property, integrity, publication, authorship, and data confidentiality have been addressed by the “Studentship Agreement” and “Assignment and Confidentiality agreement” signed by all parties: the non-academic CASE partner (The Coal Authority), The University of Edinburgh and the student (Mylene Receveur). Research-related data will be stored and made accessible under the terms set by those agreements.

As part of mandatory placements of at least 3 month throughout the PhD duration, a Coal Authority ICT User Policy and Information Risk Management Policy (IRMP) have moreover been signed. In addition, a DBS security check has been completed and a Basic Disclosure certificate obtained from Disclosure Scotland.

If any new partnership is created to access data from private companies, we will ensure that this is made through written agreement or data license, and we will guarantee to provide feedback on any results and findings obtained from these data.

13 Take home message

Flooded coal mines constitutes potential low carbon heat energy resource. However, the sustainable use of heat from coal mines can only be achieved with an appropriate dimensionning of GSHP systems, which only depends on the good understanding of the heat capacity and recharge mechanisms of the underground. A key outcome of this work will be the development of a predictive tool, model or conceptual approach that enables the scientific estimation of the extent and nature of the heat available over the long term from abandoned flooded coal mines in the UK. This tool could be used to support the design of mine-water based heat extraction schemes, the assessment of sustainable production rate, but also guide the licensing of heat with a scientific approach. In parallel, this approach would participate in determining the external energy input (i.e. injection of heat or heat from other sources) necessary to create a sustainable heat reservoir in flooded coal mines, using energy balances and numerical simulations.

A Appendix

A.1 Equations

The transient heat diffusion equation can be written as follow.

$$\langle \rho_m \beta_m \rangle \frac{dT}{dt} = -\rho_w \beta_w v_w \frac{dT}{dx} + \nabla(\lambda \nabla T)$$

The first term on the right side represents the advective term, with the mass flow a characterized by the product of the water density ρ_v and velocity v , and the second term is the conductive heat transfer. The matrix heat conductivity and capacity can be defined as the product of the porous matrix and water properties as followed:

$$\begin{aligned}\lambda_m &= \phi_e \lambda_w + (1 - \phi_e) \lambda_r \\ \langle \rho_m \beta_m \rangle &= \phi_e \rho_w \beta_w + (1 - \phi_e) \rho_r \beta_r\end{aligned}$$

The thermal diffusivity (m²/s) is defined as follow:

$$\alpha = \frac{\lambda_m}{\rho \beta}$$

In a porous rock, the total energy extractable from cooling rocks can be calculated as follow:

$$E = \Delta TV \langle \rho_m \beta_m \rangle = m_r \Delta T \beta_m$$

with E the total energy (J) extracted from cooling rocks of volume V , ΔT the change in rock temperature, $m_r = V \Phi \rho_r$ the mass of rock with Φ the rock porosity and β_r the specific heat capacity of rock (J/kg.K). Raymond and Therrien (2008) estimated that the total geothermal energy content of rock can be estimated from the sum of the energy associated with each flooded underground section, as:

$$E_r = Vz\alpha \langle \rho_m \beta_m \rangle$$

with V the volume of water in a mine section, z its average depth, α the measured geothermal gradient and E_r the energy of a given section. The rate E_{hp} at which geothermal energy can be extracted using heat pumps was calculated as followed:

$$E_{hp} = Q(T_p - T_r) \rho_w \beta_w$$

with Q the average flow rate, T_p the water temperature and T_r the exchanger return temperature. Assuming that the energy is extracted from water flowing at a rate $Q_w(m^3/s)$, recharging the system at a temperature T_i and extracted at a temperature T_{out} , the rate of cooling of the reservoir $\Delta T_r(^{\circ}C/s)$ can be expressed as follow:

$$\Delta T_r = \frac{Q_w \rho_w c_w}{V \Phi \rho_r c_r} \Delta T_w$$

with $\Delta T_w = T_{out} - T_i$. The heat fluxes induced by water advection $q(W/m^2)$ can be expressed through the coefficient of heat transfer $h(W/m^2.K)$ as $q = h \times (T_r - T_f)$.

The power exchange of water in a system with colder fluid reinjection can thus be written as followed:

$$P = \frac{C\phi\rho\beta}{t}(T_{in} - T_{system})$$

A.1.1 Fracture flow and heat transfers

The Lauwerier-Pruess-Bodvarsson model (Lauwerier, 1955; Pruess and Bodvarsson, 1983) set up a formula to predict the temperature of water T_s in a fracture of aperture $2b$ at time t and distance x , where water injection commences at $x=0$ and $t=0$.

$$T_s - T_r = (T_e - T_r)erfc(\frac{c}{2b\rho_x c_w v_w} \sqrt{\frac{\lambda\rho c}{(t - \frac{x A \rho_w}{q})}})U(\theta - \varepsilon)$$

with T_e the injected water temperature, T_r the initial rock temperature, and $erfc$ the complementary error function. With flow velocity v and injection flow rate q , the equation can be rewritten for a generalized flow channel:

$$T_s - T_r = (T_e - T_r)erfc(\frac{xP}{2qc_w} \sqrt{\frac{\lambda\rho c}{(t - \frac{x}{v_w})}})U(\theta - \varepsilon)$$

A.1.2 Periodic heating

The analytical solution for temperature change in a semi-infinite half space under periodic heating/seasonal change in temperature $T_s = T_0 + \Delta T \cos(wt)$ given by Turcotte and Schuber (XXX) is:

$$T = T_0 + \Delta T + \exp(-y\sqrt{\frac{w}{2\alpha}})\cos(wt - y\sqrt{\frac{w}{2\alpha}})$$

with $w = \frac{2\pi}{\Theta}$. A sinusoidal temperature model representing the variations in heat transferred to the soil at the surface was derived by Hillel (1982) using a sinusoidal forcing function (Ozgener et al., 2013). The soil temperature at time t and depth z can be described as:

$$T(z, t) = T_m + A_z \sin(\frac{2\pi}{P}(t - t_0) - \gamma z - \frac{\pi}{2})$$

with $\gamma = \sqrt{\frac{\pi}{\alpha P}}$ the inverse damping depth, where P is the period of the oscillations and α is the thermal diffusivity. T_m the mean surface temperature, t_0 the time lag needed for the surface soil temperature to reach T_m , $A_z = A_0 \exp(-\gamma t)$ the amplitude of temperature wave at depth z , time t , which decay exponentially with depth. The undisturbed temperature at depth z and time t taking into account daily and annual temperature variations has been expressed in Radioti (2017) as followed:

$$T(z, t) = T_m - A \exp(-z\sqrt{\frac{\pi}{365\alpha}}) \cos(\frac{2\pi}{365}(t - t_{T_{min}} - \frac{D}{2}\sqrt{\frac{365}{\pi\alpha}})) + T_g(z)$$

where A is the amplitude of air temperature oscillations, $t_{T_{min}}$ the day number corresponding to the minimum temperature, α the equivalent ground daily thermal diffusivity and T_g the product of the geothermal gradient by the testing depth.

A.1.3 Seasonal production

Angelotti et al., modelled in 3D the temperature distribution (i.e. thermal plume) in porous aquifer under seasonal production from BHE, considering different groundwater velocity. The temperature response of the medium is here expressed as follow:

$$T(x,y,t) = T_g 0 + \frac{q}{4\pi\lambda_m} \exp\left(\frac{u_x}{2\alpha_m}\right) \int_0^{r^2/(4\alpha_m t)} \frac{1}{\psi} \exp\left(-\frac{1}{\psi} - \frac{u^2 r^2 \psi}{16\alpha_m^2}\right) d\psi$$

with $u = v_x \frac{c_w}{c_m}$ the effective water velocity. A steady state temperature might be reached for high simulation time and can be defined as follow:

$$T(x,y,t) = T_g 0 + \frac{q}{2\pi\lambda_m} \exp\left(\frac{u_x}{2\alpha_m}\right) K_0\left(\frac{u\sqrt{x^2+y^2}}{2\alpha_m t}\right)$$

A.1.4 Instantaneous heating

Bauer et al. (2015) gave the solution for the calculation of the residual heat dissipated by conduction after an instantaneous heat pulse in an infinite homogeneous solid:

$$T(r,t) = \frac{Q}{\rho c (4\pi\alpha t)^{\frac{3}{2}}} \exp\left(-\frac{r^2}{4\alpha t}\right)$$

with Q the energy of the point source, r the distance from the point source, t the time elapsed after the heating pulse, ρ and c the density and specific heat capacity of the material, respectively.

For a instantaneous cooling/heating of a semi-infinite half-space, where a constant temperature T_0 is applied on the top boundary condition of a domain of initial temperature T_1 , with $T_1 < T_0$, the temperature profile or temperature change can be calculated at a time t or distance z from the boundary using the following equation (Dirichlet heat conduction problem, with q = 0 on the lower boundary):

$$T = T_1 + (T_0 - T_1) \operatorname{erfc}\left(\frac{z}{\sqrt{4\alpha t}}\right)$$

The equations to calculate the temperature distribution in a 2D plan due to a constant temperature boundary condition or a heat pulse have been written as followed:

$$T = \operatorname{erfc}\left(\frac{x-vt}{\sqrt{4\alpha t}}\right) + \exp\left(\frac{xv}{\alpha}\right) * \operatorname{erfc}\left(\frac{x+vt}{\sqrt{4\alpha t}}\right) * \frac{T_0}{2}$$

$$T = \operatorname{erfc}\left(\frac{x-v(t+\Delta t)}{\sqrt{4\alpha(t+\Delta t)}}\right) + \exp\left(\frac{xv}{\alpha}\right) * \operatorname{erfc}\left(\frac{x+v(t+\Delta t)}{\sqrt{4\alpha(t+\Delta t)}}\right) * \frac{T_0}{2}$$

In case of a heat flux boundary condition, the change in temperature on the surface T_s and at a distance z, T_z in the half space can be defined as follow (using $T \rightarrow T_1$ as $y \rightarrow \infty$):

$$T_y = T_1 + \frac{2q_0}{k} \left(\sqrt{\frac{\alpha t}{\pi}} \exp\left(\frac{-z^2}{4\alpha t}\right) - \frac{z}{2} \operatorname{erfc}\left(\frac{z}{\sqrt{4\alpha t}}\right) \right)$$

and

$$T_s = T_1 + \frac{2q_0}{k} \sqrt{\frac{\alpha t}{\pi}}$$

A.2 Figures from Chapter 1

Radiogenic heat production for the Midlothian Coalfield:

	Sandstone CM	Sandstone PGP	Siltstone CM	Mudstone CM	Limestone	Ironstone	Coal	Average Fm conductivity	Average RHP	Heat flow	Gradient	
Conductivity	3.58	2.91	2.23	1.85	3.14	2.35	0.31	Calculated harmonic mean	Busby (2019)	Calculated harmonic mean (W/m ²)	(°C/km)	
RHP*	0.896	0.896	1.392	1.392	2.066	0.7	0.5			53	30	
CARRINGTON 1												
Thickness % lithology for each formation												
LOWER COAL MEASURES GROUP	250	35	30	30		1	5	2.516	1.91	1.18E-03	?	
PASSAGE FM	210		90	5	5			2.823	2.91	9.46E-04	?	
UPPER LIMESTONE FM	165	39	20	20	20		1	2.8433	2.25	1.32E-03	?	
LIMESTONE COAL	175	35	20	20	20		5	2.7125	2.24	1.31E-03	?	
LOWER LIMESTONE FM	85	39	20	20	20		1	2.8433	1.88	1.32E-03	?	
WEST LOTHIAN OIL SHALE	492	30	25	25	20			2.722	2.1*	1.38E-03	?	
GULLANE	593+								4.19**	1.40E-03	?	
CLYDE PLATEAU VOLCANIC FM	70								2.2	?	?	
Carrington-1 (Monaghan and Brown, 2014)												
*Kirkwood Fm conductivity **Clyde Sandstone Fm Conductivity												
Length (m)	14484.06				1 feet =	0.3048 m						
Width (m)	5632.69				1 mile =	1.60934 km						
Area (m ²)	81584219.92											
Groundwater composition												
FORMATION	Volume (m ³)	LITHOLOGY	PERCENTAGE	Volume (m ³)	RHP μW/m ³	Density (kg/m ³)	HPE	H (W/kg)	Concentration			
Coal Measures	Thickness (m): Daiketh (full thickness) 457.2	Sandstone*	35%	7.14E+09	0.896	2400	K	3.40E-09	9.19E+00 mg/L			
		Siltstone / Mudstone*	60%	1.22E+10	1.392	2400	Th	2.64E-05	9.00E-03 µg/L			
Passage Formation		Limestone**	0%	0.00E+00	2.066	2789	U	9.83E-05	2.26E-01 µg/L			
		Coal**	5%	1.02E+09	0.5	1200	Al	3.58E-01	1.80E+00 µg/L			
		Ironstone**	1%	2.04E+08	0.7	2650	Fe	3.65E-02	1.22E+03 µg/L			
							SO4	2.36E+01 mg/L				
20396054980		AVERAGE RHP (μW/m ³):	1.181	TOTAL RHP (W):	2.4E+04		A		8.20E+00 μW/m ³			
Thickness (m): Passage Formation	Carrington-1: 250	Sandstone*	90%	1.54E+10	0.896	2400						
		Siltstone / Mudstone*	10%	1.71E+09	1.392	2400						
		Limestone**	0%	0	2.066	2789						
		Coal**	0%	0	0.5	1200						
		Ironstone**	0%	0	0.7	2650						
17132686183		AVERAGE RHP (μW/m ³):	0.946	TOTAL RHP (W):	1.6E+04		A					
Upper Limestone FM Limestone Coal	In Lonhead (328 m) 165 In Lonhead (320 m) 175 Lower Limestone Fm 85	Sandstone*	35%	1.21E+10	0.896	2400	K	3.40E-09	3.08E+00 mg/L			
		Siltstone / Mudstone*	40%	1.39E+10	1.392	2400	Th	2.64E-05	2.28E-03 µg/L			
		Limestone**	20%	6.95E+09	2.066	2789	U	9.83E-05	4.00E-02 µg/L			
		Coal**	5%	1.73E+09	0.5	1200	Al	3.58E-01	4.00E+00 µg/L			
		Ironstone**	0%	0	0.7	2650	Fe	3.65E-02	3.22E+02 µg/L			
34673293467		AVERAGE RHP (μW/m ³):	1.309	TOTAL RHP (W):	4.5E+04		A		2.67E+00 μW/m ³			
Carboniferous strata below	873.24	Granite*	-	?	2.827	2650						
		Basalt*	-	?	0.358	2750	GW in aquifers extensively mined for coal					
		Sandstone*	30%	?	0.896	2400	U	9.83E-05	7.80E-01 µg/L			
		Siltstone / Mudstone*	50%	?	1.392	2400	K	3.40E-09	1.99E+01 mg/L			
		Limestone**	20%	?	2.066	2789	Fe	3.65E-02	3.28E+03 µg/L			
71242604204		AVERAGE RHP (μW/m ³):	1.378	TOTAL RHP (W):			A		4.56E+02 mg/L			
TOTAL HEAT PRODUCTION: 85658 W												

*Vila et al. (2010); ** OSIMOBi et al., 2018

HPE values are from Ruedas (2017)

Midlothian Model		Thickness	%thickness	RHP (W/m ³)	RHP (J/s)	Conductivity
LOWER COAL MEASURES GROUP		125	0.125	1.20E-03	0.150	1.910
PASSAGE FM		105	0.105	9.00E-04	0.095	2.910
UPPER LIMESTONE FM		85	0.085	1.30E-03	0.111	2.250
LIMESTONE COAL		85	0.085	1.30E-03	0.111	2.240
LOWER LIMESTONE FM		45	0.045	1.30E-03	0.059	1.880
WEST LOTHIAN OIL SHALE		255	0.255	1.40E-03	0.357	2.100
GULLANE		300	0.300	1.40E-03	0.420	4.190
		Average conductivity :		2.803		
		Gradient :		0.031		
		Heat flux :		8.69E-02		

Figure A.1: Estimates of the total radiogenic heat produced in the Midlothian Coalfield based on the thickness of the strata in the Carrington-1 well (Monaghan and Brown, 2014), the percentage of lithologies in each group (Vincent et al., 2010, Table XXX) and RHP values from the literature (Table XXX). The area considered for the total volume estimates consists of the area covered by the Coal Measures Formation outcrops in the Midlothian Coalfield. The average concentration of Th, U, K, Al, SO₄ and Fe in sampled groundwaters from the Coal Measures, Clackmannan and "Mine" aquifers of the MVS are from Dochartaigh et al., (2011) and were used to calculate a radiogenic heat generation potential, based on Equation XXX. The heat production rate values for ²⁶Al, K, ⁶⁰Fe, ²³²Th and U were estimated by Ruedas (2017) using atomic and nuclear properties

Table XXX summarizes the proportion of different lithologies (i.e. sandstone, siltstone, limestone, coal, mudstone) for the Carboniferous formations of the Midland Valley of Scotland. Data are based on the analysis of geological cores and samples from the Glasgow Observatory (Geothermal Energy Research Field Site), published by Vincent et al. (XXX) and Entwistle (2019).

lithology	UCMS	MCMS	LCMS	LSC - PGP	BELOW
Sandstone	40	>40	>50	40	30
Mudstone	60	30	30	40	50
Siltstone		24	14		
Coal		6	4		
Ironstone			<1		
Limestone				20	20

Table A.1: Percentage of lithologies recorded in existing borehole data. Data for the Lower (LCMS) and Middle (MCMS) Coal Measures are from the BGS Open Report OR19019 (Entwistle, 2019). Data for the Upper Coal Measures (UCMS), Limestone Coal (LSC) to Passage (PGP) Formations and underlying Carboniferous strata (BELOW) were determined from LOGS from 9 boreholes in the MVS (from Vincent et al., 2010)

A.3 Rock properties

The thermal character of a reservoir rock is mainly dependent on the effective heat capacity C_p (J/K), thermal conductivity λ (W/m.K) and thermal diffusivity α (m²/s) of the materials that forms it, as well as the amount of saturation. Where conductive processes are dominant, the effective fluid-rock heat capacity and heat conductivity both influence heat transfers. Thermal dispersivity mostly account for heat dispersion in areas where convective heat transfers are dominant (Deethlefsen et al., 2016). However, while the specific heat capacity, conductivity and diffusivity of groundwater are well known, the thermal properties of rocks highly depend on their material composition, texture and structure (Allen et al., XXX; Deethlefsen et al., 2016).

Browne et al. (1985) noted considerable variations both in the proportion of rock types in each formation in the MVS and in the conductivity for each lithology in the Upper Palaeozoic. The average thermal conductivity for the formations of the Carboniferous succession in the MVS is shown in Table XXX together with values for common rock types reported by Lee et al. (1984), Rollin (1987, reported in Banks, 2008) and Busby (2019). Formations thermal conductivity were estimated by Busby (2019) in the UKGEOS Open Report OR19015 by combining the thermal conductivities of individual lithological units as a harmonic mean, based on the data recently acquired from cores at the Glasgow Geothermal Energy Research Field Site. Due to the absence of thermal conductivity values for the Scottish Coal Measures, the Passage Formation and the Kirkwood Formation, the thermal conductivity for representative sections in those formations were estimated from values measured on similar lithologies in 5 boreholes located in the Pennine Coal Measures of northern England.

a) Lithology	K (W/m/K)	Reference
Coal	0.31	Lee et al., 1984
Coal Measures Sandstone	3.31, 3.58*	Rollin, 1987; *Busby (2019)
Coal Measures Siltstone	2.22, 2.23	Rollin, 1987; *Busby (2019)
Coal Measures Mudstone	1.49, 1.85*	Rollin, 1987; *Busby (2019)
Coal Measures Ironstone	2.35*	*Busby (2019)
Namurian Millstone Grit Limestone	3.75	Rollin, 1987
Lower Carboniferous limestone	3.14	Rollin, 1987
Upper Old Red Sandstone	3.26	Rollin, 1987
Silurian slates	3.33	Rollin, 1987
Hercynian granites	3.3	Rollin, 1987
Basalt	1.8	Rollin, 1987
Shale	1.3	Busby (2019)**
Fireclay	0.59	Busby (2019)**
b) Formation	K (W/m/K)	Reference
Scottish Coal Measures Formation	1.91 0.25	Browne et al., 1985
Scottish Middle Coal Measures	2.02	Busby (2019)
Scottish Lower Coal Measures Formation	1.91 0.25	Busby (2019)
Passage Formation	2.91 0.15	Browne et al., 1985
Upper Limestone Formation	2.25	Busby (2019)
Limestone Coal Formation	2.24	Busby (2019)
Lower Carboniferous	2.120.25	Browne et al., 1985
Lower limestone Formation	1.88	Busby (2019)
Lawmuir formation	4.36	Busby (2019)
Kirkwood Fm	2.1	Busby (2019)
Clyde Plateau Volcanic Formation	2.2	Busby (2019)
Clyde Sandstone Formation	4.19	Busby (2019)
Ballagan Formation	3.14	Busby (2019)
Kinnesswood formation	3.66	Busby (2019)

Table A.2: a) Thermal conductivity for specific lithologies found in the MVS succession, estimated based on laboratory measurements made on water saturated samples extracted from boreholes. *representative values for the Scottish Middle Coal Measured estimated from 5 boreholes in England. ** averages from the Boreland (Anderson, 1940) and Glenrothes (Gebbski et al., 1987) boreholes. b) Average thermal conductivity for the formations of the Carboniferous succession of the MVS (from Busby, 2019), estimated from the Maryhill, Hurlet House, Clachie Bridge, Barnhill, Kipperoch (Oxburgh, 1982), Boreland (Anderson, 1940) and Glenrothes (Gebbski et al., 1987) borehole logs

A.4 Scripts

A.4.1 Calculate heat flux across 2D grid

A.4.2 Plot and output surface flux

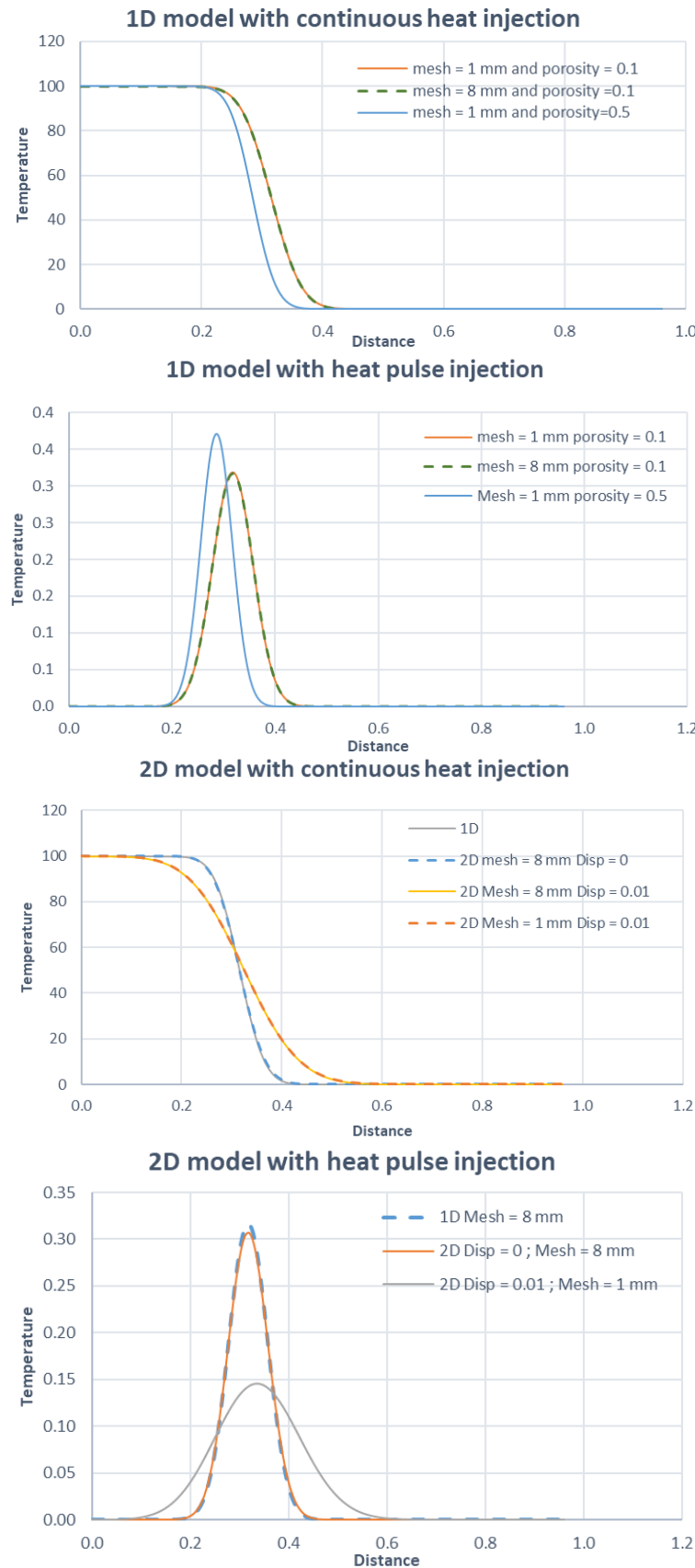
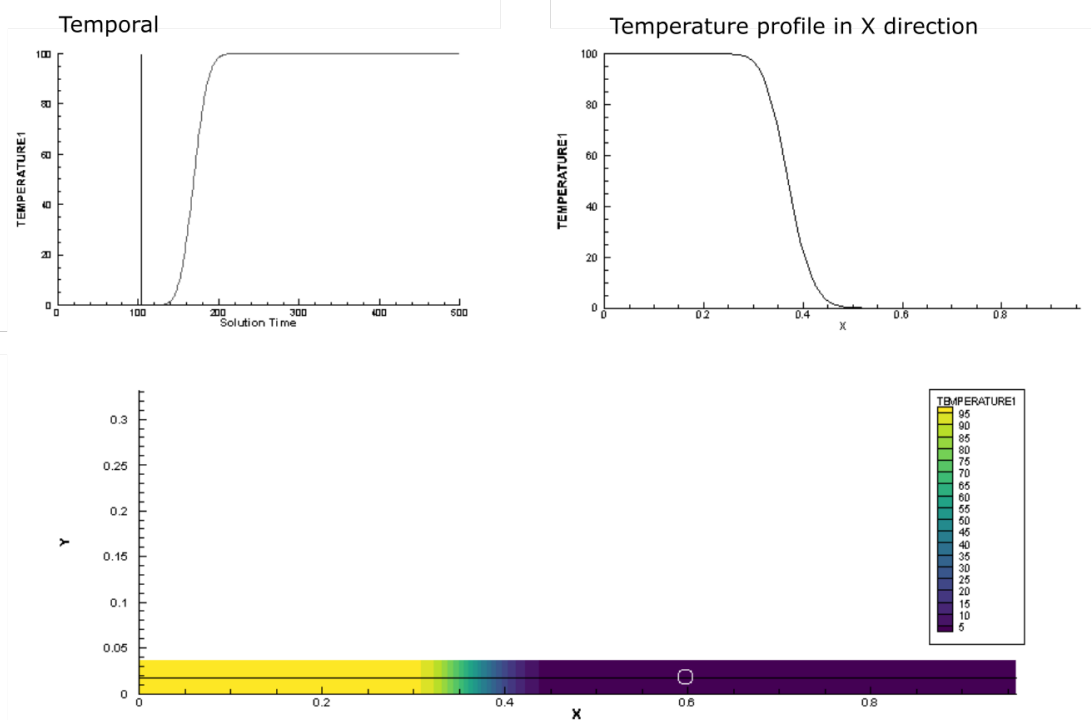


Figure A.2: Sensitivity analysis for porosity and mesh size for a 2D model with quadratic elements for the benchmarking of continuous and heat pulse injection

Continuous Injection



Heat pulse Injection

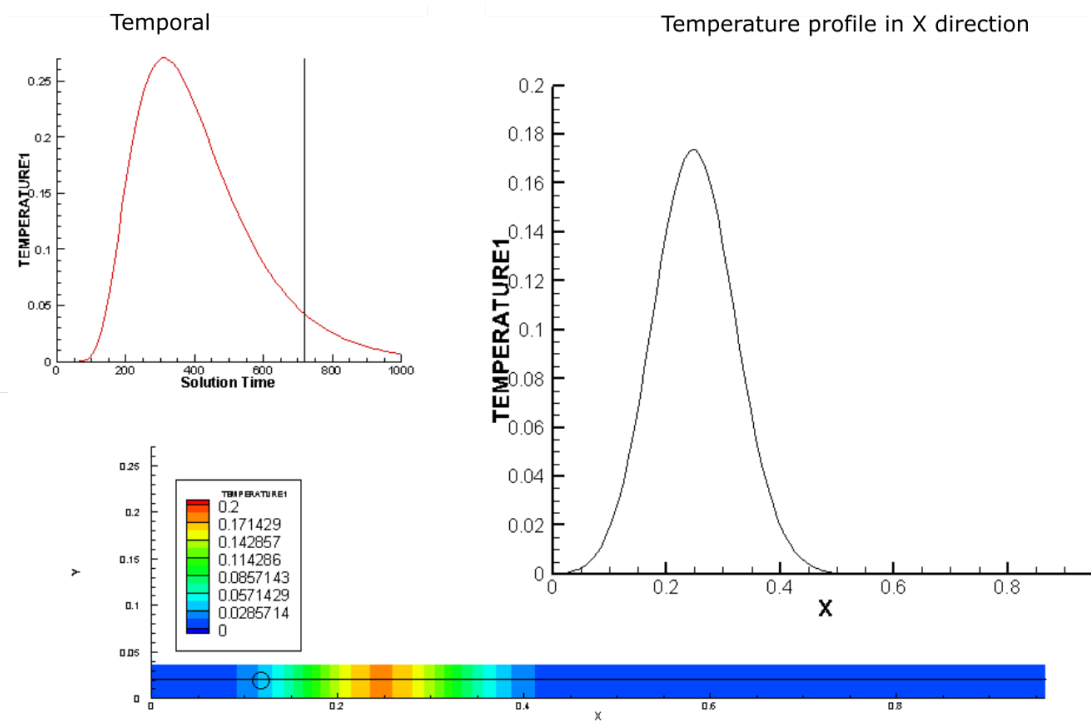


Figure A.3: Example of temperature distribution at $t=1000s$ from numerical simulation for a) continuous heat injection in 2D domain, and b) heat pulse injection in 2D domain

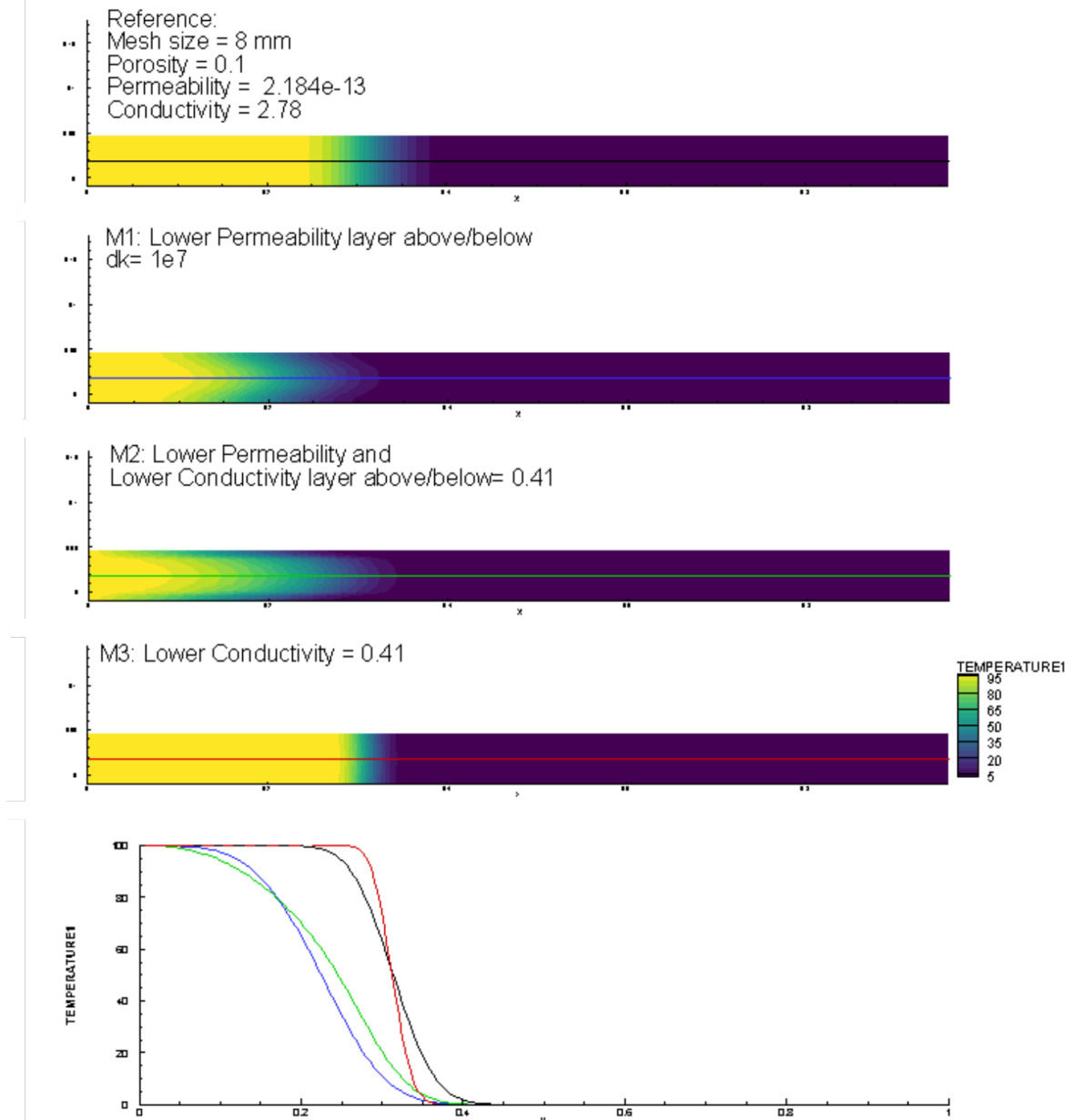


Figure A.4: Analysis of the effect of thin layer of rock with different rock properties on the final temperature distribution within the porous layer: a) Reference case with $k = 2e-13$, $K= 2.78$ and groundwater flow = $2e-4$ m/s b) with layers of 0.1m above below with lower permeability and c) with lower permeability and thermal conductivity

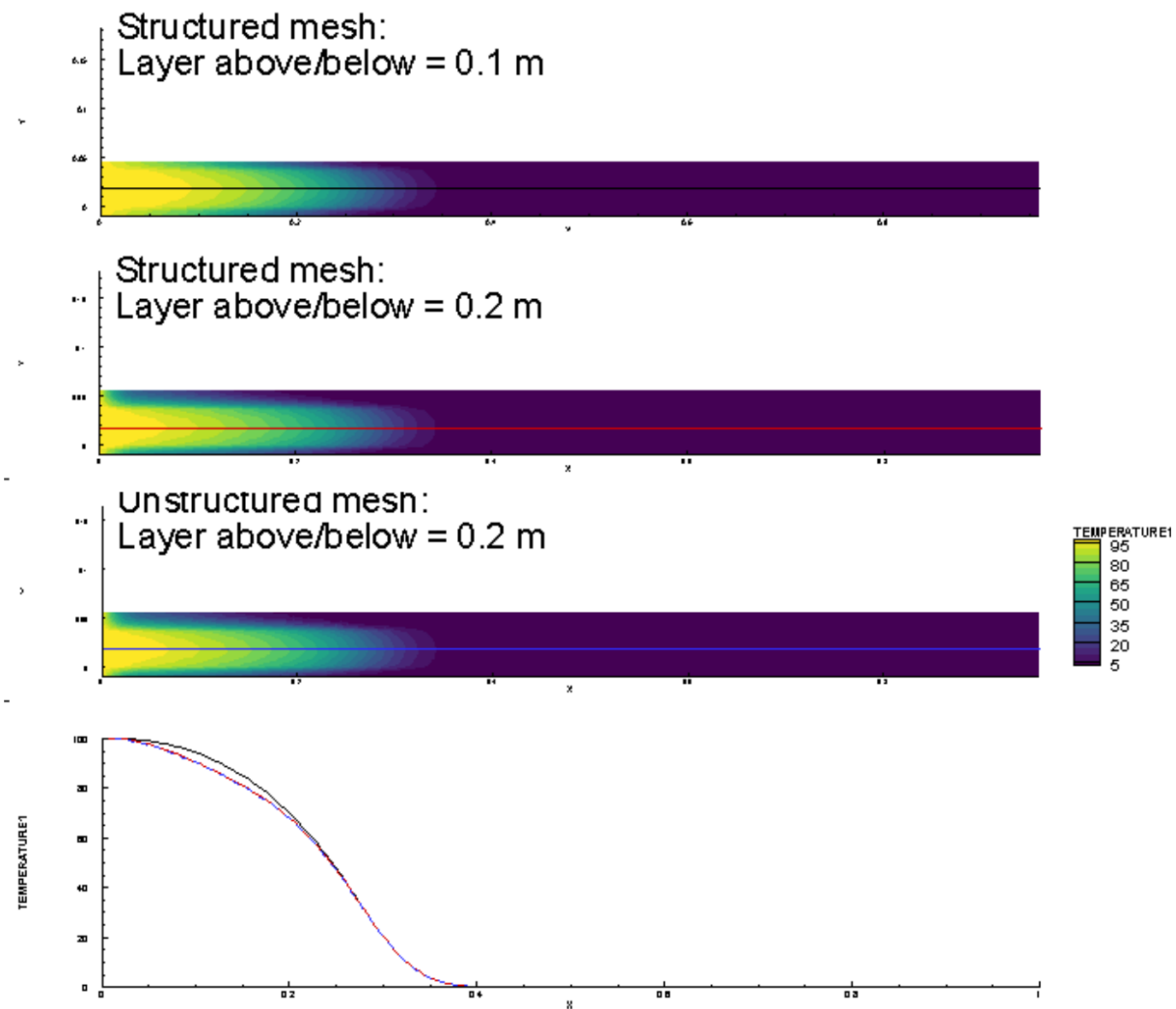


Figure A.5: Analysis of the effect of different rock properties on the final temperature distribution within the porous layer: a) Reference case with $k = 2e-13$, $K = 2.78$ and groundwater flow = $2e-4\text{m/s}$ b) with lower permeability, c) with higher porosity (0.5) and d) with conduction only (no advecting groundwater)

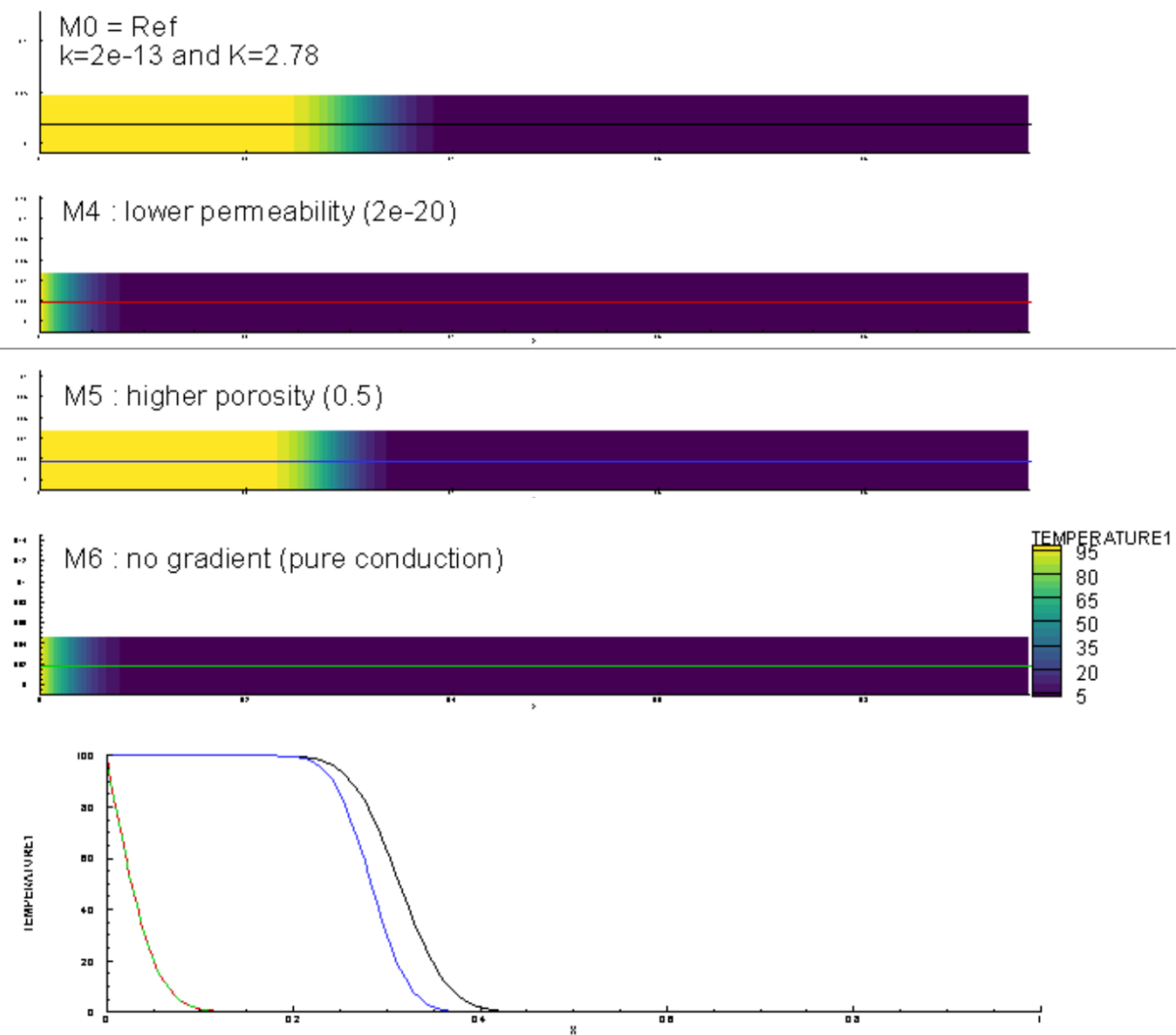


Figure A.6: Comparison of models for structure and unstructured mesh and different impermeable layer sizes

```

1 import math
2 import numpy as np
3 from scipy import special
4 import matplotlib.pyplot as plt
5 import pandas as pd
6
7 lambda_r = 2.78
8 lambda_w = 0.63
9 c_r = 1280
10 c_w = 4068
11 d_r = 2500
12 d_w = 1000
13 phi = 0.5
14 lambda_m = (lambda_r * (1-phi)) + (lambda_w * phi)
15 d_m = (d_r * (1-phi)) + (d_w * phi)
16 c_m = (c_r * (1-phi)) + (c_w * phi)
17 rho_c = (d_r*c_r)*(1-phi)+(d_w*c_w)*phi
18 D = lambda_m / rho_c # Thermal diffusion coefficient
19
20 x=0.96
21 DP=2e4
22 DP_DL=DP/x
23 k=2.184e-13
24 u= 1.8e-5
25 ux= (DP_DL * k) / u # Darcy velocity
26 vx = ux / phi # advective velocity
27 vT=(ux*d_w*c_w)/(rho_c) #effective thermal velocity of convective heat transport (Molina-Giraldo, 2011)
28 dispersivity = 0
29 DD = D + ux * dispersivity #longitudinal diffusion-dispersion coefficient
30
31 t_tot = 1000
32 dt=1
33 Ti = 0
34 T0= 100
35 Q = T0 * rho_c
36
37 # Continuous / moving infinite point source (1D)
38 #solution time
39 n=1
40 st=[]
41 for t in range(10000):
42     t1 = Q / (rho_c * (4*np.pi * DD)**((1+n)/2)) #o if n=1, rho_c * DD = lambda --> q/(4*pi*lamda)
43     t2 = - (x-vT*(t+dt))/np.sqrt(4*DD*(t+dt))
44     T = t1*math.exp(t2)
45     st.append(T)
46 plt.figure(figsize=(16,5))
47 plt.subplot(1,3,1)
48 plt.plot(range(10000),st,color='black', lw=2,label="analytical")
49 plt.xlabel('time')
50 plt.ylabel('temperature')
51 plt.legend(loc='best')
52
53 #solution distance: continuous
54 sd=[]
55 list = np.arange(0.0001,1,0.0001)
56 for x in list:
57     t1 = (x-vT*t_tot)/np.sqrt(4*DD*t_tot)
58     t2 = math.exp((x*vT)/(DD))
59     t3 = (x+vT*t_tot)/np.sqrt(4*DD*t_tot)
60     T = (special.erfc(t1)+t2*special.erfc(t3))*T0/2
61     sd.append(T)
62
63 plt.subplot(1,3,2)
64 plt.plot(list,sd,color='black',lw=2,label="analytical")
65
66 #import data
67 data = pd.read_csv('1D_Cont.csv', delimiter=',', header=0) #mesh = 1 mm poro=0.5
68 xp = data['xp']
69 Tp = data['Tp']
70 plt.plot(xp,Tp,'--', color='red',label="numerical")
71 plt.xlabel('distance')
72 plt.ylabel('temperature')
73 plt.legend(loc='best')
74
75 #solution distance: pulse
76 sd=[]
77 n=1
78 list = np.arange(0.0001,1,0.0001)
79 for x in list:
80     t1 = -(x-vT*t_tot)/np.sqrt(4*DD*t_tot)
81     t2 = math.exp((x*vT)/(2*DD))
82     t3 = (x+vT*t_tot)/np.sqrt(4*DD*t_tot)
83     T = (1/(rho_c*(16*np.pi*DD)**((1+n)/2)))*(math.exp(t1))*(special.erfc(t1)+t2*special.erfc(t3))*T0/2 |
84     sd.append(T)
85 plt.subplot(1,3,3)
86 plt.plot(list,sd,color='black',label="analytical")
87
88 #import data
89 data = pd.read_csv('1D_Pulse.csv', delimiter=',', header=0) #poro = 0.5, mesh=1 mm
90 xc = data['xc']
91 Tc = data['Tc']
92 plt.plot(xc,Tc, color='blue',label="numerical")
93 plt.xlabel('distance')
94 plt.ylabel('temperature')
95 plt.legend(loc='best')
96 plt.savefig("analytical_vs_numerical_1D.png")

```

```

1 import os
2 import numpy as np
3 import matplotlib.pyplot as plt
4 os.chdir(r'C:\Users\s1995204\Documents_LOCAL\Modeling\Heat_Models\1D')
5
6 qmax=6 #qmax=input("Enter qmax : ")
7 qmin=-qmax
8 amp=abs(qmax-qmin)/2
9
10 dt_d=1
11 dt_s=3600*24
12
13 t_y=2 #t_y=input("Enter nb year : ")
14 #t_y=eval(t_y)
15 t_d=dt_d*365*t_y
16 t_s=dt_s*365*t_y
17 time = np.arange(0, t_d, dt_d)
18 time_s= np.arange(0, t_s, dt_s)
19 time_yr = time/365
20
21 plt.figure(figsize=(14,6))
22
23 ##Plot and output daily values of surface flux
24 plt.subplot(1,2,1)
25 amplitude = amp*np.sin(2*np.pi*(time/t_d*dt_y))-0.06
26 data=np.stack((time_s, amplitude), axis=-1)
27 np.savetxt('surface_flux.txt', data)
28 plt.plot(time_yr, amplitude, "k-", label="Surface flux", linewidth=2)
29 plt.title('Surface flux and temperature')
30 plt.xlabel('Time (days)')
31 plt.ylabel('Amplitude surface flux (W/m2) ')
32 plt.ylim(-10,10)
33 plt.grid(True, which='both')
34 plt.axhline(y=0, color='k')
35
36 ##Plot output temperature at y=0 (point on surface of 1D model)
37 plt.twinx()
38 t = np.loadtxt('POINT0.txt', skiprows=0, usecols=0) # first column
39 tyr= t/(3600*24*365)
40 T = np.loadtxt('POINT0.txt', skiprows=0, usecols=1) # 2nd column
41 plt.plot(tyr[0:721], T[0:721], "r-", label="Temperature", linewidth=2)
42 plt.ylim(-2,15)
43 plt.ylabel('Temperature (degC)',color='r')
44
45
46 ##Plot and extract extraction rate
47 plt.subplot(1,2,2)
48 amplitude = -294*np.sin(2*np.pi*(time/t_d*dt_y))-1000
49 data=np.stack((time_s, amplitude), axis=-1)
50 np.savetxt('extraction_rate.txt', data)
51 plt.plot(time_yr, amplitude, "k-", label="Extraction rate", linewidth=2)
52 plt.title('Extraction rate along borehole')
53 plt.xlabel('Time (days)')
54 plt.ylabel('Extraction rate (W)')
55 plt.ylim(-1500,-600)
56 plt.grid(True, which='both')
57 plt.ylabel('Extraction rate (W)')
58 plt.tight_layout()
59
60 plt.savefig('surface_flux_extraction_rate.png')
61
62

```

References

- Adams, R. and Younger, P. (Mar. 2001). A Strategy For Modeling Ground Water Rebound In Abandoned Deep Mine Systems. *Ground Water* [online]. 39.2, pp. 249–261. ISSN: 0017-467X, 1745-6584. DOI: 10.1111/j.1745-6584.2001.tb02306.x.
- Andrés, C., Ordóñez, A., and Álvarez, R. (2017). Hydraulic and Thermal Modelling of an Underground Mining Reservoir. *Mine Water and the Environment* [online]. 36.1, pp. 24–33. ISSN: 1025-9112, 1616-1068. DOI: 10.1007/s10230-015-0365-1.
- Banks, D., Fraga Pumar, A., and Watson, I. (2009). The operational performance of Scottish minewater-based ground source heat pump systems. *Quarterly Journal of Engineering Geology and Hydrogeology* [online]. 42.3, pp. 347–357. ISSN: 1470-9236, 2041-4803, 1470-9236. DOI: 10.1144/1470-9236/08-081.
- Banks, D., Skarphagen, H., Wiltshire, R., and Jessop, C. (2004). Heat pumps as a tool for energy recovery from mining wastes. *Geological Society, London, Special Publications* [online]. 236.1, pp. 499–513. ISSN: 0305-8719, 2041-4927. DOI: 10.1144/GSL.SP.2004.236.01.27.
- Burley, A., Edmunds M., W., and Gale, I. (1984). *Catalogue of geothermal data for the land area of the United Kingdom*. Second revision. British Geological Survey.
- Clean Growth - Transforming Heating* (2018). Department for Business, Energy and Industrial Strategy, p. 136.
- Ferket, H., Laenen, B., and Van Tongeren, P. (2011). “Transforming flooded coal mines to large-scale geothermal and heat storage reservoirs: what can we expect?” In: *Mine water - Managing the Challenges*. IMWA Congress 2011. Aachen, Germany, pp. 171–175.
- Gillespie, M., Crane, E., and Barron, H. (2013). *Study into the Potential for Deep Geothermal Energy in Scotland - Volume 2*. AEC/001/11. Scottish Government, p. 129.
- Kolditz, O., Bauer, S., Bilke, L., Böttcher, N., Delfs, J. O., Fischer, T., Görke, U. J., Kalbacher, T., Kosakowski, G., McDermott, C. I., Park, C. H., Radu, F., Rink, K., Shao, H., Shao, H. B., Sun, F., Sun, Y. Y., Singh, A. K., Taron, J., Walther, M., Wang, W., Watanabe, N., Wu, Y., Xie, M., Xu, W., and Zehner, B. (2012). Open-GeoSys: an open-source initiative for numerical simulation of thermo-hydro-mechanical/chemical (THM/C) processes in porous media. *Environmental Earth Sciences* [online]. 67.2, pp. 589–599. ISSN: 1866-6280, 1866-6299. DOI: 10.1007/s12665-012-1546-x.
- Małolepszy, Z. (2003). “Low Temperature, Man-Made Geothermal Reservoirs in Abandoned Workings of Underground Mines”. In: Stanford Geothermal Workshop. Standford.
- Renz, A., Rühaak, W., Schätzl, P., and Diersch, H.-J. G. (2009). Numerical Modeling of Geothermal Use of Mine Water: Challenges and Examples. *Mine Water and the Environment* [online]. 28.1, pp. 2–14. ISSN: 1025-9112, 1616-1068. DOI: 10.1007/s10230-008-0063-3.
- Rodríguez, R. and Díaz, M. B. (2009). Analysis of the utilization of mine galleries as geothermal heat exchangers by means a semi-empirical prediction method. *Renewable Energy* [online]. 34.7, pp. 1716–1725. ISSN: 09601481. DOI: 10.1016/j.renene.2008.12.036.

- Stark, C. (2019). *Net Zero: The UK's contribution to stopping global warming*. Committee on Climate Change, p. 277.
- Todd, F., McDermott, C., Harris, A. F., Bond, A., and Gilfillan, S. (2019). Coupled hydraulic and mechanical model of surface uplift due to mine water rebound: implications for mine water heating and cooling schemes. *Scottish Journal of Geology* [online], sjg2018–028. ISSN: 0036-9276, 2041-4951. DOI: 10.1144/sjg2018-028.
- Younger, P. (2001). Mine water pollution in Scotland: nature, extent and preventative strategies. 265, pp. 309–326.
- Younger, P. L. (2004). Making water: the hydrogeological adventures of Britain in early mining engineers. *Geological Society, London, Special Publications* [online]. 225.1, pp. 121–157. ISSN: 0305-8719, 2041-4927. DOI: 10.1144/GSL.SP.2004.225.01.09.